Microwave Radiometry and Snow Water Equivalence Retrievals on Snow Covered Sea Ice in the Marine Cryosphere

Sheldon D. Drobot

A Thesis

Submitted to the Faculty of Graduate Studies

in Partial Fulfillment of the Requirements

for the Degree of

Master of Arts

Centre for Earth Observation Science

Department of Geography

University of Manitoba

Winnipeg, Manitoba

THE UNIVERSITY OF MANITOBA

FACULTY OF GRADUATE STUDIES

*****

COPYRIGHT PERMISSION PAGE

MICROWAVE RADIOMETRY AND SNOW WATER EQUIVALENCE RETRIEVALS ON SNOW COVERED SEA ICE IN THE MARINE CRYOSPHERE

BY

SHELDON D. DROBOT

A Thesis/Practicum submitted to the Faculty of Graduate Studies of The University of Manitoba in partial fulfillment of the requirements of the degree of

MASTER OF ARTS

Abstract

Snow water equivalence (SWE) derivation over sea ice requires a better understanding of how variations in the evolving snow-sea ice mixture affect microwave emission. In this thesis, the effects of (a) variation in liquid water content within a seasonally dynamic snowpack and (b) heterogeneity in underlying ice are examined. Geophysical snow data and in situ passive microwave signatures were collected in the Canadian Arctic Archipelago during the spring of 1996 under the Collaborative-Interdisciplinary Cryospheric Experiment (C-ICE). Surface based radiometer measurements were collected at 19, 37 and 85GHz (both vertical and horizontal polarizations). Snow data and Special Sensor Microwave/Imager (SSM/I) data were collected from 1993-1995 during the Seasonal Sea Ice Monitoring and Modelling (SIMMS) program.

Results indicate SWE can be derived with an in situ microwave radiometer when the snowpack is dry. Multiple regression techniques are shown to better estimate in situ SWE over the case site. With increased water in liquid phase, emission from the snowpack causes current algorithms to overestimate SWE. Variation in ice type and spatial pattern of the ice limit the applicability of SWE derivation with SSM/I. The presence of multiyear ice (MYI) lowers emissivity values that leads to an underestimation of SWE with current algorithms.

Acknowledgements

Special thanks go out to Dr. David G. Barber for his continual support and patience. In particular, I thank him for showing me the nature of scientific inquiry, and giving me the opportunity to explore the remote northern reaches of our world. I would also like to acknowledge the help my fellow colleagues provided both in the field and in the lab. John Yackel and John Iacozza were instrumental in helping me acquire the data used in this work. Thanks also to Theresa Nichols, John Hanesiak, and David Mosscrop for their editorial comments.

I will never forget the love and support of my family and friends, who have made my time in Winnipeg truly enjoyable. I would also like to recognize Walt Lipinski as being an energetic, thoughtful junior high teacher who first got me interested in this place called Earth.

Thanks also to the various institutions and agencies that have supported the final work. In particular, CRYSYS, Canadian Ice Services, NSERC, ONR, and the Northern Studies Training Program were instrumental in completing this thesis. Thanks to Polar Continental Shelf for logistical field support.

Table of Contents

List of Figures

List of Tables

CHAPTER 1 - Introduction

1.1 Introduction

The marine cryosphere consists of snow on sea ice, the underlying ocean and the atmosphere, as well as biological life living within these volumes and energy exchanges operating across them. Scientific interest centres on the marine cryosphere as an early indicator of global change resulting from its sensitivity to a series of enhanced feedback processes (IPCC, 1990). Snow, with a low thermal conductivity and high albedo, is an integral component of this marine cryosphere. Physically, the snow volume governs key energy exchanges between the ocean and the atmosphere (Barber *et al.*, 1995), which in turn controls processes such sea ice accretion and ablation. It is therefore essential to obtain improved information regarding snow covered sea ice in the marine cryosphere.

The Intergovernmental Panel on Climate Change (IPCC) projects warming in the marine cryosphere will reduce the spatial and temporal extent of snow cover (IPCC, 1995). The development of remote sensing is an important step in documenting such change, as it provides excellent spatial and temporal coverage in contrast with traditional in situ observations (Massom, 1991). In particular, derivation of snow water equivalence with

microwave radiometry appears to be one of the more promising monitoring approaches (Goodison, 1997). SWE is the amount of water a melted snowpack would yield. SWE accounts for variations in snow density as well as snow depth, which is necessary to fully document modifications in snow cover amount. Furthermore, SWE retrievals are successfully acquired over terrestrial surfaces (e.g. Goodison *et al.*, 1990). Unfortunately, the complex nature of a snow covered sea ice volume has prevented operational SWE estimation in the marine cryosphere to date (Carsey *et al.*, 1992).

The conceptual underpinnings for deriving SWE with microwave radiometry are based on the effect a snow layer has on microwave emissions originating within the underlying sea ice. Increasing snow thickness or density increases the scattering potential of a snowpack, resulting in decreases in microwave emission from the ice. However, the effect of water in liquid phase on microwave emission is not completely understood nor is the significance of variation in the underlying ice type.

Specific objectives of this thesis are linked to determining the effects snow and sea ice have on the successful derivation of snow water equivalence over the marine cryosphere. In particular, this thesis examines a relationship between snow geophysical properties, microwave emission and in situ derived SWE. It also outlines how ice type heterogeneity affects Special Sensor Microwave/Imager derived SWE.

To make this a tractable thesis, spatial and temporal restraints are applied. The investigation is spatially limited to specific field sites located within a hundred kilometer radius of Resolute Bay, NT. Geophysical samples are

only drawn from saline, smooth, first-year ice considered typical of this region. Temporally, data collection begins in the latter stages of the cold winter period and extends into the beginning of the melt onset season.

This thesis is a small part of a large, multidisciplinary, international effort to understand the complex interworkings of the cryosphere. It seeks to further our knowledge in the fields of geophysical inversion and algorithm development by improving characterization and understanding of both the snow covered sea ice volume and its interaction with microwave energy.

In the larger framework, scientific research in the cryosphere is focused on better characterization, understanding and prediction of Earth processes. Characterization represents an initial attempt to monitor and describe current conditions in the marine cryosphere. Understanding furthers that work by providing hypotheses which explain why things happen and provide knowledge as to how they happen. Finally, prediction is concerned with exploiting the knowledge gained through understanding to explain how variations in one component of the marine cryosphere will affect other processes, both locally and globally.

To accomplish the specific goals of this thesis a scientific framework will be presented in the next section. This provides an overall scientific objective and a series of research tools that provide the underlying structure for the remaining chapters.

1.2 Research Design

To make a significant scientific contribution in this thesis the following mission statement is provided:

> *Science Objective: "To provide insight on the development of SWE algorithms for snow covered sea ice using microwave radiometry."*

The tools used to assess the scientific objective are divided into four sections:

1) *In-situ Observations*: Few experiments have analyzed snow cover in the marine cryosphere owing to the hostile climate and remote location of this region. None have specialized in snow water equivalence studies over sea ice. This work provides detailed in situ snow observations from various seasonal and diurnal regimes. The snow data provides a comprehensive suite of variables needed to assess SWE variations within a case study or field context.
2) *Modelled (derived) Variables*: Passive microwave interaction is controlled by the sea ice-snow volume dielectric properties. Modelled values are used in this thesis to estimate snow pack dielectrics. The models are based upon the results in (1) and can be used in conjunction with the physical data to understand the nature of electromagnetic interaction between the snow and the passive signature in the microwave portion of the electromagnetic spectrum.
3) *Remotely Sensed Data*: Remotely sensed data can record changes in microwave emission over an ice surface. With the high cost of operating microwave radiometers and inherent calibration difficulties, few studies

have successfully coupled microwave emission with an evolving snowpack. This study provides the necessary passive microwave data to explore derivation of both in situ and SSM/I derived SWE over varying diurnal time steps. The diurnal aspect of this study is key since operational SSM/I data is available at various times of the day in the marine cryosphere.

4) *Statistical Analysis*: Assessing the scientific objective is facilitated by the use of statistical techniques as a means of ensuring that the work presented here is reproducible. In particular, correlation analysis and a full suite of general linear regression models are used to help understand the complex interaction between microwave energy and the evolving sea ice-snow mixture.

1.3 Chapter Reviews

This thesis contains six chapters, each contributing to the assessment of my stated scientific objective. The first chapter outlines the purpose, context and constraints of the project. Chapter two outlines the scientific focus and provides descriptions of sea ice, snow and their role within the marine cryosphere. It also examines how changing snow conditions could affect this region and explores evidence that changes have already occurred.

The third chapter provides the necessary microwave interaction theory to link geophysical snow and ice properties to microwave radiometry. It summarizes the historical precedent for using microwave radiometry in

the marine cryosphere and concludes with a series of research questions which structure the remaining chapters.

Chapter four examines the relationship between snow properties, microwave emission and in situ derived SWE over a case study site. Geophysical snow data collected in the Canadian Arctic Archipelago during the spring of 1996 is initially examined in a vertical profile over seasonal and diurnal time steps. Results are then exploited to improve derivation of SWE with an in situ microwave radiometer.

The fifth chapter expands upon the results of chapter four to examine the effects of heterogeneity in underlying ice type on SSM/I derived SWE. In situ and SSM/I derived SWE are compared to gain an understanding of the differences present between the two. Then a series of sensitivity trials are performed to theoretically determine how variations in ice emissivity affect SWE estimation. Specifically, these trials examine heterogeneity in both the spatial arrangement and type of ice (first-year ice vs. multiyear ice). Finally, real world diversity is examined with SSM/I and the Earth Resources Satellite (ERS-1).

The concluding chapter is utilized to summarize the relevant findings of this work. It is intended to reinforce the conclusions and provide insight into future directions of research raised by this thesis.

CHAPTER 2 - Scientific Focus

2.1 Introduction

As previously stated, snow cover is a major component of the marine cryosphere owing to its influence on energy and mass exchanges. The seasonal snow cover is a primary factor in controlling energy fluxes across the marine cryosphere due to its high albedo. Decreasing snow cover would lower the average seasonal albedo of this region, increasing energy absorption and leading to the well-known temperature-albedo feedback process described by Henderson-Sellers and Robinson (1987). Similarly, mass exchanges across the marine cryosphere are limited by the low thermal conductivity of snow.

This chapter describes the snow covered sea ice volume and the effects it has on the marine cryosphere. It begins with a brief description of the marine cryosphere and its components. Two of these components, sea ice and snow, are then examined more thoroughly. The formation and evolution of both surfaces is given to examine their relevance to SWE derivation. The seasonal snowpack is also described with respect to the effects it has on the shortwave radiation balance, mass transfer and the life cycles of various biologic entities. Finally, an examination of recent temperature and sea ice extent data points out evidence that this region is currently undergoing noticeable change.

2.2 The Marine Cryosphere

In this thesis, the marine cryosphere (Figure 2.1a) can be conceptualized as a physical system containing sea water (1), multiyear sea ice (2), first-year sea ice (3), snow (4) and the atmosphere (5). Each of these components vigorously interacts with the others through specific energy and mass exchanges (Figure 2.1b). Some of these exchanges, such as heat transfer between the ocean and atmosphere, are instrumental in regulating the global energy balance (Henderson-Sellers and Robinson, 1987). The physical properties of snow (and to a lesser degree sea ice) are important because they restrict energy and mass exchange between the underlying ocean and the overlying atmosphere. In what follows, a detailed description of the snow-sea ice mixture, from formation through evolution, will be presented in order to better understand how their physical properties affect the marine cryosphere.

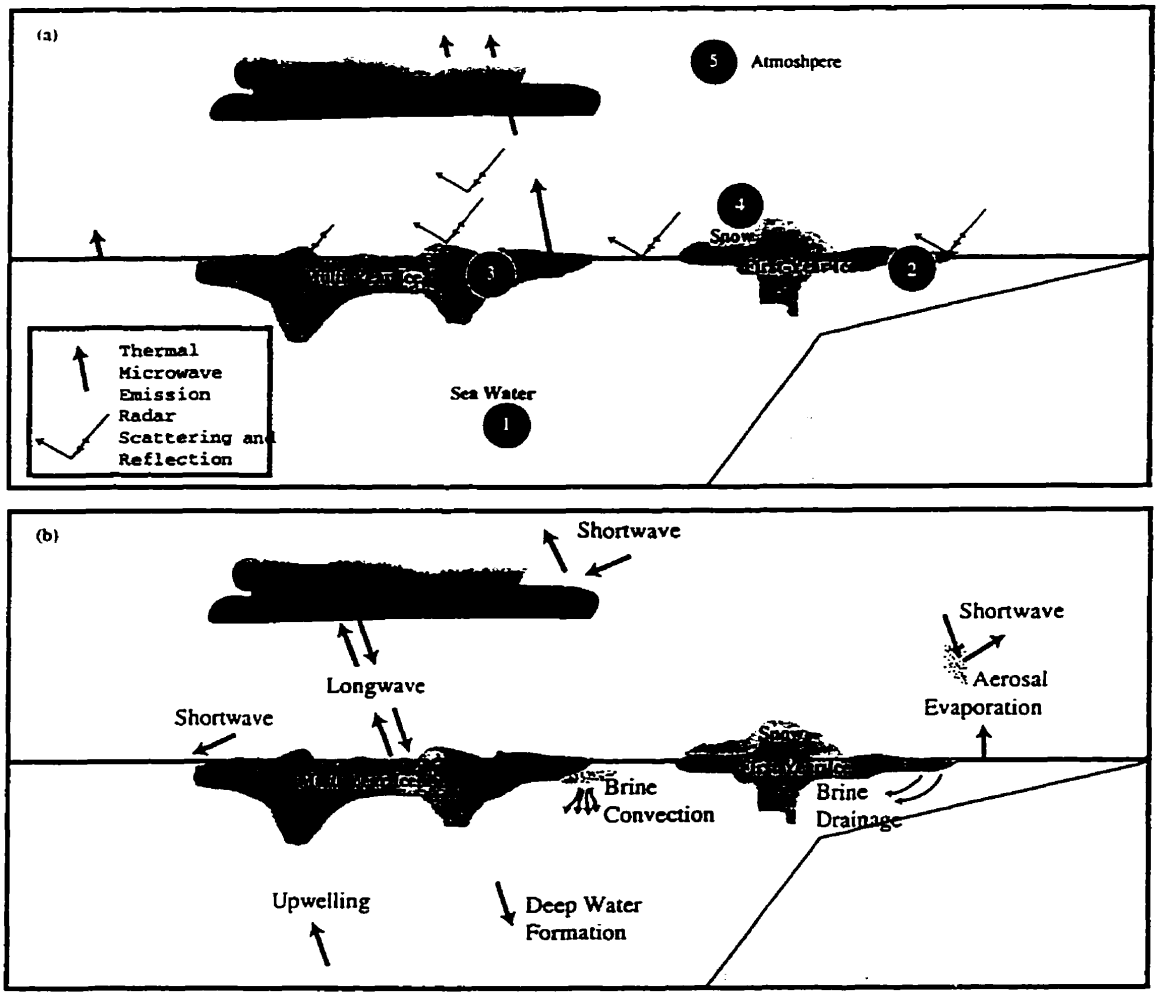

Figure 2.1 (a) Microwave interactions and (b) processes within the marine cryosphere. *(adapted from Carsey, 1992)* Numbers referenced in section headings below.

2.2.1 Sea Ice (2,3)

The polar oceans are seasonally covered by a dynamic, uneven layer of frozen water termed sea ice (Carsey *et al.*, 1992). The spatial coverage of this ice exhibits a strong seasonal bias (Figure 2.2). During the spring maximum, sea ice coverage can be as high as 15 x 10^6 km^2 (LeDrew, 1990). However, in the summer sea ice retreats to the remote northern regions of the marine cryosphere, where it covers as little as 8 x 10^6 km^2 (LeDrew,

1990). The 7 x 10^6 km^2 differential is larger than the area of all the Canadian provinces combined (Barber, 1993).

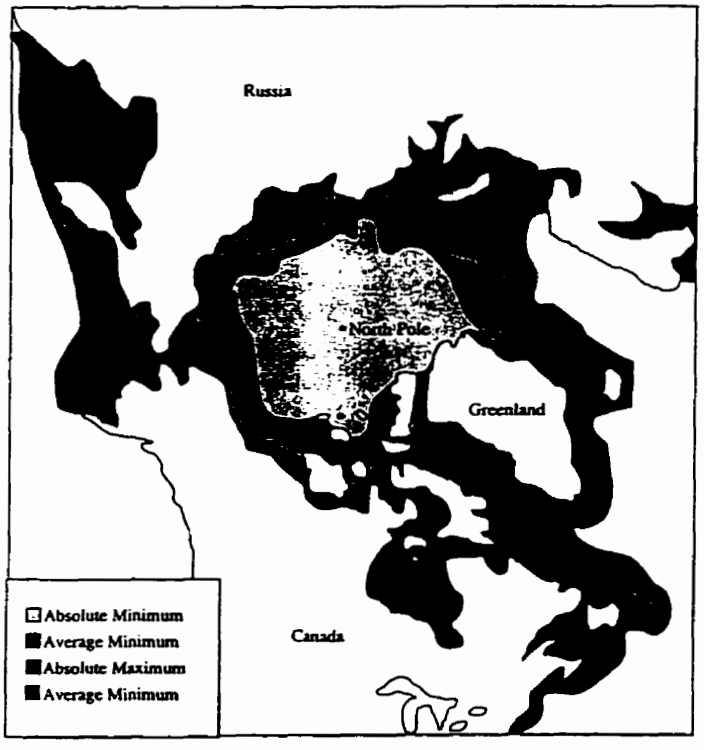

Figure 2.2 Minimum and maximum sea ice extent. *(adapted from Henderson-Sellers and Robinson, 1987)*

In this work, two distinct types of sea ice are examined: FYI and MYI. FYI is a mixture of pure ice, salt, liquid brine and air inclusions typically 30cm to 200cm thick (World Meteorological Organization, 1970). MYI is ice that has survived at least one summer melt season. Since it is older, MYI tends to grow thicker, with 3.0 to 4.0m depths being common (Maykut and Understeiner, 1971), although great variability exists. It also tends to be more topographically diverse and less saline than FYI.

Formation of First-year Sea Ice (2):

Initial ice formation occurs at the water surface where heat transfer between the cool atmosphere and warm ocean is greatest. Growth begins with the formation of small platelets and needles termed frazil (Tucker *et al.*, 1992). Since growth occurs in a brine-rich environment, several considerations are important. First, the presence of salt depresses the freezing point of water according to [2.1] (Neumann and Pierson, 1966)

$$T_f = -0.003 - 0.0527S_w - 0.00004S_w^2 \qquad [2.1]$$

where S_w is the salinity of water in parts per thousand (‰). Under typical conditions seawater freezes at -1.8°C.

The second important condition relates to water density. For seawater greater than 24.7‰ the maximum density is less than the freezing point. Therefore, continued cooling of seawater above this salinity threshold leads to a vertically unstable density distribution. Consequently, the entire convective layer, generally 10-40m (Doronin and Kheisen, 1975), must cool to the freezing point before sea ice formation begins.

Continued clumping of frazil crystals results in a conglomerate of unconsolidated crystals and seawater labeled grease ice. In the absence of wind primary formation ends when frazil coalesces into a solid, elastic ice cover termed nilas. Conversely, pancake ice forms if windy conditions prevail. Pancakes, normally 0.3 to 3.0m in diameter (Tucker *et al.*, 1992), have slightly raised edges because they adhere new frazil crystals to their edges and continually bump into one another.

Once ice covers the ocean surface any further ice growth must occur on the ocean side of the ice sheet. The growth rate of this congelation ice is governed by a temperature gradient across the ocean-sea ice-atmosphere boundary (Tucker *et al.*, 1992).

Evolution of First-year Sea Ice (2)

From a microwave radiometry perspective, evolution of the ice is mainly concerned with the incorporation and rejection of brine in the volume (Perovich and Gow, 1991; Arcone *et al.*, 1986). Initial ice salinity is governed by water salinity and the growth rate, which is highly temperature dependent. Laboratory measurements (Cox and Weeks, 1988, 1975; Weeks and Lofgren, 1967) suggest the initial salinity of ice (S_i) is related to sea water salinity (S_w) by [2.2]:

$$S_i = K_{eff} S_W \qquad [2.2]$$

where K_{eff} is the effective distribution coefficient.

As ice thickness increases over time, the average salinity generally decreases from 20‰ (during formation) to 5‰ after 2 to 4 weeks (Eide and Martin, 1975). In cold ice two separate regression equations adequately describe ice salinity as a function of ice thickness (Figure 2.3). Below 40cm, [2.3] explains 61% of the salinity variation, while [2.4] explains 88% of the salinity variation when ice is greater than 40cm thick.

$$S_1 = 14.24 - 19.39 h_1 \qquad [2.3]$$

$$S_2 = 7.88 - 1.59h_2 \qquad [2.4]$$

where S is salinity in ‰, h_1 is for ice less than or equal to 40cm and h_2 is for ice greater than 40cm.

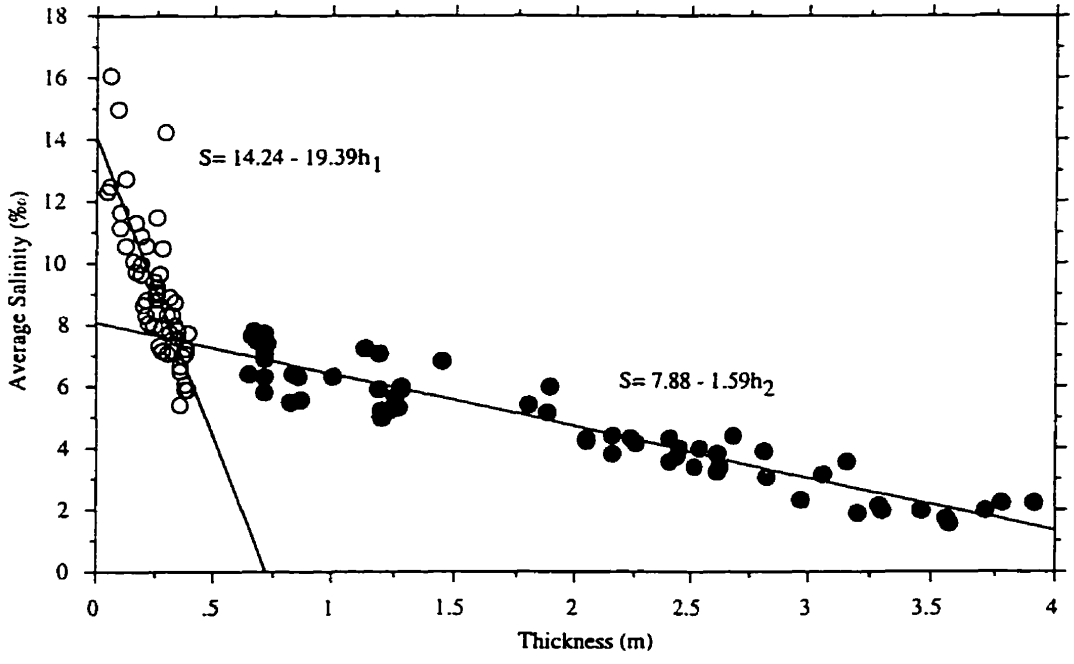

Figure 2.3 Average salinity of sea ice as a function of ice thickness for cold sea ice during the growth season. *(adapted from Cox and Weeks, 1974)*

Brine volume is a function of salinity and temperature. After formation brine begins to drain from the ice sheet. Subsequent brine content is determined by the physics of phase equilibrium (Weeks and Ackley, 1986), which essentially correlates a brine volume with a given temperature. The dominant mechanisms of brine drainage are expulsion and gravity drainage (Eide and Martin, 1975). Brine expulsion is governed by pressure differences arising from ice formation. As water freezes, it physically expands, forcing brine to be transported away through cracks in the ice

(Tucker *et al.*, 1984). The majority of the brine channels downwards, although some is forced onto the sea ice surface (Martin, 1979) and even wicked into the basal snow layers (Drinkwater and Crocker, 1988). Tucker *et al.* (1992) suggest expulsion dominates brine movement only in the upper ice layers, while Cox and Weeks (1975) show the effect of expulsion on brine transport diminishes with time. Gravity drainage dominates brine transit over much of the year (Tucker *et al.*, 1992). Over time the desalinization process leads to lower ice salinities throughout the middle of the ice volume (Figure 2.4). Salinity remains high in the upper layers because it entrapped more during formation. The bottom layers remain high because they have not lost much of the brine entrapped during ice formation and they receive a continuous supply of brine drained from above (Tucker *et al.*, 1992).

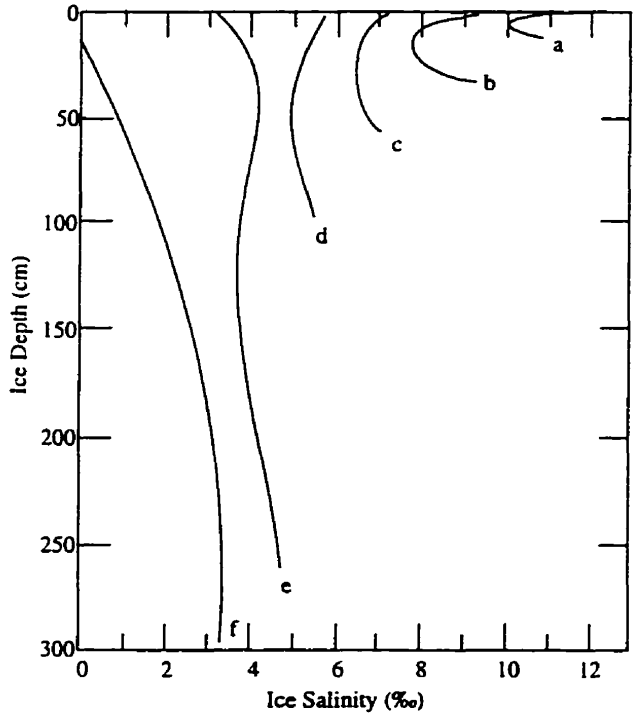

Figure 2.4 Idealized ice salinity curves for first-year ice (a-d) and multiyear ice (e,f). *(adapted from Tucker et al., 1992)*

Desalinization also leads to local variations in salinity. Several researchers have noticed significant variations in ice salinity within metres of each other, even if the structure of the ice is similar (e.g. Eicken *et al.*, 1991; Tucker *et al.*, 1984). These irregularities are likely a result of variations in the maturity of brine drainage channels (Tucker *et al.*, 1992). Where drainage channels are well established, ice salinity is decreased.

Evolution of Multiyear Ice (3)

In terms of this thesis the most important physical difference in MYI relates to its internal structure. The pattern of summer melt and winter freeze in MYI growth gives rise to a topographically diverse structure consisting of rounded hummocks and low-lying meltponds. During the summer melt season, brine drainage rapidly increases as a result of two processes. First, warming expands the brine pockets, leading to the formation of drainage channels that facilitate the brine drainage process. Second, the large influx of snowmelt from above flushes brine downwards into the ocean. As a result, salinities in the upper 50- 100cm of the ice sheet are generally 1‰, compared with 4-7‰ for FYI (Tucker *et al.*, 1992)

2.2.2 Snow (4)

Snow cover is ubiquitous over the sea ice surface in the marine cryosphere. Its presence or absence significantly affects a host of energy and mass

fluxes that control heat transfer rates and sea ice formation. The evolving snowpack also exerts an influence over biogeochemical cycles while the spring melt provides the marine cryosphere with a significant source of fresh water.

Snowfall over the marine cryosphere is dominated by a bimodal distribution pattern. A large amount of snow falls during autumn freeze up and again during the onset of spring. This is principally a result of increased storm activity during these times. The intervening polar winter is characterized by lower precipitation, primarily because little energy is in the system (Figure 2.5). As a result, snow on sea ice often contains a complex mixture of layers, each physically distinct due to their differing evolutionary histories. Snowpack conditions at any given time are a result of this history, which begins with the formation of snow in the atmosphere.

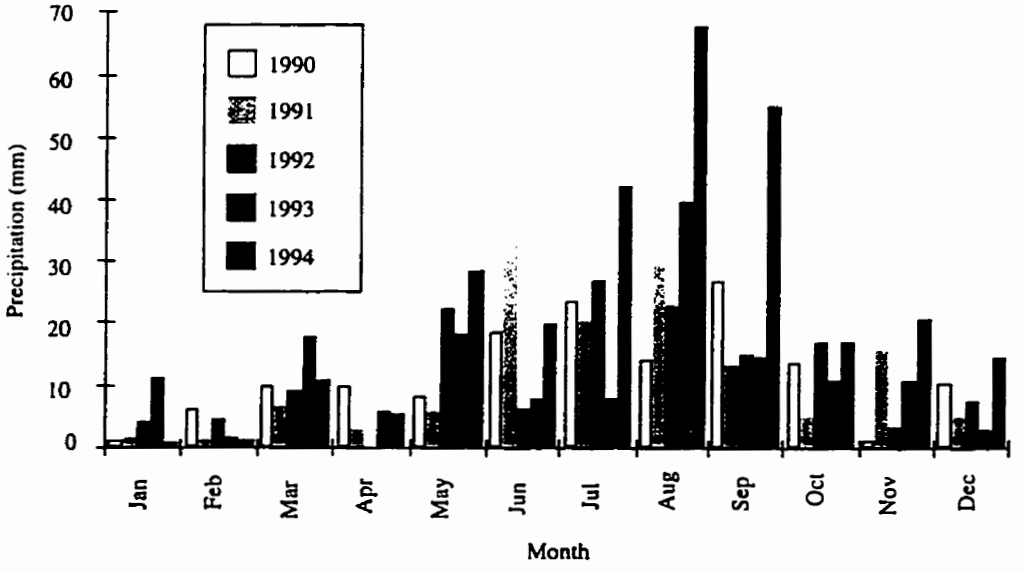

Figure 2.5 Precipitation recorded at Resolute Bay. *(courtesy Arvids Silis, personal communication)*

Formation

At approximately -5°C, ice nucleation within a cloud initiates the process of snow formation. A snowflake fuses together through interlocking the arms of ice particles and more importantly, by water vapour condensing onto the interlaced particles (Mason, 1992). In the special case where a large amount of frozen water dominates the snowflake growth process, a hard snow pellet termed graupel forms (Schemenauer *et al.*, 1981). When the snowflake reaches the ground it is termed a snowgrain.

Evolution

For SWE derivation, evolution of the snowpack is primarily concerned with understanding how snow cover variations affect microwave emission. Barber *et al.* (1995) provided statistical characterization of a seasonally evolving snow cover based on crystal geometry. In the colder regime (-20°C), only large basal (bottom of the snow cover) crystals could be separated from the rest of the snowpack. However, in the warmer part of the season (-5°C), the basal layer was distinguishable from an original snow layer with medium sized crystals and a new snow layer consisting of smaller crystals which had been deposited over the field campaign. As temperatures approached 0°C, Barber *et al.* (1995) also noticed grain sizes grew larger in the 9 to 18 cm region above the sea ice. Furthermore, growth in the new snow layers proceeded more rapidly, with grain sizes doubling in a matter of days.

Typically, evolution of the snow results in slight increases in density as well as grain size. When snow is transported by saltation the crystal's dendrites

break off due to frictional forces, causing grain compaction upon settling (Male, 1980). Solidification can also occur through vapour transfer and especially melt-freeze cycles. Barber *et al.* (1995) showed how a seasonally evolving snowpack over first-year ice increased from an initial value of 250 $kg \bullet m^{-3}$ to 375 $kg \bullet m^{-3}$. The evolutionary process is largely controlled by metamorphic action within the snowpack.

Metamorphism in Dry Snow

Upon deposition, snowgrain evolution begins with the continual process of metamorphism. Thermodynamically, the system seeks a status of free energy equilibrium. Physically, this is achieved when the snowgrain surface area to volume ratio is minimized (Langham, 1981). A temperature gradient is constructed between the top of one snowgrain and the bottom of a neighbour to facilitate the equilibrium process. An associated vapour gradient transfers water from high pressure to low pressure sections of the snowpack (in terms of temperature, from warm sections to cool sections).

When the snowpack remains dry, water vapour mass is transferred from the top of one grain to the bottom of another grain through a "hand-to-hand" process (Yoshida, 1955). Since the effective conductivity of ice is about one hundred times that of air (Colbeck, 1987), conduction through the snowgrains is likely more important than vapour transport through the air. This is especially true in cold, dense snowpacks (Fukusako, 1990). The determining factor leading to growth of highly faceted "kinetic form" grains (Figure 2.6), or more rounded "equilibrium form" grains (Figure 2.6), is the

strength of the temperature gradient (Burton *et al.*, 1951). The separation point is somewhere between 10 and 20°C•m^{-1} (Colbeck, 1986; LaChapelle and Armstrong, 1977), with equilibrium grains evolving below the threshold and kinetic grains growing above. This threshold increases with increasing density because crystal growth rates are larger with the greater separation present in low density snow (Colbeck, 1983). Yoshida (1955) experimentally determined temperature gradients of 15 to 70°C•m^{-1} grew faceted crystals, while temperature gradients of 6°C•m^{-1} formed equilibrium crystals.

In the equilibrium form of dry snow metamorphism relatively small, rounded crystals form. Generally, the dendrites begin to decompose into smaller fragments and large crystals grow at the expense of smaller crystals (Langham, 1981). Eventually larger grains form bonds through sintering (de Quervain, 1963), which increases snowpack strength.

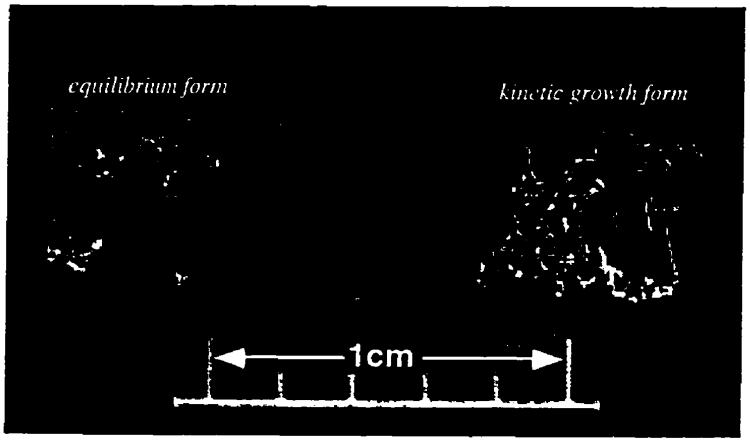

Figure 2.6 Equilibrium and kinetic growth snowgrains.

The kinetic form of dry snow metamorphism leads to large, geometrically shaped crystals. These crystals develop when a significant temperature

gradient is established and maintained for an extended period of time. Under larger gradients mass is removed from the lower portions of a snowpack, hastening the development of depth hoar crystals. These crystals are permeable, low in density and weak of strength. Akitaya (1975) has determined two distinct types of depth hoar: "solid-type", with platy or columnar shape, have sharp edges and flat surfaces. These crystals are fairly firm and may appear to be compacted fine-grained snow. Conversely, "skeleton-type" depth hoar is highly faceted with stepped or ribbed surfaces. These crystals are larger than "solid-type", but have very little shear strength. Akitaya also discovered the "solid-type" formed when temperature gradients are less than $25°C \bullet m^{-1}$ and "skeleton-type" formed when the gradient is greater than $25°C \bullet m^{-1}$.

Metamorphism in Wet Snow

Metamorphic action in wet snowpacks causes rapid alteration in the snowgrains and eventually destroys the layered character of a snowpack (Barber *et al.*, 1994). With low liquid water contents grains cannot exist individually and join to form crystal agglomerates (Colbeck, 1987). This typically occurs when bulk water contents are less than approximately 7%. This is known as the pendular regime (Figure 2.7). Densities in the grain clusters may be upwards of 600 $kg \bullet m^{-3}$, but overall snowpack density is far less due to water pockets and continuous air spaces running through the snow pack (Colbeck, 1986). The exact nature of crystal growth in low liquid water content snow is a matter of some uncertainty, since measurement is difficult. However, it appears thermal diffusion plays a more important role, while conduction plays a less important role (Colbeck, 1987). Liquid

water between the snowgrains provides channels whereby thermal diffusion could be accentuated.

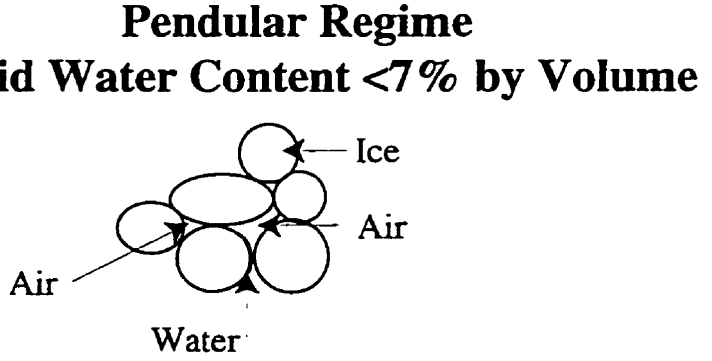

Figure 2.7 Sketch of snowgrains, air and water distributions in the pendular regime. *(adapted from Garrity, 1993)*

In the funicular regime liquid water contents are greater than 7% (Figure 2.8). Surface tension is no longer sufficient to keep snowgrains bonded. As a result, they normally form larger, more spherical shapes (Colbeck, 1987). Air spaces become discrete in nature, while water channels may run continuously through the snowpack. When the snowpack becomes saturated with water crystal growth leads to individual spherical particles. The resulting slushy mixture is weak in strength (Colbeck, 1987). Since saturated snow conditions were not encountered in C-ICE 96, they merit no further attention.

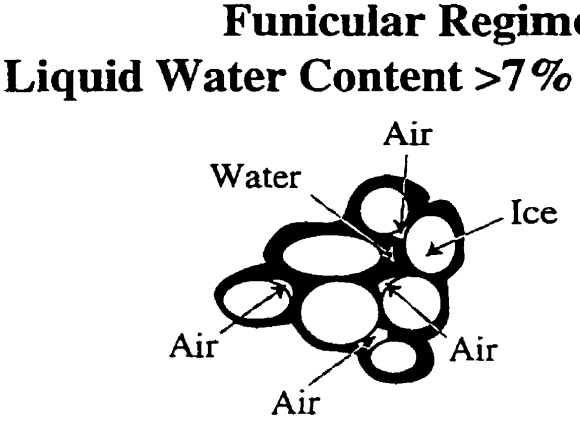

Figure 2.8 Sketch of snowgrains, air and water distributions in the funicular regime. *(adapted from Garrity, 1993)*

It can be appreciated that the evolving snow-sea ice mixture is complex. From initial formation, both snow and sea ice undergo an extensive pattern of metamorphism. At any particular time energy and mass transfer in the marine cryosphere is linked to the physical state of the snow-sea ice mass. By governing these energy exchanges over the seasonal evolution, the snow covered sea ice volume controls many of the key physical and ecological aspects of the marine cryosphere. The next section will examine some of the processes intimately related to an evolving snow covered sea ice volume.

2.3 The Role of Sea Ice and Snow in Marine Cryospheric Processes

The marine cryosphere is dominated by the seasonal evolution of a snow covered sea ice volume, which acts to (a) increase the surface albedo and (b) regulate heat flows across the marine cryosphere. The snow cover is particularly important in controlling energy and mass transfer owing to its extremely high albedo and low thermal conductivity. As a result, the

presence or absence of snow dictates light transmission and influences ecological life in the marine cryosphere. Furthermore, the low thermal conductivity of snow governs the sea ice accretion and decay process, which in turn affects brine fluxes and the thermohaline circulation. The following section will outline some of the relevant cryospheric responses governed by a snow covered sea ice volume and how changes in snow cover could affect them.

Since this thesis is concerned with snow water equivalence monitoring, snowpack effects will be emphasized, with a smaller focus on sea ice.

2.3.1 Influence of Snow Optical Properties

The optical snow properties drive metamorphism and energy fluxes within the snowpack (Mellor, 1965). For instance, the shortwave surface energy balance is largely controlled by the albedo of snow. Shortwave radiation refers to energy emitted from the Sun (Ahrens, 1991) and it exhibits a marked seasonality in the Arctic. Irradiance at the top of the atmosphere can be over 800 $W \bullet m^2$ at solar noon during the summer, but drops to zero during the periods of polar darkness (Barber, 1993; Oke, 1987).

When shortwave energy is incident upon the marine cryosphere, it will be reflected, transmitted, or absorbed. The high albedo of snow is the primary factor restricting shortwave energy exchanges between the ocean and the atmosphere because a large percentage of insolation is reflected before it reaches the water. Albedo, α, is defined as the portion of downwelling radiation which is reflected from a surface [2.5].

$$\alpha = \frac{K\uparrow}{K\downarrow} \qquad [2.5]$$

where $K\uparrow$ is upwelling shortwave radiation and $K\downarrow$ is downwelling shortwave radiation.

Seasonal albedos in the Arctic are largely dependent on the nature of the snowpack, with larger grains and increasing density both reducing the albedo (Table 2.1). Evolution of the snowpack tends to lower albedo owing to increased water in liquid phase, increased grain size and the transition of snow grains to the "equilibrium form". The net effect is absorbed energy over a snow covered surface may be an order of magnitude lower than that of an open water surface (Barber, 1993; Grenfell and Perovich, 1984; Mellor, 1977). Thus, sea ice albedo is a critical component in determining the energy balance of the marine cryosphere.

Table 2.1 Typical albedo values in the marine cryosphere.

Ocean State	Snow Cover State	Albedo
FYI	Dry	0.90
FYI	Water saturated	0.70
FYI	Meltponds	0.60
Thin Ice (<30cm)	None	0.40
FYI	None	0.20
Water	N/A	0.03-0.10

adapted from Langleben (1969); Grenfell (1979); Barber (1993)

Shortwave energy not reflected must be transmitted or absorbed, in accord with the conservation of energy law. Although transmission can be

approximated by Beers law [2.6], Barber (1993) has shown transmission through snow is almost double the predicted value at the lower (0.5 μm) portion of shortwave spectrum. Mellor (1965) conducted a series of experiments on the absorption properties of snow in the visible portion of the EM spectrum. He found absorption increased with increased grain size and density and was also frequency dependent, with increased absorption at higher wavelengths. Ledley (1991) modelled the effect of changing snow conditions on the shortwave energy balance. With no snow cover, mean absorbed shortwave energy at 75°N was 49.5 $W \bullet m^{-2}$. With the full snow model (28cm), this value dropped to 35.3 $W \bullet m^{-2}$.

$$K\downarrow_z = K\downarrow_s e^{-az} \qquad [2.6]$$

where $K\downarrow_z$ is the shortwave radiation at depth 'z' in the snow, $K\downarrow_s$ is shortwave radiation at the snow surface and a is the extinction coefficient. The extinction coefficient is a function of snow depth, density and grain size (Barber, 1993; Oke, 1987; Mellor, 1965).

Several lifeforms, such as the epontic (sub-ice) communities, are governed by the optical properties of snow (Welch and Bergmann, 1989). These groups utilize photosynthetically active radiation (PAR; 0.4 to 0.7 μm) transmitted through the snowpack to grow. Welch *et al.* (1991) illustrated a negative exponential relationship between snow depth and underlying chlorophyll production (Figure 2.9). As a result, slight changes in snow cover will be amplified substantially in the algae life cycle.

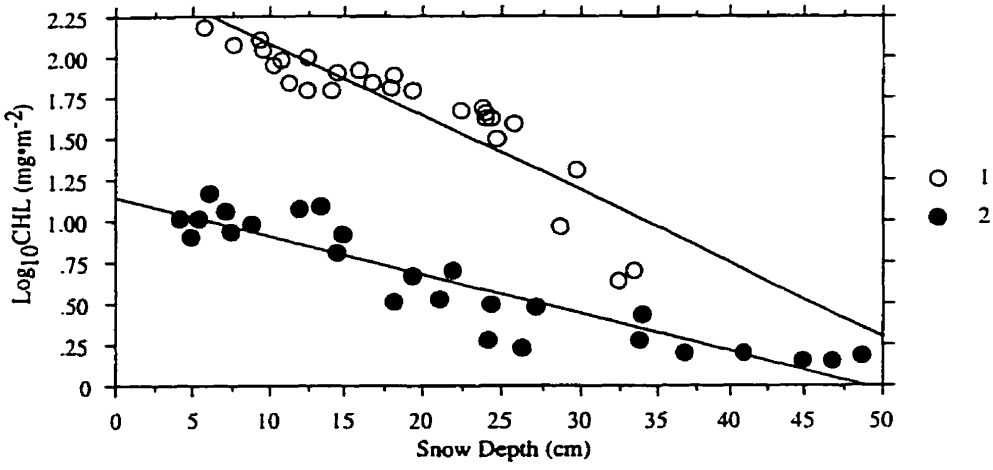

Figure 2.9 Snow-chlorophyll relationships in the Arctic. Station 1 R^2= 0.84; Station 2 R^2= 0.86. *(adapted from Welch et al., 1991)*

Higher levels of the trophic system are also governed by snow cover amount. Ringed seals (*Phoca hispida*) utilize the snow cover on sea ice for protection from predation and the harsh Arctic winter (Smith and Stirling, 1977). Jewett and Feder (1980) hypothesize the disappearance of bottom feeding fish populations along coastal shelves is attributable to increased water temperatures resulting from lack of snow.

2.3.2 Influence of Snow Physical Properties

Sea ice growth and decay is largely a function of the overlying snow cover, owing to the low thermal conductivity of snow, λ_{se}. Snow conductivity is highly dependent upon snow density with some dependence upon temperature as well. As density increases, the number and size of intergranular contacts increase, resulting in higher values of thermal conductivity (Fukusako, 1990). Conversely, as temperature increases the thermal conductivity decreases (Sakazume and Seki, 1978). Langham (1981) attributes the negative relationship to vapour diffusion along an

associated temperature gradient. The accompanying energy loss through latent heat of evaporation would affect λ_{se}. The net effect is that λ_{se} is approximately 8 to 10 times smaller than the thermal conductivity of sea ice (Kotlyakov and Grosswald, 1990). Since ice growth is a function of heat loss to the atmosphere (Maykut, 1986), lower heat transfer rates will reduce sea ice thickness. Thicker and less dense snow covers increase the insulating properties of snow, further restricting energy transfer across the marine cryosphere.

Both modelling (Ledley, 1991) and empirical studies (Brown and Cote, 1992; Nakawo and Sinha, 1981) have demonstrated increased snow cover leads to decreased ice thickness. Ledley (1991) used a coupled energy balance climate-thermodynamics sea ice (CCSI) model to study the effect of snow and sea ice on climate. After running the model for 20 years, the no snow scenario resulted in a sea ice thickness of 2.85m, while the full snow model, with an 80 cm depth, concluded with a 2.76m ice depth. Brown and Cote (1992) monitored sea ice thickness in relation to snow cover at 4 sites across the Canadian Arctic Archipelago. In all cases an increased snow cover lead to decreased ice thickness and vice versa (Table 2.2).

Table 2.2 Linear trend analysis of snow depth and ice thickness.

Site	Period	Ice ($cm \cdot yr^{-1}$)	Snow ($cm \cdot yr^{-1}$)
Alert Inlet	1956-87	-0.71	+0.43*
Alert (Dumbell Lake)	1957-87	-0.90*	+0.30
Eureka	1952-89	-0.00	+0.04
Mould Bay	1954-89	-0.29	+0.20
Resolute	1952-89	+0.99*	-0.33*

* indicate statistical significance at α=0.05 *(adapted from Brown and Cote, 1992)*

During spring the low thermal conductivity of snow limits heat transfer from the relatively warm atmosphere to the relatively cool ocean (opposite to the fall scenario). Furthermore, the high albedo mentioned previously reflects much of the incoming solar radiation, further slowing melt. In addition, the snowpack acts as a significant heat sink owing to its large latent heat of fusion (Barry *et al.*, 1995). Combined, these physical snow properties reduce the rate of ice melt in the spring.

By regulating sea ice growth and decay snow contributes to determining the brine flux of the Arctic Ocean. Cold, dense water expelled during ice formation sinks from the ocean surface and is replaced by warmer, less dense water from the surrounding seas (Aagaard and Carmack, 1989). This perpetuates a global oceanic conveyor belt, often termed thermohaline circulation, that moves cold water to the equator and warm water to the poles. Aagaard and Carmack (1989) suggest the "Great Salinity Anomaly" of the late 1960s-1970s (Dickson *et al.*, 1988) may be an example of past climatic eras in which the oceanic conveyor belt was suppressed by large influxes of fresh water. Increased snow melt could dilute the brine rich waters such that they lack the density to sink and maintain the conveyor belt. Paleoclimatic analysis by Broeker and Peng (1989) and modelled results from Bryan (1986) and Manabe and Stouffer (1988) imply the non-circulating conveyor belt system is also a stable ocean-atmosphere regime. Therefore, increased snow cover could affect the current dominance of the deep water conveyor belt circulation pattern in the future.

This section has shown the physical snow properties exert substantial influence over conditions in the marine cryosphere. The nature of the snowpack contributes to defining everything from sea ice growth and ablation through to the development of life in the marine cryosphere. With an indirect influence on thermohaline circulation, the snow also affects climate on a global basis. It stands to reason that changes in the physical make-up of the snow would alter the nature of its interaction with the marine cryosphere. As a result, conditions in this region would likely be altered. The following section provides some evidence that conditions in the marine cryosphere are already changing.

2.4 Evidence for Change in the Marine Cryosphere

Nansen (1902) was one of the first researchers to theorize changes in the physical Arctic system could affect climate. Although these claims have yet to be proven conclusively, a growing body of literature points to the fact that physical parameters and temperature in marine cryosphere are changing. This section examines that theory, specifically focusing on air temperature and sea ice extent.

One of the major reasons the marine cryosphere is considered susceptible to climate change is due to the sea ice-albedo feedback mechanism (Rind *et al.*, 1995). As temperatures increase, the snow and sea ice volume will likely melt, reducing the albedo. With lower albedos, more energy will be absorbed, 'feeding back' into the original warming cycle.

Chapman and Walsh (1993) have collected satellite based temperature measurements confirming a rise in temperature over the Arctic (Figure 2.10 and 2.11). Although winter temperature anomalies are higher, correlation analysis found a statistically significant decrease in ice extent only in summer. Others have noted a similar warming trend in ocean water (Carmack *et al.*, 1995; Mikhalevsky *et al.*, 1995; Aagaard and Carmack, 1994) but have not correlated it to ice extent.

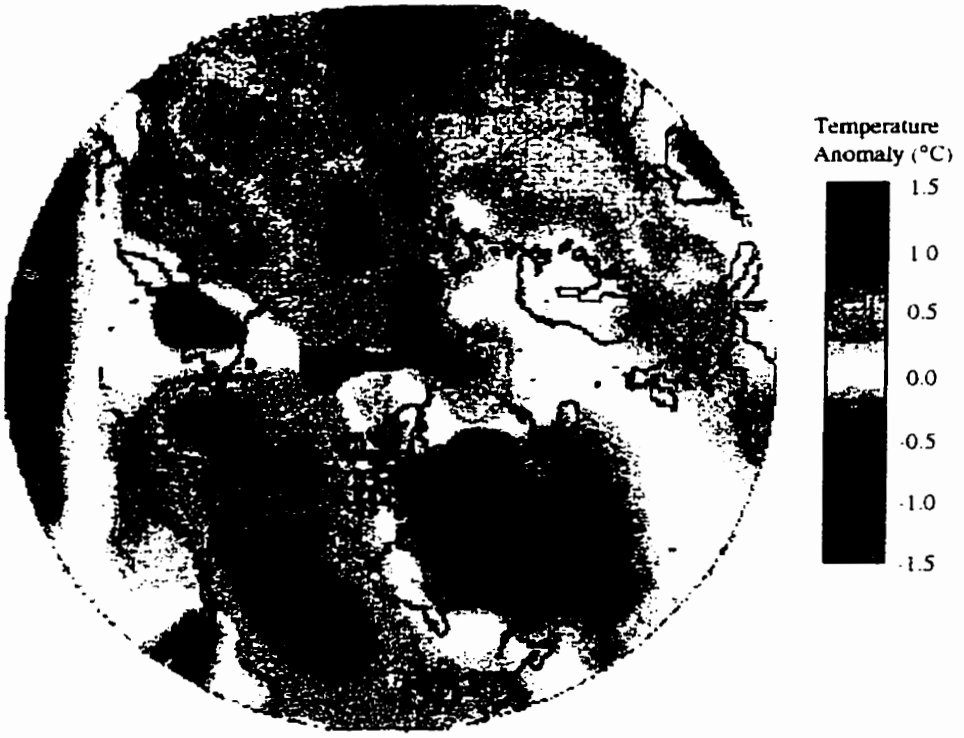

Figure 2.10 Observed trends of Arctic winter mean temperatures from 1961-1990 *(adapted from Chapman and Walsh, 1993)*

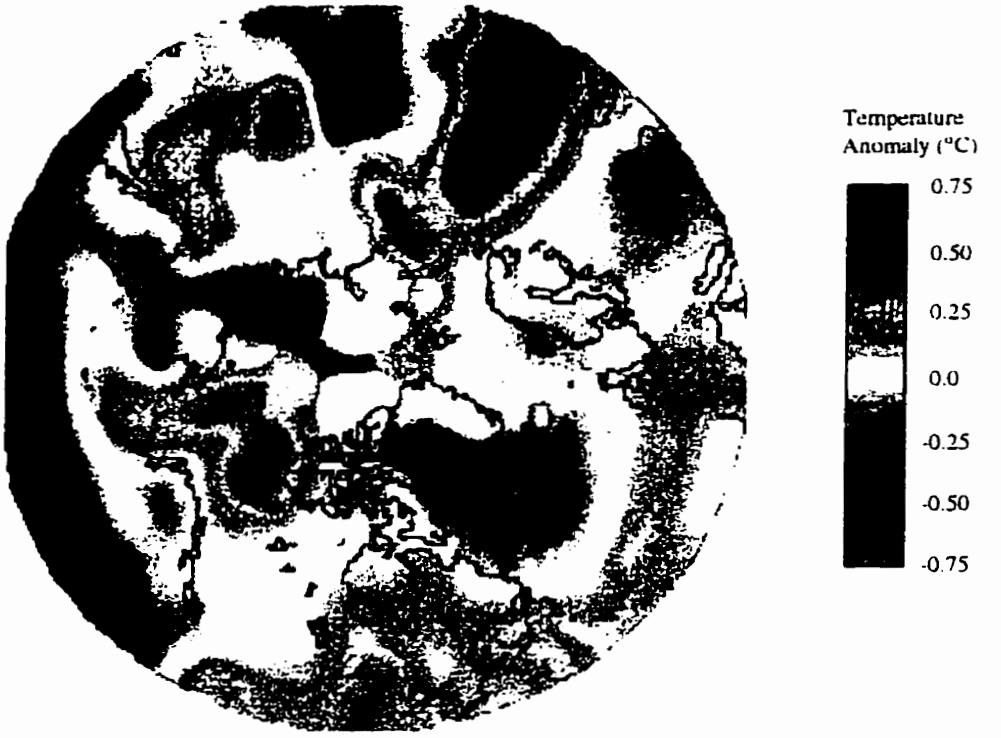

Figure 2.11 Observed trends of Arctic summer mean temperatures from 1961-1990. The warming trend is not as apparent. *(adapted from Chapman and Walsh, 1993)*

Gloerson and Campbell (1991) reported a statistically significant decrease in sea ice extent was observed in the Scanning Multichannel Microwave Radiometer (SMMR) data (Table 2.3). Johannessen *et al.* (1995) extended the time series to 1994 with the SSM/I sensor. Their -0.54×10^6 km^2yr^{-1} decrease in ice extent, statistically valid at a p-value < 0.05, is significantly greater than the -0.0315×10^6 km^2yr^{-1} decrease observed by Gloerson and Campbell. Unfortunately, neither study associated this with air or ocean temperatures.

Table 2.3 Trends in Arctic sea ice covers, 1978-1994.

Variable	Slope ($10^6 km^2 yr^{-1}$)	Standard Deviation ($10^6 km^2 yr^{-1}$)	%Change per decade	p-value
Sea Ice Extent				
1978-1987	-0.032	0.008	-2.5	<0.05
1987-1994	-0.054	0.017	-4.3	<0.05
Sea Ice Area				
1978-1987	-0.030	0.009	-2.8	<0.05
1987-1994	-0.049	0.016	-4.5	<0.05

Data from 1978-1987 is from the SMMR sensor and those for 1987-1994 are from the SSM/I sensor. *(adapted from Johannessen et al., 1995; Gloerson and Campbell, 1991)*

A compilation of modelling studies predicts the observed rise in temperature will continue to increase with a CO_2 doubling (Figure 2.12). These models, termed general circulation models (GCMs), can be used to predict future changes in the climate over the marine cryosphere. Typically, they segment the Earth into a series of grid cells. In each cell they use numerical equations to solve for conservation of mass, energy and momentum both within a grid cell and between grid cells (Henderson-Sellers and Robinson, 1987). They also consider physical processes such as the sea ice-albedo feedback mechanism. However, caution must be taken in interpreting results from these models, as even the most advanced models are relatively coarse and often treat the physical processes in a highly simplified manner. For instance, a comparison of the snow-climate feedback mechanism produced by 17 GCM models showed very different results. Some models classified this as a weak negative feedback, while others classified it as a strong positive feedback (Cess *et al.*, 1991).

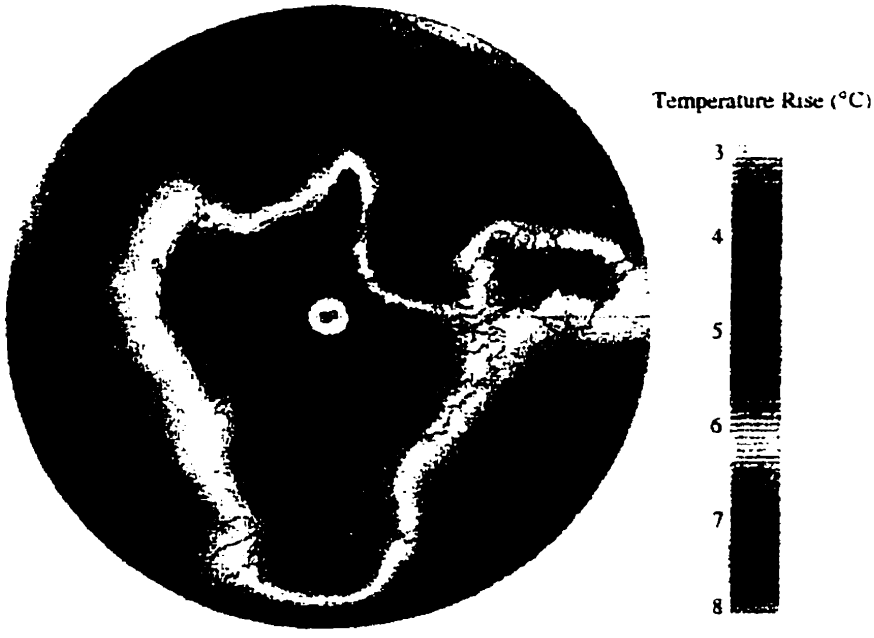

Figure 2.12 Composite greenhouse warming projections as predicted by seven Global Climate Models is presented as the difference between current conditions and those under doubled CO_2. (*adapted from http://www.circles.org/cdroms/CIESIN/HTMLAOTG/5ArcRole/E3Scen.htm*)

The modelling studies associate substantial alterations in precipitation patterns (Figure 2.13) with increasing temperature. With increased snowfall many of the processes controlled by the snow cover would change. For example, an increase in snow cover would increase the albedo of the marine cryosphere, which may delay ice melt in the summer. Conversely, the thicker snowpack would also prevent the ice from growing thicker in the fall. The thinner sea ice may then melt sooner, counterbalancing the higher albedo.

In the context of this thesis, the predicted precipitation change is one of the most critical results presented in this chapter. It provides clear impetus that improved methods of monitoring the snow cover are needed.

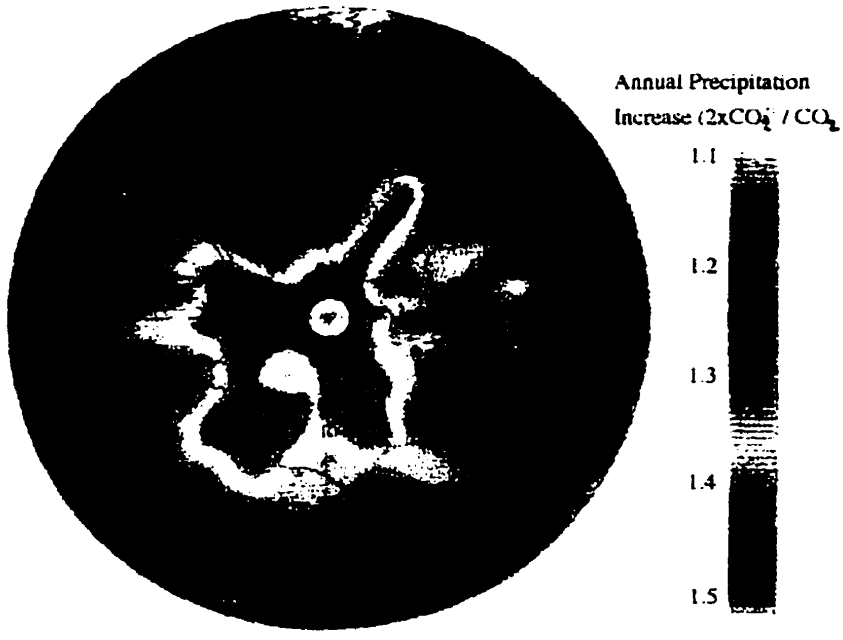

Figure 2.13 Composite of greenhouse precipitation projections as predicted by seven Global Climate Models is presented as the ratio between a doubled CO_2 scenario and current conditions. (*adapted from http://www.circles.org/cdroms/CIESIN/HTMLAOTG/5ArcRole/E3Scen.htm*)

2.5 Conclusions

The marine cryosphere is characterized by the dynamic properties of a snow covered sea ice volume. From initial formation, these properties are continually evolving and altering the environment around them. In particular, energy fluxes are controlled by the high albedo of snow, while physical processes are intimately linked to the snow's low thermal conductivity. Small perturbations in the physical properties of a snow cover may bring about large changes in local climate and ecology. If these snowpack changes altered the thermohaline component of ocean circulation, the global climate could be affected. Although few studies exist to document interannual variability in

the snowpack, several works point out the air temperature in the Arctic has warmed in the past thirty years. Furthermore, significant decreases in sea ice extent have also been noted. On the basis of current general circulation models, it seems likely this warming will continue, with an associated increase in precipitation. These models point out the need to find better methods to characterize snow conditions across the entire marine cryosphere. The use of microwave radiometry for SWE retrievals is one such method and the next chapter outlines the principles behind using microwave radiometry for SWE derivation.

CHAPTER 3 - Background

3.1 Introduction

Improved characterization of the snowpack is necessary to understand climatic conditions and trends (Barry *et al.*, 1995). The large spatial scales, hostile environmental conditions and relatively sparse in situ observational networks suggest remote sensing is a more effective measurement technique to pursue. Microwave sensors, with all-weather, all-light capabilities, offer greater flexibility in monitoring the cryospheric snow cover, since cloud and darkness often prevail in this region.

Although several indices of snow cover amount could be monitored (for instance snow depth), SWE is the best estimator because it accounts for changes in snow density as well as depth. On the basis of measuring snow depth alone, a one metre thick, 400 $kg \bullet m^{-3}$ snowpack would appear significantly different from a two metre thick, 200 $kg \bullet m^{-3}$. However, this

difference could be chiefly a product of different evolutionary histories. If the 200 $kg \cdot m^{-3}$ snowpack is dominated by new snowfall, it will soon increase in density (Barber, 1993) and begin to settle. Conversely, SWE can estimate snow amount without regard to the evolutionary pattern of the snow, as the two situations described above would yield the same SWE value. Furthermore, the passive microwave signature is intimately linked with snow water equivalence (Figure 3.1), at least over terrestrial surfaces (Chang *et al.*, 1987). Several researchers have successfully extracted SWE over terrestrial surfaces, ranging from the Canadian prairies (Goodison *et al.*, 1990), to mountain basins (Chang *et al.*, 1991) and forested land (Hall *et al.*, 1982).

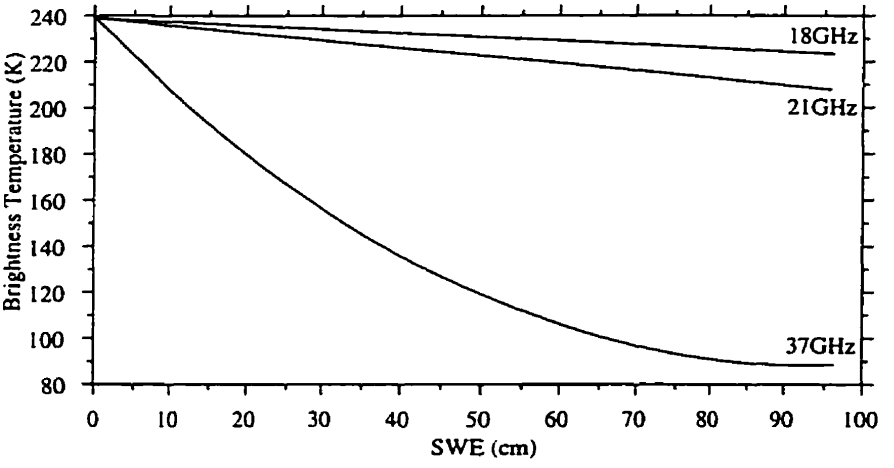

Figure 3.1 Calculated brightness temperature as a function of snow water equivalence. Calculations are based on horizontal polarization and a 50° incidence angle. *(adapted from Chang et al., 1987)*

In what follows, the interaction of microwave energy and the physical properties (covered in section 2.2) will be discussed. Both sea ice, where microwave emission originates from and the snow, where attenuation occurs, will be covered here. Finally, historical use of microwave

radiometry in the marine cryosphere is detailed as a precedent for using passive microwaves in this work.

3.2 Microwave Interaction Theory

Microwave energy occupies frequencies from 1GHz to 300GHz in the electromagnetic spectrum. Within this range, passive microwave measurements record emission from a target in selected "atmospheric windows" (Figure 3.2) where attenuation is minimized. Common passive microwave frequencies are 10GHz, 19GHz, 21GHz, 37GHz, 85GHz and 94GHz (Carsey, 1992).

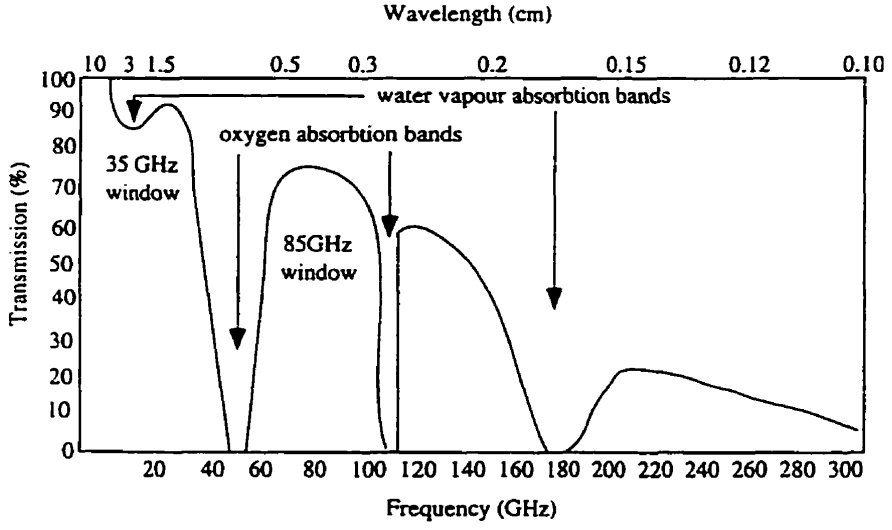

Figure 3.2 Atmospheric windows facilitating microwave remote sensing. *(adapted from Ulaby et al., 1986)*

Over the marine cryosphere microwave emission is a function of ice and snow physical properties. Sea ice is known to be the major source of microwave emission in dry snow covers (Eppler *et al.*, 1992). However, FYI

and MYI have strikingly different emission properties owing to their internal structures. Brine drainage during the warm summer creates a porous structure in MYI which is an excellent volume scattering source (Grenfell, 1992). This accounts for the decreased emission noted in MYI. Furthermore, Eppler *et al.* (1992) state variability in the physical properties of multiyear ice leads to much larger variance in emission as compared with FYI. Interest in the snow relates to its role as the dominant medium of microwave attenuation in microwave emission from sea ice (Eppler *et al.*, 1992). Both Lohanick (1993) and Lohanick and Grenfell (1986) have observed increasing grain sizes lowered brightness temperatures (Table 3.1). Table 3.1 also points out increases in SWE lowers emission, while water in liquid phase increases emission. By increasing the volume's emission, liquid water complicates the SWE retrieval process.

Table 3.1 Response of Microwave Emission With Various Snow Geophysical Properties

Geophysical Property	Microwave Emission Response
Snow Water Equivalence	Decreases as SWE increases
Grain Size	Decreases with increasing grain size
Liquid Water Content	Increases rapidly with increasing water in liquid phase

(adapted from Hallikainen and Jolma, 1986)

Although emission is a function of the snow covered sea ice volume's physical temperature, the volume emits only a fraction of the energy a perfect emitter would radiate. This fraction is described by the emissivity. The signature recorded by a microwave radiometer, expressed as a brightness temperature (T_B), is therefore a function of temperature and emissivity [3.1]:

$$T_B(f,\theta_i) = eT_{si} \qquad [3.1]$$

where f is frequency, θ_i is the incidence angle, e is emissivity ($0<e<1$), T_{si} is the physical temperature of the snow-ice combination in Kelvin.

In the context of microwave radiometry, the average emissivity is a function of frequency, polarization, incidence angle, physical composition of the sea ice (i.e. ice type) and spatial pattern in the field of view (Ulaby *et al.*, 1986). With respect to a particular frequency and polarization, variations in T_B are primarily due to variations in emissivity and secondarily to variations in the physical temperature (Steffen *et al.*, 1992). In FYI, Grenfell *et al.* (1988) have shown FYI has a fairly stable emissivity once it thickens to 10mm (Figure 3.3).

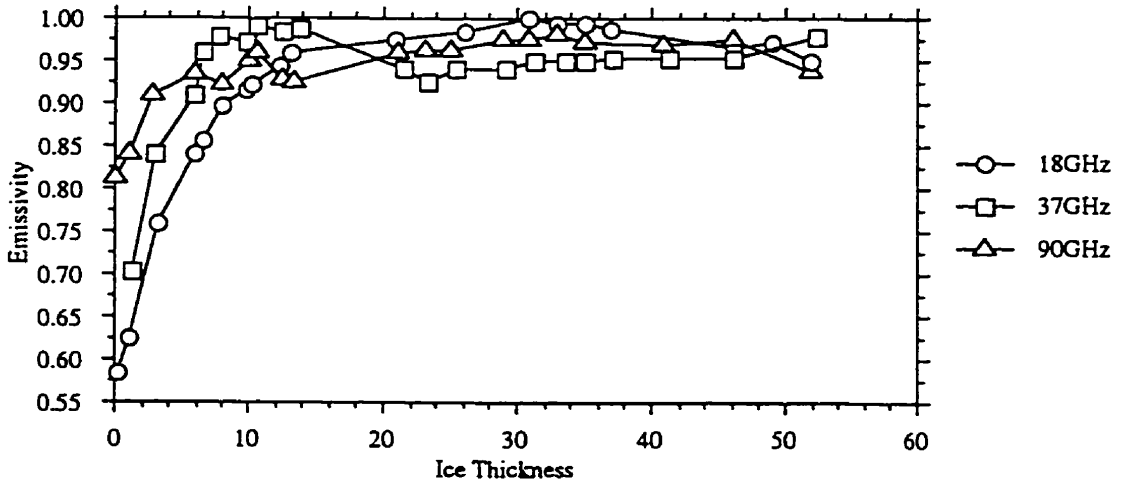

Figure 3.3 Emissivity as a function of ice thickness. *(adapted from Grenfell et al., 1988)*

In defining a relationship between SWE and T_B, we take advantage of the fact that emissivity decreases with increases in the scattering potential of an

overlying snow cover (Haykin *et al*, 1994). The nature of the scattering can be described by the principles of volumetric scattering.

Scattering in Snow Covered First-year Sea Ice

The partial fractions of ice, air, brine and liquid water create a complex medium in which emitted energy is not simply reflected or redirected, but rather scattered in a variety of directions. With respect to frequency and polarization, scattering is dependent on the physical structure and electrical properties of the snow covered-sea ice volume (Carsey, 1992). In dry snowpacks volume scattering dominates at frequencies above 20GHz (Figure 3.4) (Hallikainen, 1986). Scattering strength is proportional to the dielectric discontinuities within the volume and density of the embedded particles. The angular scattering pattern is governed by roughness of the discontinuity surface, dielectric properties of the volume and geometric size of the scattering particles relative to the impinging microwave energy (Ulaby *et al.*, 1986). A good estimator for volume scattering within a snowpack is provided by Marshall and Gunn (1952). It is applicable with frequencies over 30GHz and snow grain particles less than 1.5mm in diameter [3.2].

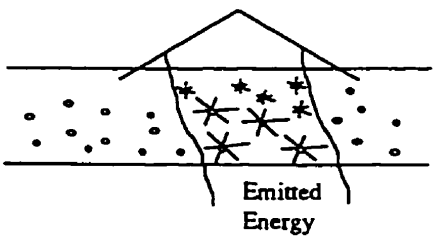

Figure 3.4 Volume scattering phenomena. *(adapted from Ulaby et al., 1986)*

$$\sigma_{bs} = 16\pi^5 \frac{r_i}{\lambda_o} \qquad [3.2]$$

where σ_{bs} is the magnitude of backscatter in dB, r_i is the size of snowgrains and λ_o is the wavelength of free space.

Sea Ice and Snow Dielectrics

The complex dielectric constant [3.3] is used to describe the scattering properties of a snow covered sea ice volume. Permittivity, ε', characterizes the relative permittivity with respect to free space (ε_{air}=1), while the dielectric loss, ε", defines the electromagnetic loss of the material. Permittivity describes what happens to EM energy when it impinges upon a boundary. Loss describes the electromagnetic loss once energy has penetrated into the material. The total electromagnetic loss (Hallikainen and Winebrenner, 1992) is a combination of absorption loss (transformation of energy into another form) and scattering loss (energy deflected to travel in directions other than incident).

$$\varepsilon^* = \varepsilon' + j\varepsilon'' \qquad [3.3]$$

Where $j = \sqrt{-1}$

The complex dielectric constant of sea ice, ε_{si}, is mainly a function of the partial fractions of ice, air and brine within the scattering volume, relative to the incidence angle (Ulaby *et al.*, 1986). Modelling the permittivity of sea ice, ε'_{si}, has focused on coupling brine volume with the permittivity of sea ice, since brine permittivity is much higher than ice or air permittivity (Mätzler and Wegmuller, 1987; Cumming 1952). Several researchers have provided models (e.g. Arcone *et al.*, 1986), with results from Hoekstra and Cappillino (1971) (Figure 3.5) shown below [3.4].

$$\varepsilon'_{si} \equiv \frac{\varepsilon_i}{1-3V_b} \qquad [3.4]$$

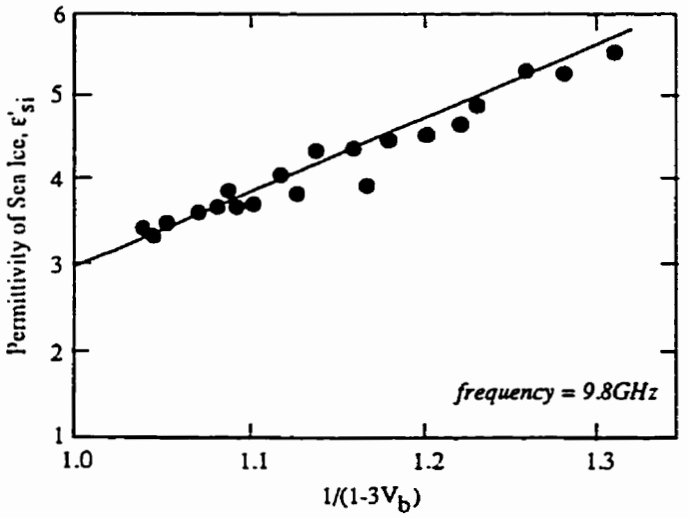

Figure 3.5 Measured permittivity of artificially grown sea ice as a function of brine volume fraction. *(adapted from Hoekstra and Cappillino, 1971)*

Using the same theory employed in calculating [3.4], Hoekstra and Cappillino (1971) provide [3.5] as an approximation for the dielectric loss of sea ice.

$$\varepsilon''_{si} = V_b \varepsilon''_b \qquad [3.5]$$

The complex dielectric constant of snow, ε_S, is mainly a function of the partial fractions of ice, water, brine and air within the scattering volume, relative to the incidence angle (Ulaby *et al.*, 1986). In the upper portion of a dry snowpack, permittivity can be described solely by the relative portion of ice and air. Since both parameters are consistent over the microwave portion of the EM spectrum, a simple equation [2.6] of the type reported by Hallikainen *et al.* (1986) accurately describes ε'_{ds} (Figure 3.6). Dielectric loss in a dry snowpack can be computed based on the models supplied by Tinga *et al.* (1973) [3.7].

$$\begin{aligned} \varepsilon'_{ds} &= 0.51 + 2.88\rho_{ds}, \rho_{ds} > 500 kg \bullet m^{-3} \\ \varepsilon'_{ds} &= 1 + 1.9\rho_{ds}, \rho_{ds} \leq 500 kg \bullet m^{-3} \end{aligned} \qquad [3.6]$$

where ρ_{ds} is the density of dry snow in $g \bullet cm^{-3}$.

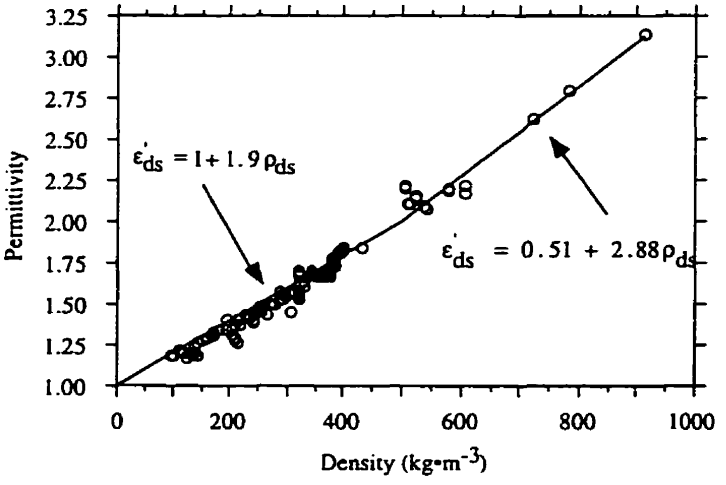

Figure 3.6 Permittivity as a function of density in dry snow. Experimental data provided by Nyfors (1983), Hallikainen (1977), Cumming (1952) and Hallikainen *et al.* (1986). *(adapted from Hallikainen et al., 1986)*

$$\varepsilon''_{ds} = \varepsilon''_i \left\{ \frac{9V_i}{\left[(2+V_i)+\varepsilon''_i(1-V_i)\right]^2} \right\} \qquad [3.7]$$

where ε''_i is the dielectric loss of ice and V_i equals [2.12a]

$$V_i = \frac{\rho_{ds}}{\rho_i} \qquad [3.7a]$$

and $\rho_i = 0.916$, the density of ice in $g \cdot cm^{-3}$.

Since the permittivity of water is roughly 40 times that of dry snow (Tiuri *et al.*, 1984), even small amounts of water in liquid phase will strongly influence wet snow dielectrics. The modified Debye-like model takes advantage of this fact in estimating the permittivity, ε'_{ws} [3.8] and loss, ε''_{ws} [3.9] of wet snow.

$$\varepsilon'_{ws} = A + \frac{Bw_v^x}{1+\left(\frac{f}{f_o}\right)^2} \qquad [3.8]$$

$$\varepsilon''_{ws} = \frac{C\left(\frac{f}{f_o}\right)w_v^x}{1+\left(\frac{f}{f_o}\right)^2} \qquad [3.9]$$

w_v is the percent water volume in liquid phase, f is the frequency and f_o is the relaxation frequency of water, 9.07 GHz in the microwave region (Hallikainen and Winebrenner, 1992). A, B, C and x are defined by fitting the model to measured data. Full details are presented in Hallikainen *et al.* (1986).

Based on Debye models, Tiuri *et al.* (1984) provide descriptions of ε'_{ws} (Figure 3.7) and ε''_{ws} (Figure 3.8) from 0 to 40GHz.

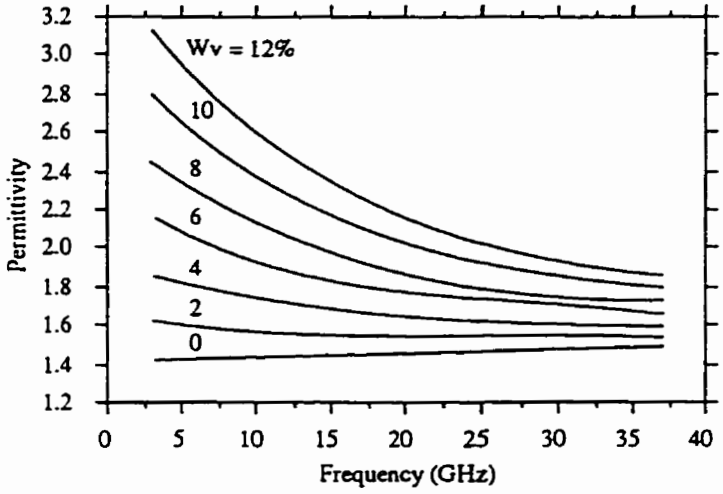

Figure 3.7 Modified Debye-like model permittivity of snow as a function of frequency and water in liquid phase. *(adapted from Tiuri et al., 1984)*

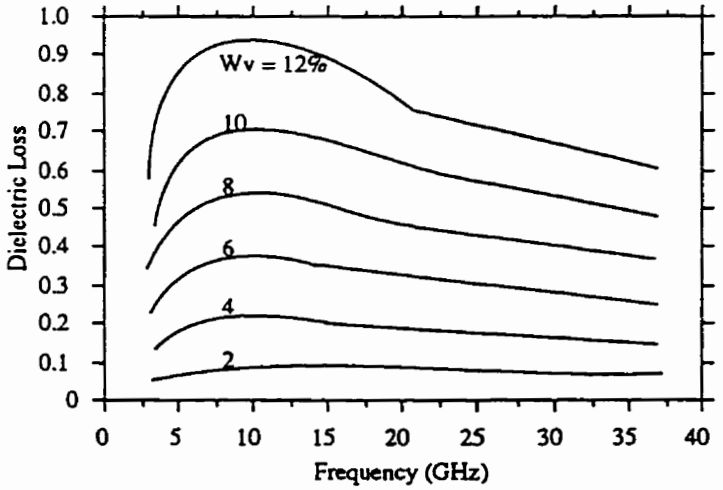

Figure 3.8 Modified Debye-like model loss of snow as a function of frequency and water in liquid phase. *(adapted from Tiuri et al., 1984)*

In the lower portion of a dry snowpack brine content dominates the microwave response. Barber (1993) used mixture models based on the work of

Drinkwater and Crocker (1988) to describe the dielectric properties under these conditions. The complex mixture models predict an overall dielectric property based on the dielectrics of the constituent parts, namely ice, air and brine. When water in liquid phase appears, the models presented in [3.8] and [3.9] are appropriate.

3.2.1 Experimental Results

Dielectric values used in this thesis are modelled results based on physical properties. This is mainly due to the difficulty in acquiring experimental dielectric values. However, it is important to illustrate the findings of several authors who have empirically determined dielectric properties, as empirical measurements are important to develop the models.

Sea Ice Dielectrics

The vast majority of empirical studies on sea ice dielectrics have occurred over first-year ice surfaces or artificial ice, with very little data available for multiyear ice (Hallikainen and Winebrenner, 1992). Vant (1976) and Hallikainen (1983) examined permittivity changes at 1GHz with respect to temperature and salinity (Figure 3.9). They noted increases in permittivity and loss with increases in salinity and rapid increases as temperatures approached 0°C.

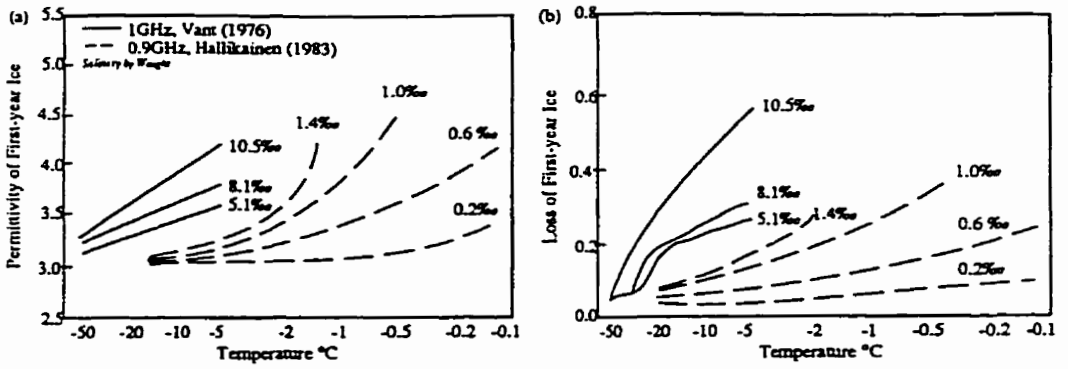

Figure 3.9 Experimental values obtained by various authors for sea ice at 1GHz: (a) permittivity, (b) loss. *(adapted from Hallikainen and Winebrenner, 1992)*

From 9 to 16GHz, several researchers have measured both permittivity and loss of real and artificially created sea ice (Figure 3.10). In all cases, researchers noticed rapid increases in permittivity as the temperature approached 0°C and slight increases with increasing salinity content.

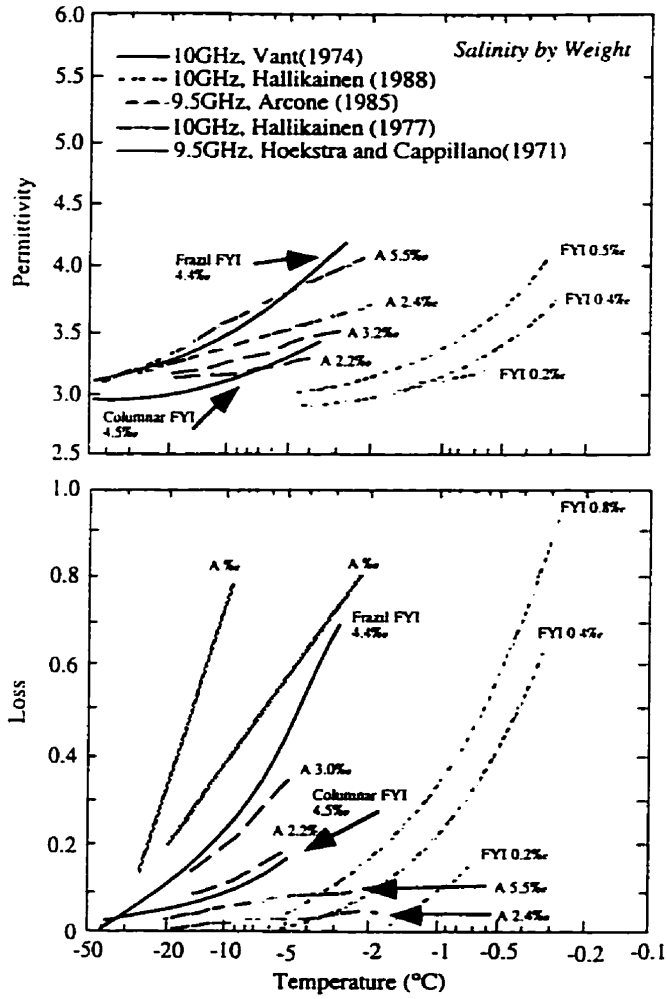

Figure 3.10 Experimental values obtained by various authors for sea ice between 10 and 16GHz: (a) permittivity, (b) loss. *(adapted from Hallikainen and Winebrenner, 1992)*

Snow Dielectrics

Perla (1991) outlined the permittivity of snow at 0°C for 1MHz. He found average permittivity increased from 1.98 when liquid water volume was 0% to 7.10 when w_v was just under 1%. Tiuri *et al.* (1984) examined permittivity of new and old snow at 5.6 and 12.6GHz. They found ε_{ds} is independent of snow geometry, as old, new, fine grained and coarse snow all yielded similar results. With the inclusion of liquid water they noticed

increases in permittivity and loss, with loss values rising more rapidly. The modified Debye-like models presented in [3.8] and [3.9] were found to agree well with experimental observations. From 3 to 37GHz Hallikainen *et al.* (1986) reported ε'_{ds} concurred with the results of Tiuri *et al.* (1984). Permittivity increases due to wet snow (Figure 3.11) closely followed predicted values from the modified Debye-like models. Dielectric loss in wet snow also resembled modelled values (Figure 3.12)

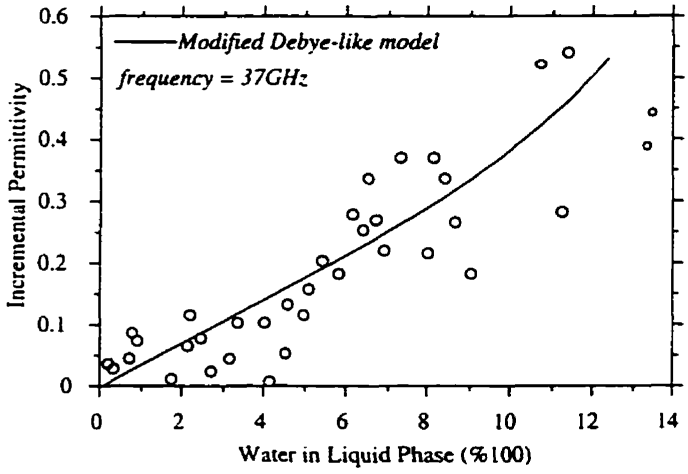

Figure 3.11 Changes in permittivity as a result of increasing water in liquid phase. The incremental permittivity equals $\varepsilon'_{ws} - \varepsilon'_{ds}$. *(adapted from Hallikainen et al., 1986)*

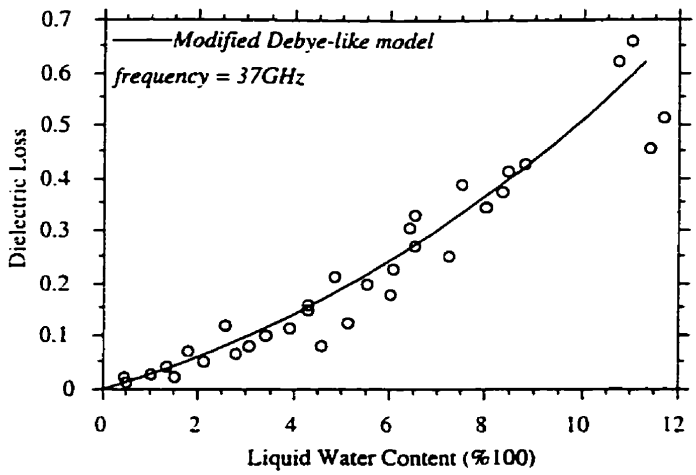

Figure 3.12 Wet snow dielectric loss as a function of water in liquid phase. *(adapted from Hallikainen et al., 1986)*

The dielectric theory shown here provides the basis for understanding the interactions of a snow covered sea ice volume with microwave energy emission. The next section will describe some of the historical research conducted with microwave radiometers in the marine cryosphere. It is not intended to be an exhaustive account of all microwave research in the Arctic, but rather to (a) provide a precedent for using microwave radiometry in this work and (b) outline the previous research from which this thesis builds upon.

3.3 Historical Use of Microwave Radiometry within the Marine Cryosphere

Figure 2.2 outlined the large seasonal variability present in ice coverage over the marine cryosphere. It also shows why satellite remote sensing is an important research tool in this region. The vast spatial scales mean many in situ observations are necessary to characterize the area. However,

the hostile climate makes in situ operations difficult, costly and dangerous. Thus, the use of remote sensing, with its large spatial coverage, is an obvious research tool for the marine cryosphere. Since this region is enshrouded in darkness over the winter and covered in cloud much of the spring, microwave remote sensing is a more effective measurement tool than visible or infrared sensors. The following section is intended to outline some of the historical research conducted in the marine cryosphere. Although it is not practical to provide an exhaustive account of microwave radiometric research in the marine cryosphere, the works which have bearing on this thesis are noted.

Satellite based passive microwave measurements began in 1968 with the Russian Cosmos 243. The instrument supported four nadir-looking radiometers operating from 3.5GHz to 37GHz (Basharinov *et al.*, 1971). NASA's (National Aeronautics Space Agency) first spaceborne imaging radiometer, launched in 1972, was the 19.35GHz Electronically Scanning Microwave Radiometer (ESMR). Six years later a more robust Scanning Multichannel Microwave Radiometer system was launched on the Nimbus-7. SMMR operated from October 1978 through August 1987 on alternating days to conserve power. Data was collected at 6.6, 10.69, 18.0, 21.0 and 37.0GHz. The latest addition to orbital imaging systems was launched onboard the United States Defense Meteorological Satellite Program (DMSP) satellite. Termed the Special Sensor Microwave/Imager (SSM/I), the instrument is a 7-channel, 4-frequency, passive microwave system. Dual-polarization information is available at 19.35GHz, 37.0GHz and 85.5GHz, while vertical polarization data is available at 22.235GHz. The SSM/I sensor provides daily coverage of the Arctic with a swath width of

approximately 1400km, excluding a 2.4° radius around the north pole (NSIDC, 1996). Sensor precision is measured with respect to a calm ocean surface and varies from 1.0K to 2.7K for the vertical channels and 1.8K to 2.0K for the horizontal channels (Hollinger, 1989). Instrument accuracy is compared in relation to modelled T_B for calm water and varies from -4.3K to 1.1K for V polarization and -1.1K to 0.9K for H polarization. Onboard radiometric sensitivity ranges from 0.4K for 19GHz and 37GHz, through 0.7K for 22GHz, to 1K for 85GHz (Hollinger, 1989).

Some of the earliest science missions with microwave radiometry were run under the Arctic Ice Dynamic Joint Experiment (AIDJEX). Wilheit *et al.* (1972) used airborne microwave radiometers in June 1970 to distinguish ice from open water. However, they noted a diversity in measured ice emissivities which could not be explained. Gloersen *et al.* (1973) followed by using surface based radiometers to classify multiyear ice flows and refrozen leads that were observed on the airborne imagery. Meeks *et al.* (1974) conducted similar experiments with ground based radiometers and successfully delineated FYI from MYI in a $110m^2$ study area based on emissivity differences between the ice types. Campbell *et al.* (1976) reanalyzed AIDJEX aircraft data to distinguish five "zones" of ice that they felt were typical of the Beaufort, Kara, Laptev and East Siberian Seas. The first zone consisted of shorefast FYI, the second was characterized as a shear zone containing FYI and MYI, while the third contains FYI and small MYI floes. The fourth zone was described as being similar to zone 2, while the 5th zone contained almost exclusively MYI. The first AIDJEX experiments concluded by stating changes in T_B were due to variations in ice salinity as well as the distribution of air bubbles and brine pockets.

Results from these experiments led to the formation of ice differentiation algorithms that worked adequately under dry snow conditions (e.g. Cavalieri *et al.*, 1984). Using the SMMR instrument researchers could compute sea ice concentration, multiyear ice fraction and the ice temperature. Errors in multiyear fraction were encountered when heavy cloud cover dominated, or if a strong surface wind persisted. For example, Cavalieri *et al.* (1984) noted a 6 $m \bullet s^{-1}$ surface wind could cause MYI fraction miscalculations by as much as 16%. In all situations the presence of a wet snowpack negated the operational abilities of the algorithms.

Radiometric observations made in these experiments have discovered emissivities over cold, dry FYI are very consistent (Figure 3.3) Steffen and Maslanik (1988) have documented ice salinities remain above 6‰ over the winter and do not introduce large emissivity variations. The largest change in T_B over FYI is associated with the overlying snow cover (Eppler *et al.*, 1992). Conversely, large variation in emissivity has been noted over MYI surfaces, especially with increasing frequency (Figure 3.13). This large fluctuation introduces significant error into SWE derivation, as variations in T_B are due to the ice in addition to the snow.

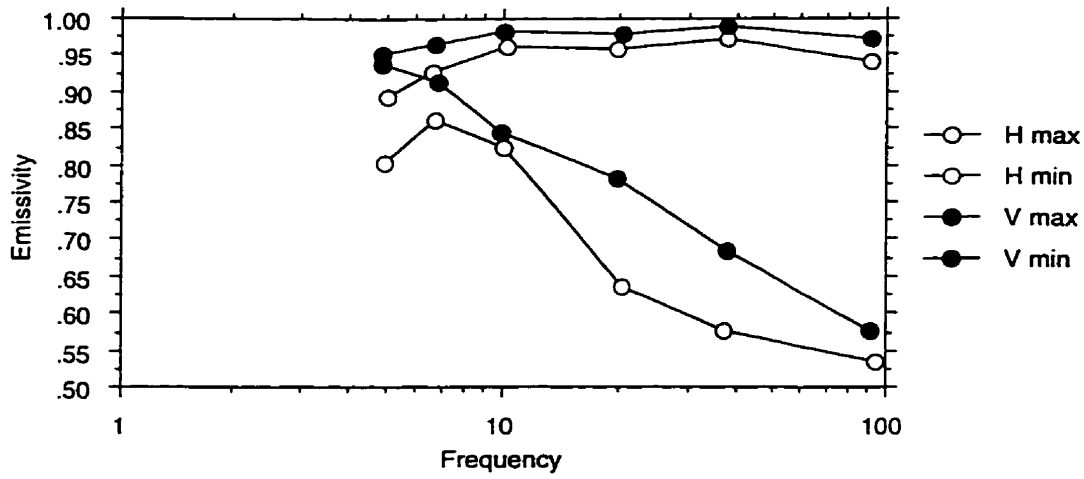

Figure 3.13 Emissivity variations in MYI as a function of frequency (incidence angle = 50°). *(adapted from Eppler et al., 1992)*

Research on the link between snow cover and microwave radiometry lagged years behind sea ice studies. Although correlation analysis between a land based seasonally dynamic snow pack and T_B had occurred in the 1970s, (e.g. Kong *et al.*, 1979, Chang *et al.*, 1976), work by Mätzler *et al.* (1982) was the first to formalize the influence of snow cover on sea ice brightness temperatures. They discovered a snow pack with greater than 1% liquid water volume affected the emissivity of the combined sea ice-snow volume. They also noted strong attenuation in microwave response from 5 to 35GHz, which was presumed to be an effect of volumetric scattering. As a result, it was stressed the successful application of algorithms would require understanding of the evolving snow cover.

Beginning in the early 1980s, significant effort began to focus on understanding the interaction of passive microwave energy with a wet

snowpack. In 1982, Grenfell and Lohanick (1985) operated a ground based radiometer unit at Mould Bay, NWT, to investigate the changes in T_B as they related to melt-freeze cycles and meltpond formation. In the early spring, it was found FYI T_Bs were independent of frequency and closely associated to the physical temperature of the ice surface (i.e. snow cover had negligible effects). MYI signatures decreased with frequency. During the summer, both FYI and MYI signatures increased with increasing frequency, owing to the effects of a wet snow pack. However, if a slush layer was present, a significant decrease in T_B was noted. No explanations were given to account for this. By late summer, with the formation of meltponds, MYI and FYI signatures were equal.

Comiso (1986) noted the use of dual polarization, single frequency observations were beneficial in discriminating information under wet snow conditions. He reported emissivity increased in both MYI and FYI signatures when snowpack liquid water volumes were above 0%, but less than 5%. Under melt-freeze cycles decreases in T_B were ascribed to increased volume scattering within the snow volume.

Grenfell (1986) provided strong evidence on the scattering effect of a thick snow pack with the assistance of in situ microwave radiometers. He measured T_Bs at 10, 18, 37 and 90GHz over snow with thickness of (a)<3mm, (b) 3 to 50mm and (c) >50mm. In shallow snow, brightness temperatures were approximately equal (Figure 3.14), while T_Bs decreased with frequency in the thickest snowpacks, owing to volumetric scattering. Under laboratory conditions, Grenfell and Comiso (1986) noticed decreasing

T_B at high frequencies after a snowfall event. Comiso *et al.* (1989) continued this work by systematically removing snow from a first-year ice surface while simultaneously obtaining microwave measurements at 90GHz. They found T_B rose tens of Kelvin with the removal of snow.

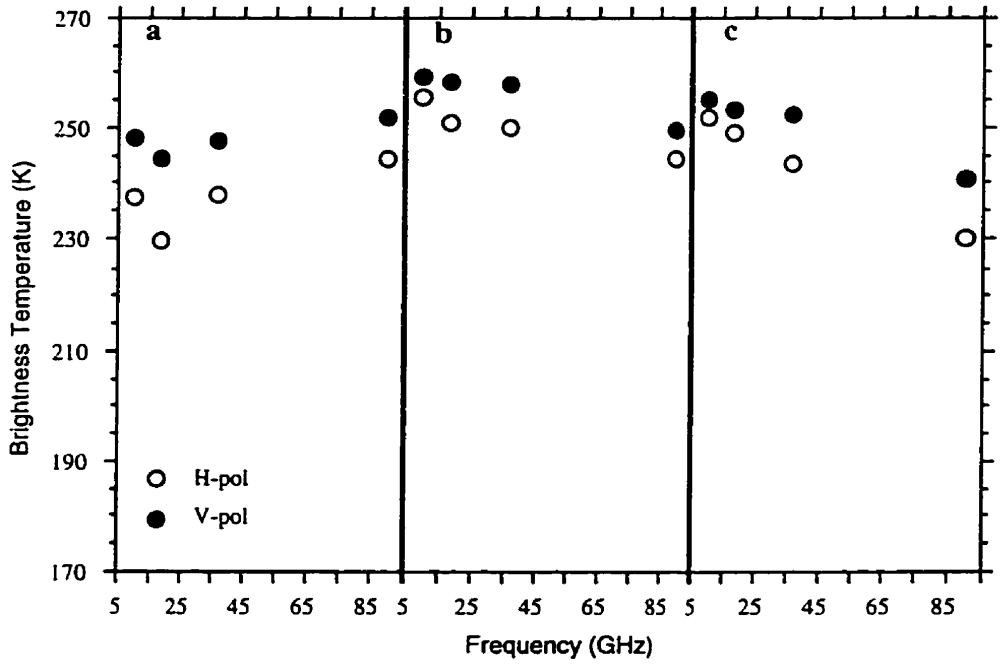

Figure 3.14 Average brightness temperature as a function of frequency over snow covered first-year sea ice for snow thicknesses of (a) <3mm, (b) 3 to 50mm and (c) >50mm. *(adapted from Grenfell, 1986)*

Lohanick and Grenfell (1986) continued the work from Mould Bay by correlating T_B with snow and ice properties near Tuktoyaktuk, NWT. They measured brightness temperatures at 10, 19, 34 and 37GHz, as well as snow/ice interface temperature, ice and snow salinities, snow depth and snow grain geometry. Results indicated a strong linkage existed between T_B and the brine volume in the ice. Snow depth also appeared to correlate

negatively with microwave emission. As snow thickness increased, the acquired brightness temperature decreased. They also noted combining snow depth with snow/ice interface temperatures lead to better correlations with T_B.

The monitoring work eventually led to several attempts at modelling changes in T_B based on an evolving snow cover. Onstott *et al.* (1987) were the first to provide qualitative models from the spring to summer season to describe the interaction of snow and T_B. From 5 to 94GHz, they postulated decreases in emissivity were resultant from enhanced volume scattering in the upper snowpack. As the temperature warmed, large scattering grains formed through metamorphism. During meltpond formation they noticed decreased emissivities, but large inter-day variations. They concluded fluctuations in the snowpack caused major difficulties in developing algorithms for determining ice and snow information remotely.

Lohanick (1990) examined the importance of snow basal layers on microwave emission. Over a first-year ice surface, he noted the bottom 50mm of a 250mm dry snowpack supplied an additional 20K to the acquired brightness temperature at 33GHz. As a result, T_B did not correlate well simply with underlying ice conditions or the overlying snow depth. Lohanick (1993) continued with an examination of microwave emission on an evolving snow cover over artificial sea ice. He noted a drop in T_B by as much as 100K at 10GHz when a slush layer developed after snowfall. More importantly to this thesis, he noted slight drops in T_B as the snow grains grew over time.

Garrity (1993) furthered previous research by looking at diurnal variations in a snowpack. It was found that changes in snow liquid water content and snow structure affected the daily T_B if cold nights followed warm days (Garrity, 1991). Garrity exploited this information to successfully classify FYI from MYI even during the melt onset. Her classification is based solely on the snowpack and how temperature gradients in the snow layers over FYI and MYI are different at varying parts of the day. The thinner FYI snow cover is generally affected by increasing air temperatures more rapidly than MYI snowpacks. Using a 37GHz microwave radiometer, she concluded by saying the morning is the best time for ice differentiation in the mid-spring, while the afternoon is superior during the latter stages of spring.

Results from the past 30 years have shown the T_B of a particular feature at any time is a product of scattering and emission from the ice and snow cover. We now understand the importance of quantifying snow in passive microwave studies. Furthermore, we have begun to exploit the information in the T_B caused by variations in the snow. In fact, the volume scattering principles of a snowpack provide the theoretical foundation of this thesis.

3.4 Research Questions

The scientific objective provided in section 1.2 gave a general scope for the research. Now that the variables of interest and the rationale for studying the work have been discussed, more detailed questions can be raised. A series of research questions are listed below, followed by specific rationale for analyzing each. They provide the framework for chapters 3 and 4.

1 - *How does variation in the snowpack affect in situ derivation of SWE over FYI?*

Uncertainties in the spatial and temporal extent of snow cover under projected warming scenarios can be monitored with derived SWE only if definitive links can be drawn between SWE and microwave emission. As a result, this work begins with an analysis of the snow cover and then exploitation of that analysis to obtain a statistical connection between SWE and T_B. Previous research by Goodison (1990) pointed out water in liquid phase is a key problem with current SWE algorithms, so it is a primary focus here.

2 - *How does variation in the underlying ice type affect SSM/I derivation of SWE?*

Variations in the underlying ice leads to a mixture of emissivities within an remotely sensed pixel. It is not clear how that variation will affect SSM/I brightness temperatures, or even how much variation exists. Theoretical case studies are constructed to understand the effects of spatial variability in the underlying ice type on derived SWE. SSM/I and synthetic aperture radar images are classified to document the real world variability in ice type.

3.5 Conclusions

This chapter has introduced the marine cryosphere as a integrated system which is key to understanding global change. The sea ice and snow volumes were described in detail, from initial formation to continued evolution. This was followed with a broader description of how snow is relevant to the larger scientific community. As well, this chapter outlined the microwave interaction theory necessary to link SWE with microwave radiometry. A series of examples were given showing some of the historical work done with passive microwaves in the marine cryosphere. Finally, detailed research questions were presented to frame the remaining chapters.

Information from the previous two chapters will now be exploited to better understand SWE derivation over the marine cryosphere. Specifically, I will comment on the abilities of a microwave radiometer to measure in situ SWE and on the affects water in liquid phase has on the SWE derivation.

CHAPTER 4 - In Situ Derived SWE and the Effect of Water in Liquid Phase

4.1 Introduction

Investigating SWE derivation with an in situ microwave radiometer provides the possibility to concurrently monitor changes in brightness temperature with changes in the snow cover, specifically the SWE. The resultant data set provides a suite of radiances that can be related to known changes in SWE. In addition, the small spatial resolution of the in situ microwave radiometer means heterogeneity in the underlying ice type will be small, further enhancing the interpretability of the measurements (Eppler *et al.*, 1992). This chapter will examine in situ SWE derivation with respect to the research question labeled in section 3.4:

1 - *How does variation in the snowpack affect in situ derivation of SWE over FYI?*

A series of sub-objectives are helpful in assessing this question:

1A - How do the geophysical properties of snow over first-year sea ice vary over seasonal and diurnal time steps?

1B - Can the information from 1A, specifically water in liquid phase, be exploited in SWE derivation over first-year sea ice with an in situ microwave radiometer?

The main objective in this chapter is to investigate the relationship between SWE and microwave emission through an evaluation of the in situ physical and electrical properties which give rise to this connection (1). It will specifically focus on the co-occurrence of brightness temperatures at 50° (near SSM/I incidence) and the diurnal and seasonal evolution of the scattering. The intention is to investigate the statistical relationships between T_B and SWE and to explain these empirical results by assessing the physical and electrical characteristics which drive this relationship.

The initial step will be to examine how the snow properties vary over a daily time span (1A). It is important to completely characterize and understand how the snow is developing before it can be exploited for SWE derivation. Question 1B will focus on statistical linkages between the microwave brightness temperatures and snow properties. In particular, the effects of

water in liquid phase on the SWE retrievals with an in situ microwave radiometer will be analyzed.

4.2 Methods

Data were collected as part of the Collaborative Interdisciplinary Crysosphere Experiment (C-ICE '96) from May 11 to June 15, 1996. The field site was located approximately 70km northeast of Resolute Bay, Cornwallis Island, NWT, Canada (Figure 4.1).

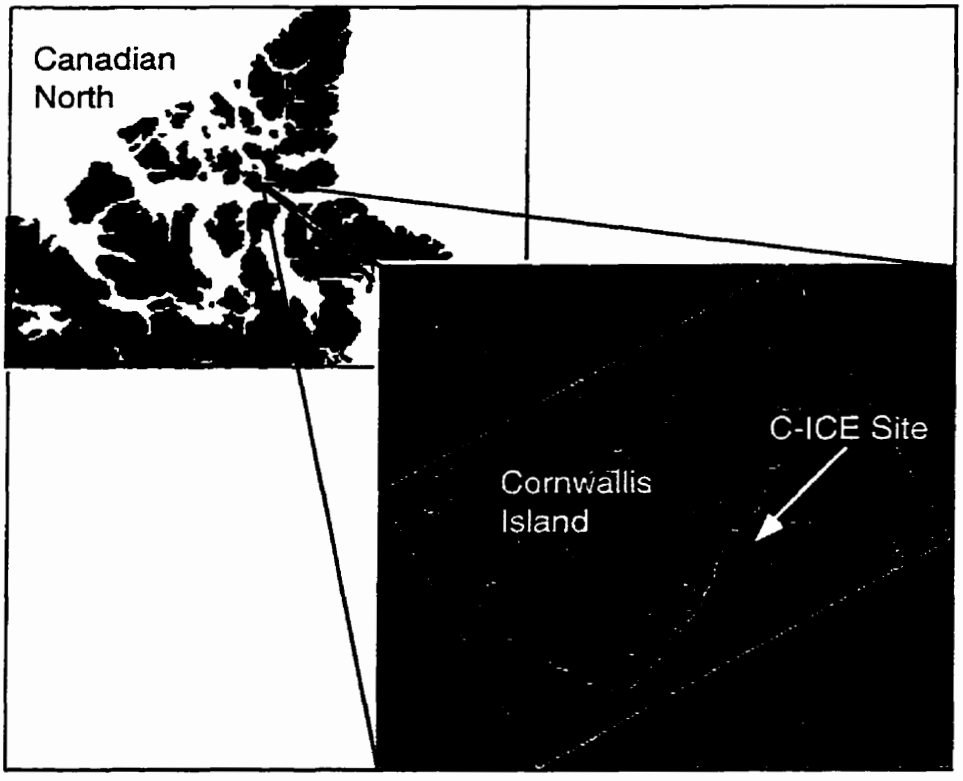

Figure 4.1 C-ICE '96 Field Site.

4.2.1 Snow and Sea Ice Sampling

Snow profiles were collected from an area adjacent to the radiometer site (Figure 4.2). Sampling was performed without replacement in a 0.375 m^2 'crystal pit'. All measurements were taken on the diffusely illuminated snow wall (perpendicular to the solar disk) in order to minimize the effect of solar insolation. Data were gathered three times daily, at approximately 7:30 am (*am*), 1:30 pm (*noon*) and 6:30 pm (*pm*) CST.

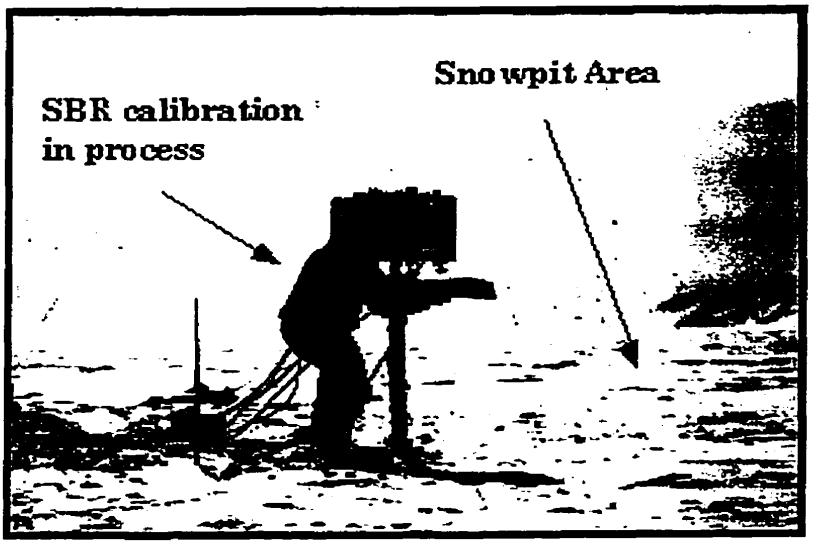

Figure 4.2 Radiometer sampling site during C-ICE'96.

During each measurement set snow depth, density, volumetric liquid water content, ice surface and snow salinity and ice and snow temperatures were recorded. Depth was recorded to the nearest half cm with a metre stick. Density samples were removed at 2 cm vertical intervals with a 66.36 cc density cutter and placed into a sealed plastic bag. Each sample was then weighed to the nearest 10th of a gram on a digital scale and subsequently converted to $kg \bullet m^{-3}$ using the gravemetric technique. This is precise to ± 40 $kg \bullet m^{-3}$ based on replicate sampling and previously published results

(Garrity and Burns, 1988). The percent water in liquid phase was estimated with a capacitance plate (dielectric device). Values were recorded from the plate at intervals of 1 m above the snow surface (relative calibration to air), on the snow surface and at the midpoint of each 2 cm snow sample on the pit wall. The 0 to 6cm layers above the ice surface contain brine which negates the capacitance approach to estimating liquid water content. In these basal layers liquid water content is estimated by extrapolation based on the values observed in the brine free layers of the upper snow pack. Snow salinity was measured by melting the snow density samples to room temperature and measuring bulk salinity using an optical refractometer. Ice surface salinity was measured by scraping the top 2 mm of the ice surface for measurement using an optical refractometer. Snow temperature data were recorded continuously with 24 AWG, Cu-Co thermocouple junctions and recorded as 15 minute averages by Campbell Scientific Instruments data loggers (model 21X). The junctions were embedded in brass tubing (9 x 0.5 cm) which in turn were fastened at 3cm levels into a wooden dowel. The sensor arrays (including leads) were painted white to minimize thermal contamination. The snow was packed evenly during backfilling and the sensor leads, which extended to the data logger, were buried to further minimize thermal contamination. Further details of these methods are presented elsewhere (Barber *et al.*, 1994, 1995).

Physical properties of the snowpack were subsequently divided into 6 layers for analysis purposes. Layers containing brine at 2cm, 4cm and 6cm, were unaltered due to the significant effect salinity has on dielectrics at these depths. The remaining snowpack was stratified into three equal segments.

Layering the snowpack in this manner allows for meaningful intercomparisons between days with different snow depths.

Electrical properties derived in this chapter are based on the models of Barber (1993), which were discussed in chapter three.

4.2.2 Microwave Radiometry

Brightness temperatures were measured with three dual polarized Russian ATTEX radiometers at 19, 37 and 85GHz. All measurements were taken on an undisturbed snow surface flanked by the snowpit sampling grid (Figure 4.2). The Surface Based Radiometer (SBR) system was operated coincident in both time and space with the snow sampling program.

During each data acquisition set samples were recorded at 5 degree increments from 20° through 70°. A custom designed software program automatically controlled radiometer operations. The SBR system recorded a voltage which was then converted to a T_B. Samples were integrated over a 50 second look period, providing an error estimate of less than 1K.

Calibration of the SBR system was based upon linear regression between an Ecosorb® hot load and cosmic background radiation. Due to the need for clear skies, only 10 calibrations were performed over the field season. Consequently, all calibrations (Figure 4.3a) were averaged into one general calibration equation for each frequency. All voltages were then re-analyzed using this general calibration. It is felt that this is the best option to minimize sensor effects which could obscure the results. Relative stability

(Figure 4.3b) appears adequate. A nonparametric Kruskal-Wallis test confirms the 5 sample runs are statistically equivalent (p-value = 0.96).

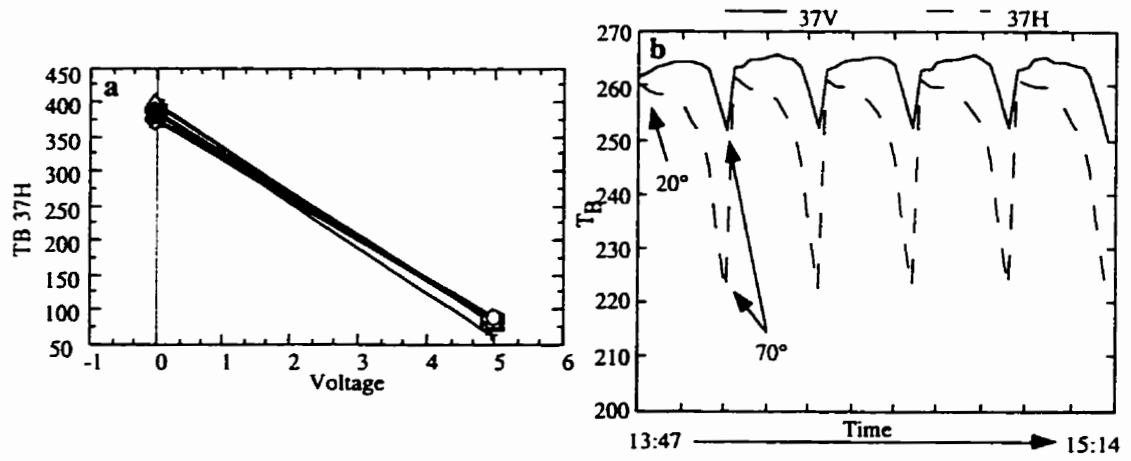

Figure 4.3a. Absolute and **4.3b.** Relative Calibration curves for the SBR system.

4.3 Results and Discussion

4.3.1 Geophysical Properties

Snow depth began at 15cm and quickly rose to near 30cm, where it fluctuated for the rest of the field project (Figure 4.4).

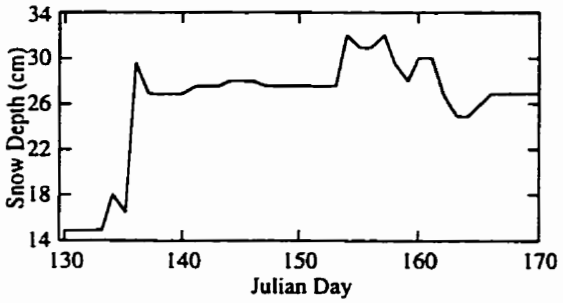

Figure 4.4 Snow depth

Profile Distributions

Over the field season the vertical profile of liquid water (Figure 4.5a) exhibits noticeable increases towards the ice surface. This is a result of increased temperatures and drainage as the spring season advances. Modelled loss values at 37GHz (Figure 4.5b) closely correspond to liquid water volumes. This result is expected due to the influence water in liquid phase has on the complex permittivity of snow (Ulaby *et al.*, 1986). A third variable of interest, snow pack density, shows some diversity in the profile (Figure 4.5c). Densities are highest in the middle layers and decrease towards the snow-ice boundary as well as the snow-air boundary. New snowfall with low densities accounts for the lower values in the upper pack, while the formation of large kinetic growth grains explains the lower densities in the basal layers. Interestingly, results from previous research (e.g. Barber *et al.*, 1995) indicate density in the basal layers (1-3 in this study) should be significantly less than the middle and upper snowpack layers. However, during C-ICE '97 an abnormal amount of ice mass agglomerates were evident in the snowpack, especially in the basal layers. Further, ice lenses with densities approaching 900 $kg \bullet m^{-3}$ were apparent in the lower 3 snow layers. Modelled permittivity at 37GHz ε' (Figure 4.5d) closely resembles density measurements due to the influence density has on permittivity. Finally, significant variation in salinity is present (Figure 4.5e). Snow wicks brine from the ice surface and salinity decreases with distance from the ice.

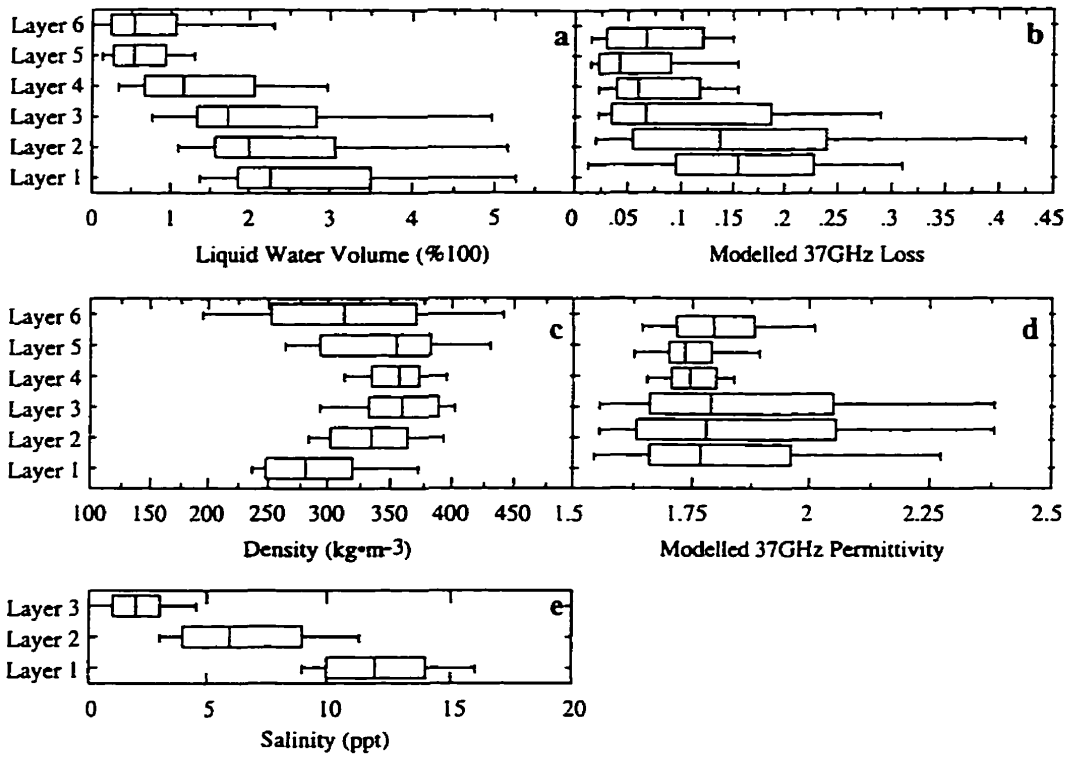

Figure 4.5 Profile distribution of (a) liquid water volume, (b) modelled 37GHz loss, (c) density, (d) modelled 37GHz permittivity and (e) salinity.

Seasonal Evolutions

Seasonally, the water content remains relatively constant during the first half of the field season and then shows an increased variability in the latter half (Figure 4.6a). As the season progressed towards spring, the incidence of warm storm fronts increased, explaining the increased variance of liquid water. The general increase in the late season is a result of elevated air temperatures corresponding to the spring temperature evolution. Modelled 37GHz loss values (Figure 4.6b) do not increase as substantially as liquid water because of the corresponding loss in snow salinity as wetness increases. Both density (Figure 4.6c) and derived 37GHz permittivity (Figure 4.6d) show a slight increase, especially in the upper layers, as the

spring progresses. Natural compaction, wind effects and melt-freeze cycles will all increase snowpack density, especially in the uppermost layers. Salinity reduces slightly as spring advances (Figure 4.6e). With warmer temperatures brine drainage begins and correspondingly lower salinity concentrations are observed.

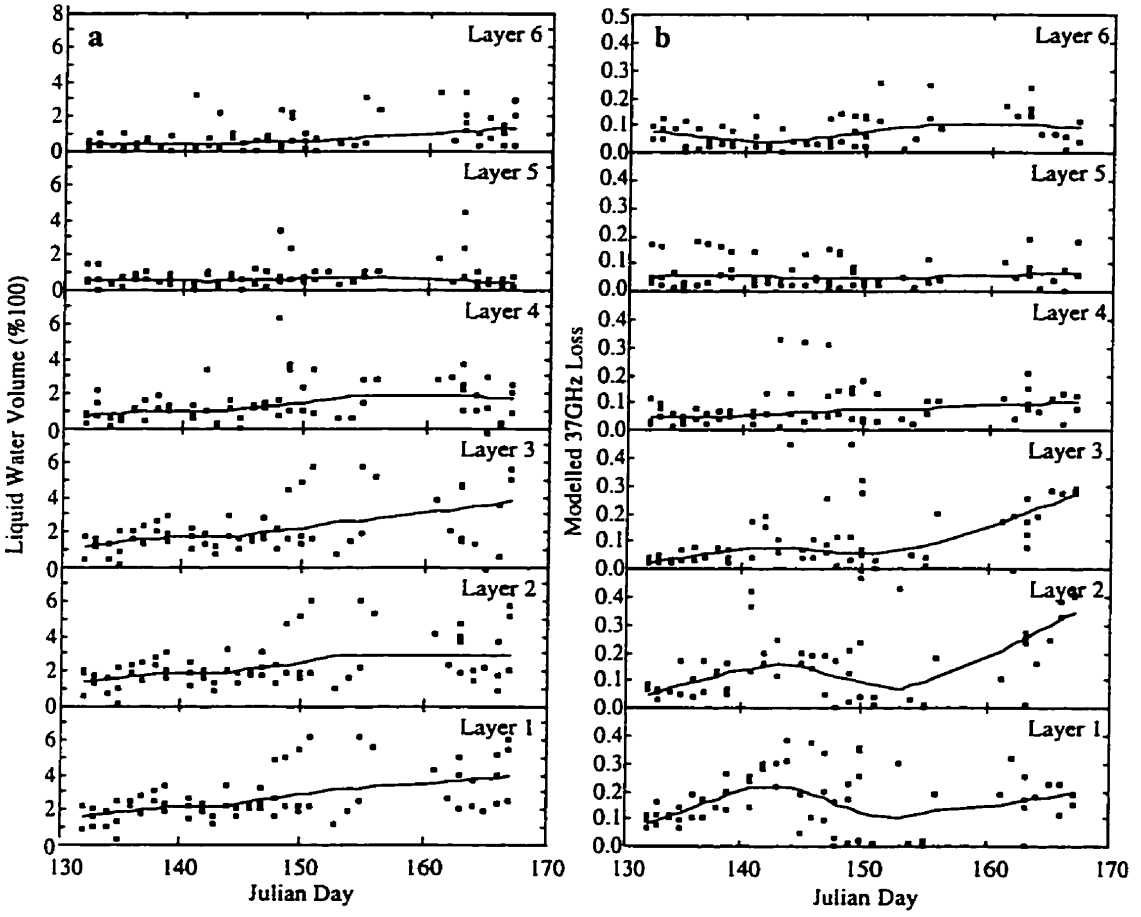

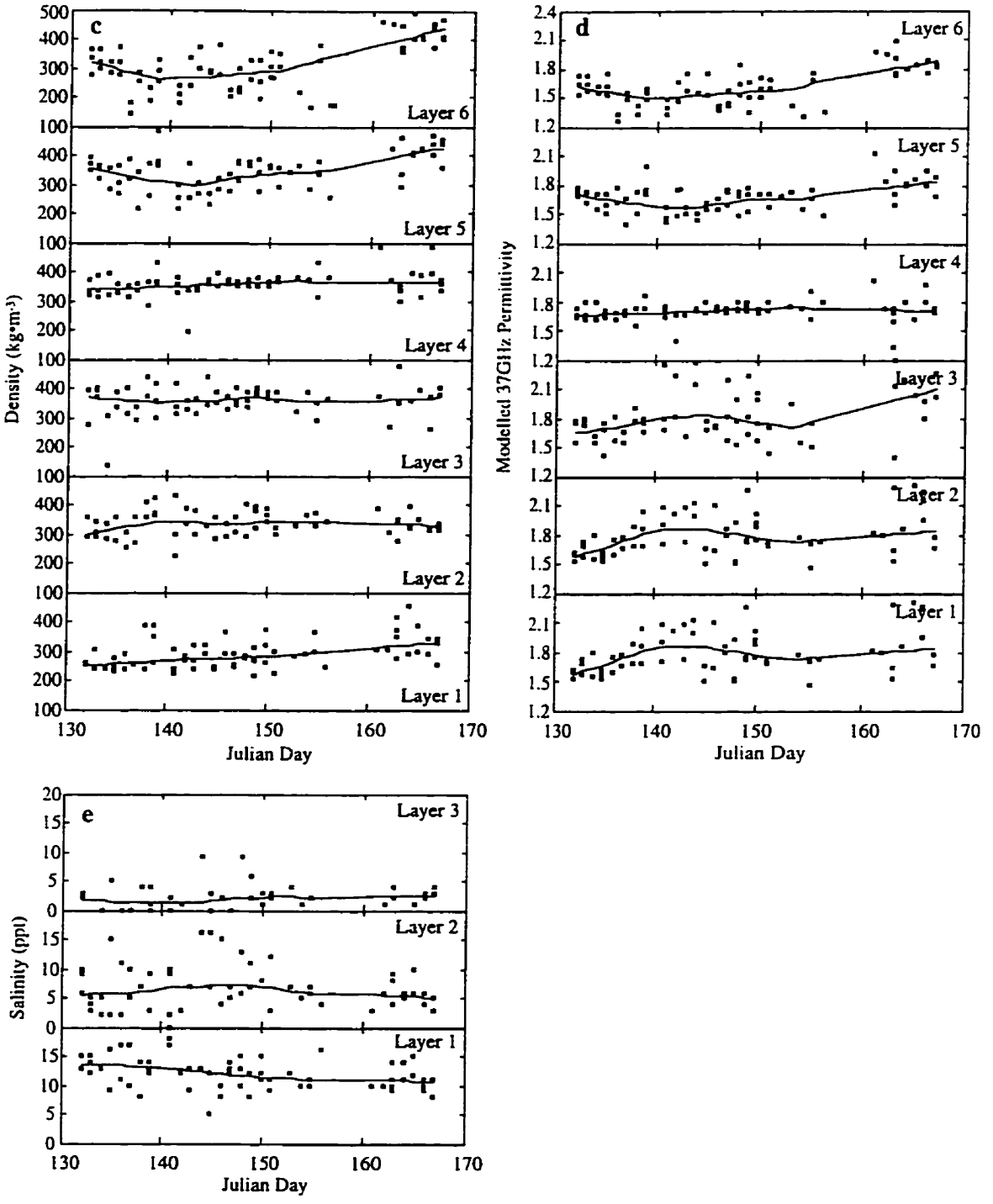

Figure 4.6 Seasonal evolution of (a) liquid water volume, (b) modelled 37GHz loss, (c) density, (d) modelled 37GHz permittivity and (e) salinity.

Diurnal Variations

Diurnally, a noticeable difference between the 3 sample sets for liquid water content (Figure 4.7a) and modelled 37GHz loss (Figure 4.7b) becomes clear towards the end of the field project. *Am* water contents remain fairly stable, while *noon* and especially *pm* sets showed a marked rise in liquid water content. Little difference in either density (Figure 4.7c) or modelled 37GHz permittivity (Figure 4.7d) is noted, as expected. Density will change mainly through metamorphic action, which is more noticeable over seasonal scales rather than diurnal scales - during the course of a few hours, the density is unlikely to substantially change. Finally, the small observed decrease in salinity (Figure 4.7e) implies that gravity drainage of water in liquid phase is small over the sampling period.

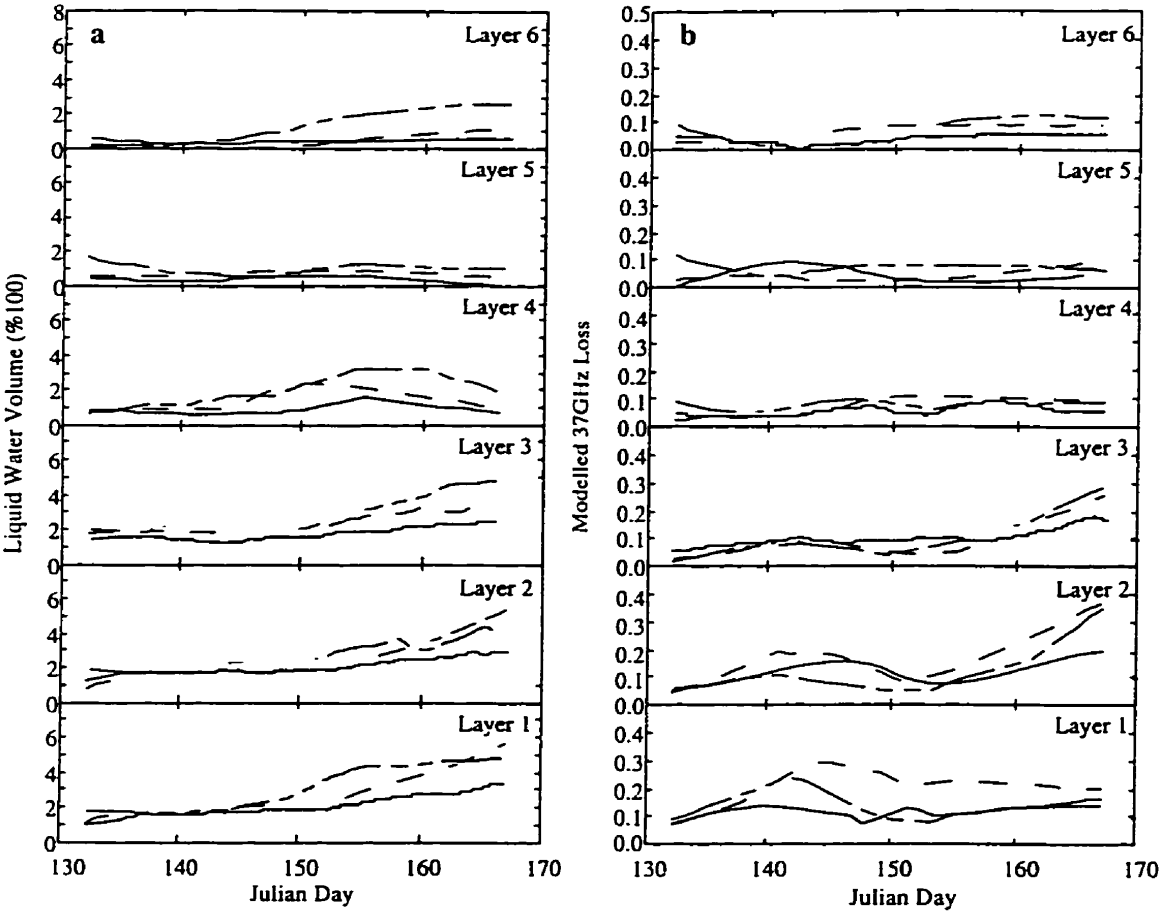
a
b
Layer 6
Layer 5
Layer 4
Layer 3
Layer 2
Layer 1
Liquid Water Volume (%100)
Modelled 37GHz Loss
Julian Day
Julian Day

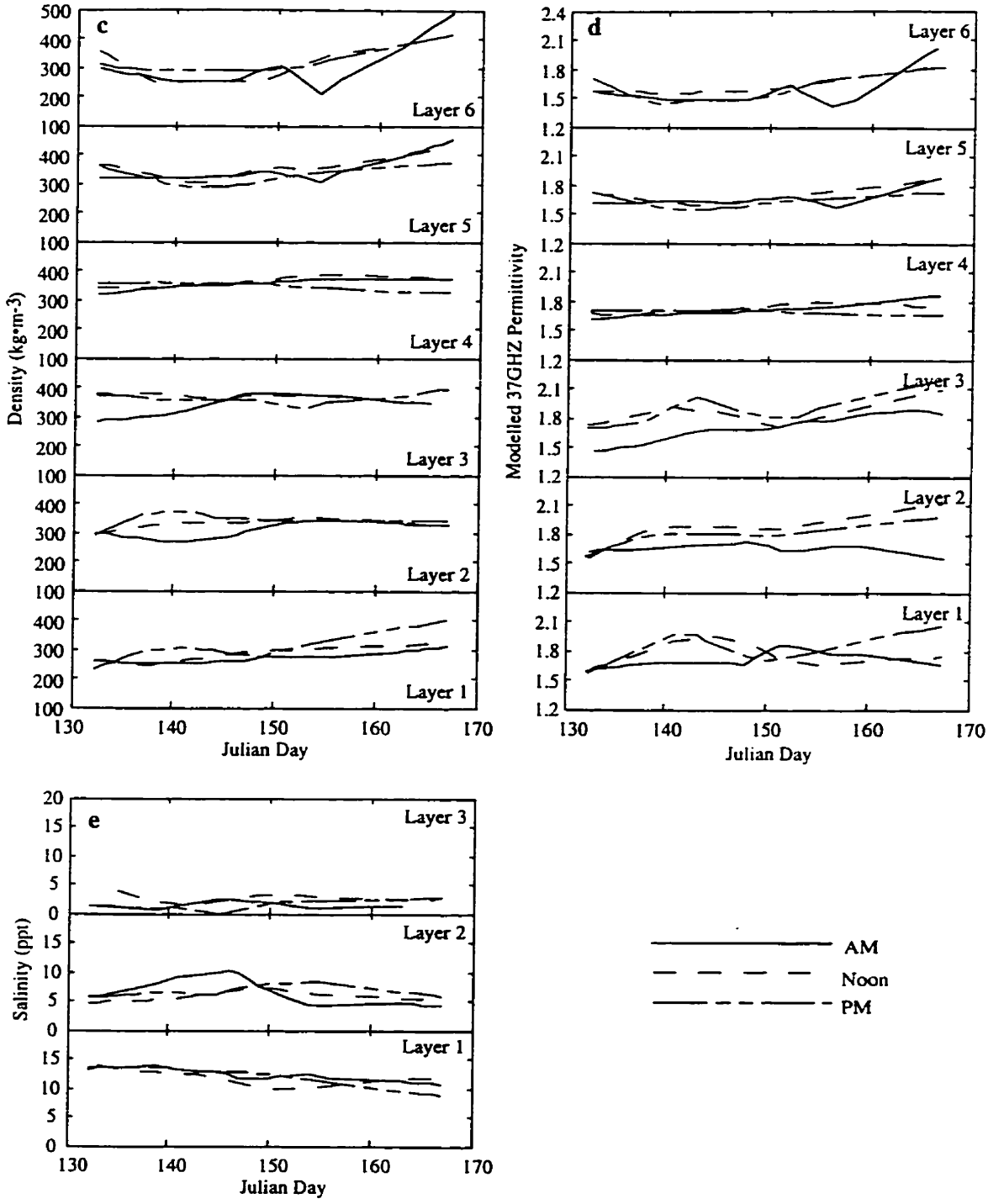

Figure 4.7 Diurnal separation of the seasonal evolution in (a) liquid water volume, (b) modelled 37GHz loss, (c) density, (d) modelled 37GHz permittivity and (e) salinity.

4.3.2 Microwave Radiometry

Geophysical effects on SWE monitoring

Comparison between snow density and microwave brightness temperatures (Table 4.1) indicates a consistent negative correlation. Increasing densities induce more volume scattering, thereby reducing the T_B.

Table 4.1 Correlation Matrix between snowpack layers and brightness temperatures.

Layer	19H	19V	37H	37V	85H	85V
6	-0.23	-0.23	-0.28	-0.32	-0.30	-0.17
5	-0.08	-0.10	-0.13	-0.09	-0.08	-0.05
4	-0.23	-0.19	-0.17	-0.13	-0.08	-0.07
3	-0.25	-0.18	-0.24	-0.21	-0.20	-0.40
2	-0.25	-0.22	-0.31	-0.30	-0.44	-0.46
1	-0.13	-0.17	-0.31	-0.36	-0.26	-0.29

Disregarding natural variability in snow properties will adversely affect the SWE predictive capabilities of microwave radiometry. Variability which can be explained by combinations of frequency and polarization is low with combined data from *am*, *noon* and *pm* sets (Figure 4.8). At horizontal polarization, 85GHz results are the weakest; 37GHz are strongest. For vertical polarization, 19GHz is the poorest estimator, while 85GHz is best. 19GHz is the least sensitive frequency to changes in the snowpack and this explains the lower R^2 values. Inversely, 85GHz is known to be very responsive to slight variations in liquid water content and this likely weakens the relationship between SWE and T_B at H polarization.

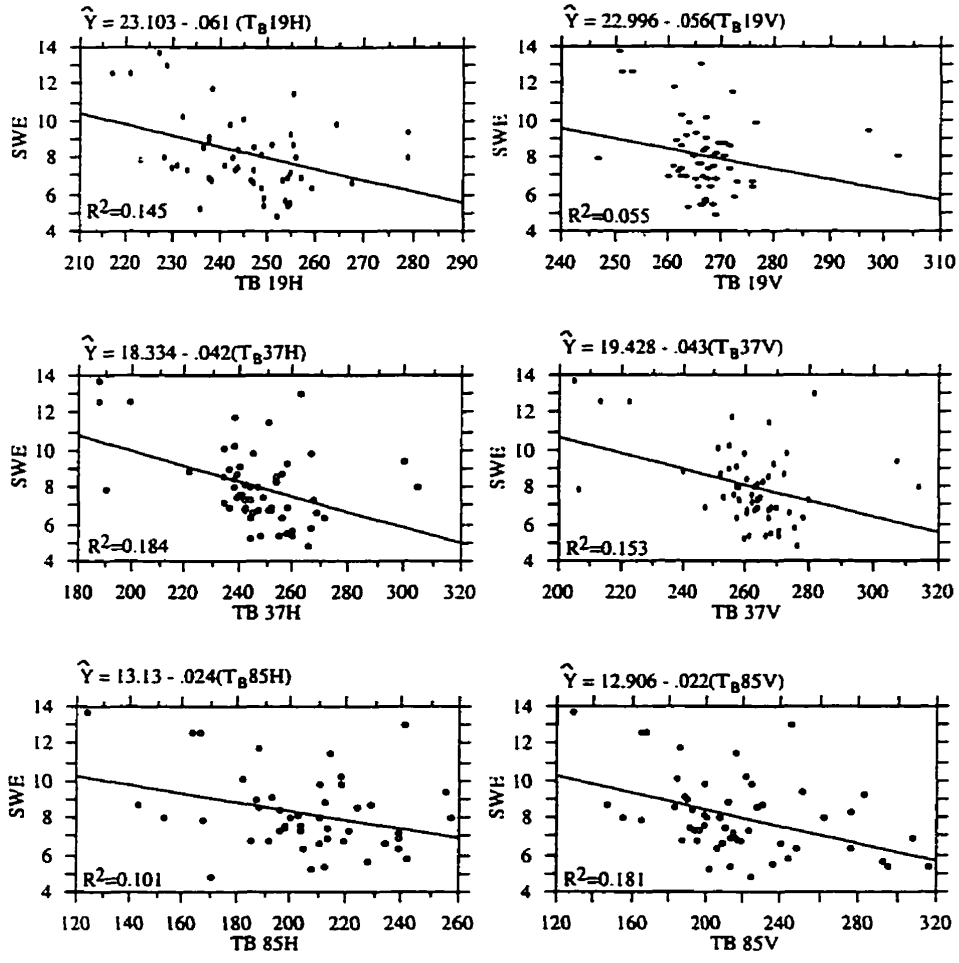

Figure 4.8 Initial regression plots which include all 3 diurnal sampling periods lumped over the full duration of the field experiment.

Improving microwave radiometric SWE measurements necessitates understanding sources of error such as liquid water, density and dielectrics. Figure 4.7 showed that water content and modelled 37GHz loss were higher in the *noon* and *pm* sets. To further illustrate, the seasonally averaged liquid water volume (Figure 4.9) clearly displays the *pm* set has the most liquid water, followed by *noon* and then *am*.

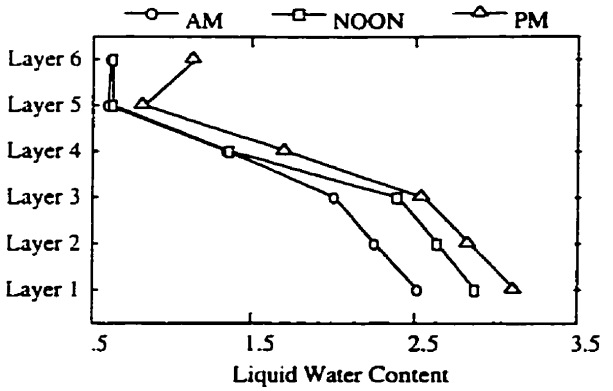

Figure 4.9 Water Volume by Subset.

Subsetting the data into *am*, *noon* and *pm* sets shows that *am* data explains a much higher percentage of the observed variability than either *noon* or *pm* results (Table 4.2). Normal probability plots and Durbin-Watson statistics validate parametric analysis in all but 85V. Note the lowest R^2 value (*pm*) coincides with the highest liquid water content and dielectric loss values. Dielectrically, the *pm* snowpack is emitting noticeable energy which elevates the brightness temperature; lowering the predictive capabilities. The *noon* set, with a slightly lower water content, exhibits a similar effect on a smaller scale. Once the effects of liquid water and dielectric loss are analyzed, SWE prediction from microwave radiometry improves dramatically.

Table 4.2 Subsets of 50° T_B vs. SWE

Frequency	R^2		
	am	*noon*	*pm*
19H	0.70	0.27	0.04
19V	0.73	0.26	0.01
37H	0.91	0.34	0.03
37V	0.89	0.27	0.01
85H	0.85	0.38	0.01
85V	0.71	0.32	0.05

SWE Algorithm Development

Operational SWE prediction includes various combinations of polarization and frequency. Although the initial and subset analyses use only single frequencies, the majority of SWE retrieval algorithms use a combination of 19 and 37GHz. Two of the more popular algorithms, after Chang *et al.* (1987) [4.2] and Goodison *et al.* (1990) [4.3] are analyzed with *am* data in this study.

$$SWE = K_1(T_{19H} - T_{37H}) \qquad [4.2]$$

$$SWE = \frac{K_1(T_{37V} - T_{19V})}{19} + K_2 \qquad [4.3]$$

where *Kx* is an orbital correction based on geographic location and *Tx* is the brightness temperature at a particular frequency and polarization.

Results (Table 4.3) based on [4.2] and [4.3] are poorer SWE estimators than single 37H or 37V for the conditions observed in this case study. Combining the V and H polarizations from [4.2] and [4.3] show no improvement over 37H (refinement 1), or a much worse result (refinement 2). Adding 85GHz to 37GHz provides is also less precise. Similarly, polarization information is of little value. It seems even the smallest amount of liquid water negates the potential of using polarization information or 85GHz to predict SWE. Simple combinations of frequency and polarization do not improve the SWE predictive ability of microwave radiometry.

Table 4.3 Single and Multi-Frequency/Polarization R^2.

Variables	R^2	*Comments*
19H-37H	0.72	Based on Chang *et al.*, 1987
37V-19V	0.89	Based on Goodison *et al., 1990*
19V-37H	0.90	Refinement 1
19H-37V	0.68	Refinement 2
85V-37V	0.12	85GHz
85H-37H	0.08	85GHz
19V-19H	0.10	Polarization Effect
37V-37H	0.18	Polarization Effect
85V-85H	0.04	Polarization Effect

Examination of the incidence angles show 20° through 60° are fairly uniform as SWE estimators (Figure 4.10). 60° is the best estimator for 3 frequencies, while 20°, 30° and 40° each estimate one frequency the best. However, the differences in R^2 values are not considered statistically distinguishable. Overall, 60° is marginally the best, while 70° is clearly the worst. Although varying the incidence angle appears to be of limited value in SWE prediction, the data is too limited to provide a definitive answer.

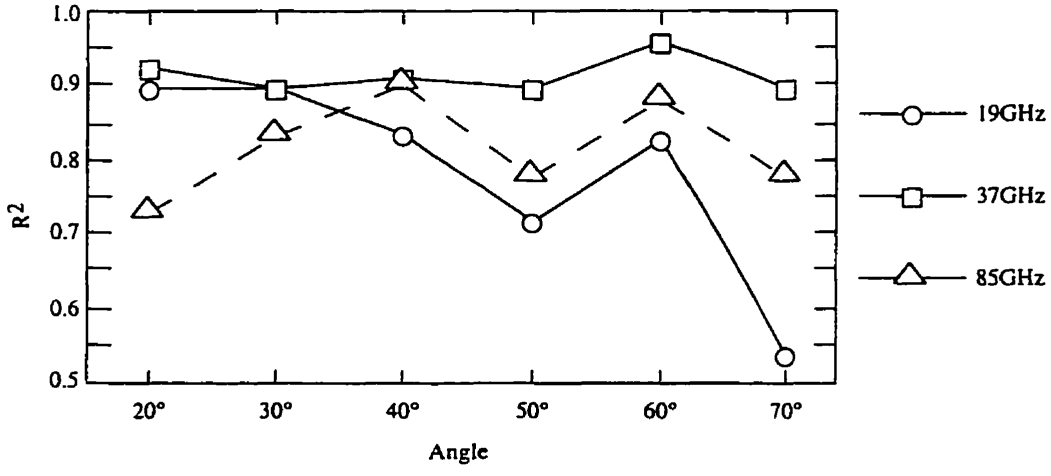

Figure 4.10 Incidence angle effects on SWE estimation.

Multiple regression techniques appear to improve the SWE derivation abilities of the microwave radiometer. Using all 6 channels, 96.8 percent of the observed variation can be explained (Table 4.4). Separating into H polarizations (92.9%) and V polarizations (91.5%) across all frequencies yields equally good estimators, while 37GHz (90.7%) is slightly better than 19GHz (89.1%) and 85GHz (85.7%). Caution must be noted because the improvement is, at least in part, due to the statistical artifact of increasing the number of independent variables. This given, continued research into multivariate approaches to SWE estimation is still recommended.

Table 4.4 Multiple Linear Regression Results.

Variables	R^2	*Comments*
All Freq/Pol	0.97	Multiple Linear Regression
V Pols	0.92	Multiple Linear Regression
H Pols	0.93	Multiple Linear Regression
19GHz	0.89	Multiple Linear Regression
37GHz	0.91	Multiple Linear Regression
85GHz	0.86	Multiple Linear Regression

4.4 Conclusions

In the introduction to this chapter, the following questions were noted:

1 - *How does variation in the snowpack affect in situ derivation of SWE over FYI?*

1A - How do the geophysical properties of snow over first-year sea ice vary over seasonal and diurnal time steps?

1B - Can the information from 1A, specifically water in liquid phase, be exploited in SWE derivation over first-year sea ice with an in situ microwave radiometer?

In this chapter it was found snowpack density and permittivity were largest in the middle of the snowpack, while water in liquid phase and dielectric loss were greatest in the basal layers. Salinity was greatest at the snow-ice interface and rapidly decreased to 0ppt above 6cm. Over the seasonal evolution snowpack density, water in liquid phase, permittivity and loss slightly increased, while salinity showed a slight drop. On a diurnal time step snowpack density, permittivity and salinity remained fairly constant, while water in liquid phase and loss showed larger variation. Typically, water contents were highest in the evening and lowest in the morning. Exploiting the diurnal separation of the seasonal evolution was shown to be an effective approach in remotely monitoring SWE. By using samples when liquid water content was lowest, statistically significant relationships were determined between SWE and the microwave brightness temperature.

This chapter has demonstrated that snow water equivalence retrievals can be made with a microwave radiometer, so long as the liquid water content is accounted for. However, even under dry snow conditions, heterogeneity in the ice type could negatively affect SWE derivation. This problem is compounded when the large spatial scales of the marine cryosphere are considered. For instance, considerable diversity in ice type has been observed over the central Arctic (Cavalieri *et al.*, 1991; Comiso, 1990, Carsey, 1982). Since monitoring the spatial and temporal variations in snow cover over the marine cryosphere will require a microwave radiometer with a larger spatial coverage, the next chapter examines the effect of ice diversity on SSM/I SWE derivation.

CHAPTER 5 - Effects of Sea Ice Heterogeneity on SSM/I SWE Derivation

5.1 Introduction

Accurate SWE retrievals over large spatial regions are necessary to characterize the spatial and temporal variation of snow in the marine cryosphere. The main disadvantage with using in situ measurements is the finite spatial scale. While they may be representative with respect to local conditions, the observational network is limited in the marine cryosphere. Conversely, the advantage of satellite microwave radiometry is

the ability to monitor the entire marine cryosphere on a daily time step irregardless of darkness or cloudiness (Eppler *et al.*, 1992). Furthermore, since SSM/I observations have been recorded since 1987, an operational SSM/I SWE algorithm could yield a long term record of snow cover variation over the marine cryosphere. This would provide insight into whether the projected climatic warming outlined in chapter two has already affected the snow cover. The disadvantage in going from in situ to satellite based measurements is increased diversity in the field of view. With spatial resolutions on the order of $25km^2$, a SSM/I pixel can contain a mixture of ice types and snow conditions. This chapter will examine heterogeneity in the underlying ice type with respect to the research question noted in section 3.4:

2 - *How does variation in the underlying ice type effect SSM/I derivation of SWE?*

In order to assess this a series of sub-objectives are provided:

- *2A - Are the SWE derivations from an in situ microwave radiometer and a satellite based microwave radiometer associated?*
- *2B - To what extent does variation in the underlying ice type (FYI vs. MYI) statistically affect brightness temperatures on the F-13 SSM/I sensor?*
- *2C - What does real world underlying ice type variability look like?*

The main objective is to address the operational use of SSM/I for sea ice SWE estimation with respect to problems of heterogeneity in the underlying ice type (2). Since the preceding chapter reported fairly good success with an in situ radiometer, the first step will be to investigate the link between in situ SWE measurements and SSM/I derived SWE from 1993 and 1994 (2A). Then a series of sensitivity trials will be performed to better understand what effect spatial heterogeneity has on emissivity (2B). Specifically, the effects of (a) ice type heterogeneity and (b) spatial pattern on emission will be studied. Finally, this chapter will examine real world variability with the both SSM/I and Earth Resources Satellite (ERS-1) images (2C).

5.2 Methods

The methods will be outlined in three sections which correspond to Objectives 2A, 2B and 2C.

5.2.1 In Situ vs. SSM/I SWE Estimation

Data were collected over two different field campaigns, 1993 and 1994, from the Seasonal Sea Ice Monitoring and Modelling Site (SIMMS). Both field sites (Figure 5.1) are located around Resolute Bay, NT, Canada.

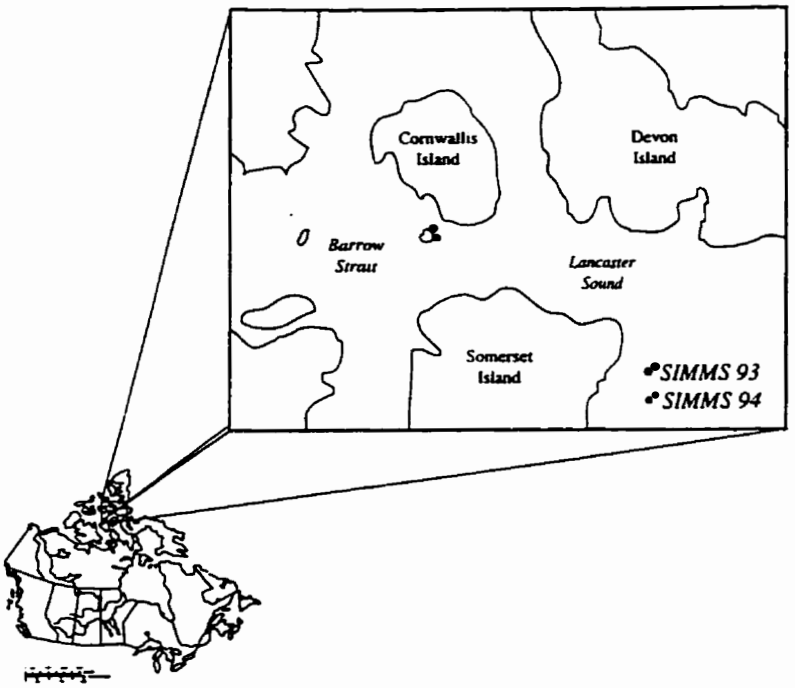

Figure 5.1 SIMMS Field Sites.

In Situ Data Physical Data

Data collection methods were identical to those presented in section 4.2.1, with the following exceptions (Misurak, 1994, 1993):

- Profile samples were collected every 3cm in a 100cc density cutter.
- Samples were taken at 1:30pm only.

SSM/I

SSM/I imagery used in this project were computed from gridded swath data, as opposed to the commonly available daily SSM/I EASE-Grid Northern Hemisphere brightness temperatures. Using a single pass minimizes averaging of daily T_B, which could have deleterious effects on SWE estimation. Grids represent spatially interpolated data and were

processed to facilitate the operational and scientific use of the SSM/I sensor. The interpolation technique maximizes radiometric integrity of the original brightness temperatures, while maintaining high spatial and temporal precision (NSIDC, 1996). Resolution in the grid series is 12.5km^2 for 85GHz data and 25km^2 for all other channels. Derived SWE was computed with [5.1], based on the terrestrial algorithm supplied by Walker and Goodison (1993). Five separate dates over the field seasons were used (Table 5.1). In 1993, Julian days 138 and 162 appeared to have substantial amounts of liquid water. Based on the effect of water in liquid phase presented in the previous chapter, these days should not correlate well with in situ SWE.

$$SWE = \frac{-20.7 - 49.27(37V - 19V)}{18} \qquad [5.1]$$

where 37V is 37 GHz V polarization and 19V is 19 GHz V polarization.

Table 5.1 Derived SWE data acquisition dates.

Year	Julian Day In-situ	Julian Day SSM/I	Water Volume (%100)
1993	126	125	0.00
1993	138	139	2.22
1993	162	163	8.42
1994	127	126	0.89
1994	130	128	0.30

5.2.2 Spatial Heterogeneity as a Source of Variation

For the sensitivity trials used here, frequency, polarization and incidence angle were held constant. Nine separate case studies were created based on the configuration and composition of ice types (Figure 5.2; Table 5.2).

Each case is composed of a 25x25 square grid, which represents the surface imaged in one SSM/I pixel.

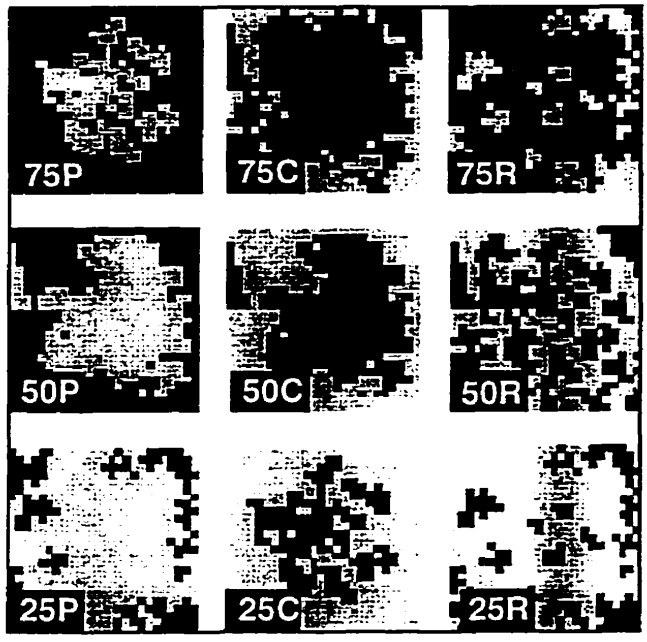

Figure 5.2 Case study diagram of underlying ice types. Dark grey shades represent FYI, while light grey shades represent MYI.

Table 5.2 Case study table of underlying ice types.

Case	%FYI	%MYI	Spatial Distribution of FYI
75P	75	25	Perimeter of FOV
75C	75	25	Centre of FOV
75R	75	25	Randomly Distributed
50P	50	50	Perimeter of FOV
50C	50	50	Centre of FOV
50R	50	50	Randomly Distributed
25P	25	75	Perimeter of FOV
25C	25	75	Centre of FOV
25R	25	75	Randomly Distributed

FOV = field of view.

Emissivities (Table 5.3) collected from Eppler *et al.* (1992) were used in a random number generator to calculate the 25^2 grids with respect to polarization and frequency. Average emissivity was first calculated without the SSM/I antenna patterns to examine the effect of ice type. Then the average emissivity was re-calculated with the F-13 SSM/I antenna patterns (Figure 5.3) to examine the effect of spatial differences in ice. For each frequency and polarization, the antenna patterns were converted into a weighted function with sum equal to 625 (25x25 grid). Emmisivity values in the centre of the field of view received more weight.

Table 5.3 Microwave emissivities of sea ice used in case studies.

Ice Type	Polarization	19GHz	37GHz	85GHz
First year	H	0.888	0.913	0.886
		(0.019)	(0.020)	(0.031)
	V	0.941	0.955	0.926
		(0.019)	(0.015)	(0.045)
Multiyear	H	0.780	0.706	0.650
		(0.080)	(0.115)	(0.011)
	V	0.850	0.764	0.680
		(0.068)	(0.079)	(0.105)

( ) = standard deviation of pooled emissivity values. *(adapted from Eppler et al., 1992)*

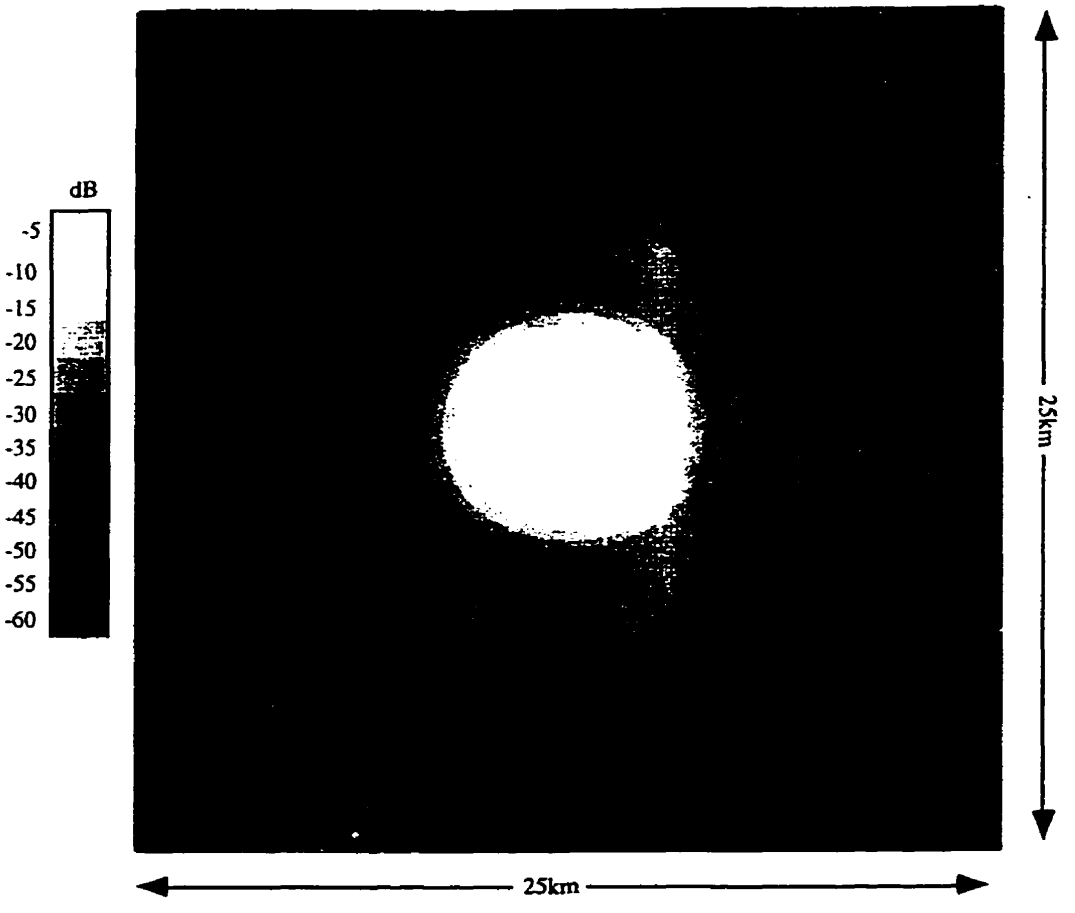

Figure 5.3 F-13 SSM/I antenna patterns. *(courtesy Gene Poe, personal communication)*

5.2.3 SAR Characterization of Spatial Heterogeneity

Spatial heterogeneity in real world situations was examined with the NASA Team Algorithm (Cavalieri *et al.*, 1984; Gloerson and Cavalieri, 1986) for SSM/I imagery and Bayesian classification with ERS-1 imagery. The NASA algorithm [5.2] presumes FYI, MYI and open water (OW) dominate the cryospheric icescape. It uses a spectral gradient ratio [5.1] and a polarization ratio [5.3] to determine the combination of MYI, FYI and

OW in a particular cell. All SSM/I pixels within 96 to 99°N and 74 to 75°W were included for this study.

$$GR(19V,37V) = \frac{T_B(37V) - T_B(19V)}{T_B(37V) + T_B(19V)} \quad [5.2]$$

$$PR(19GHz) = \frac{T_B(19V) - T_B(19H)}{T_B(19V) + T_B(19H)} \quad [5.3]$$

Since the spatial resolution of a low-res ERS-1 image is $100m^2$, it follows the synthetic aperture radar (SAR) image will be able to examine ice type variation at a much smaller scale in comparison with the NASA Team Algorithm. Segmentation of a SAR scene from 1993, 1994 and 1995 was performed with a supervised classification scheme. To be consistent with the NASA Team Algorithm, ice types were classified as either FYI or MYI. Rubble zones were grouped with MYI. Multiple training sites were selected for each ice type (land areas were visually masked out beforehand) and a Bayesian maximum likelihood processor was used to calculate the entire scene.

5.3 Results and Discussion

The results will be presented in three parts, identical to the methods section.

5.3.1 In Situ vs. SSM/I SWE Estimation

Based on the success of chapter three in-situ SWE values from SIMMS 1993 and 1994 were compared (Table 5.4). A relationship appears to be present (Figure 5.4), but the limited data cannot be statistically analyzed. This

small data volume is a result of limited snow measurements in 1993 and 1994 and an absence of SSM/I data in 1995 and 1996. Except for May 14, 1994, the SSM/I algorithm underestimated SWE. This may be a result of water in liquid phase. With the appearance of water, the microwave radiometer increasingly begins to monitor a return only from the water in the top portion of the snowpack. Radiances increase sharply and begin to merge at 19 and 37GHz (Eppler *et al.*, 1992). As a result, 37V-19V in [5.1] approaches zero and SWE is underestimated. The Walker and Goodison (1993) algorithm can separate wet snow areas, while Mote and Anderson (1995) delineated wet snow areas in the Arctic. Therefore, it should be possible to determine if the snowpack on the marine cryosphere is wet.

Table 5.4 Brightness temperatures from the test dates.

Year	Julian Day	37GHz V	19GHz V	Derived SWE	In-situ SWE
1993	126	242.900	251.200	21.570	30.298
1993	138	260.800	264.500	8.990	30.766
1993	162	262.000	266.200	10.350	21.162
1994	127	240.500	253.900	35.530	43.584
1994	130	241.200	254.600	35.960	35.497

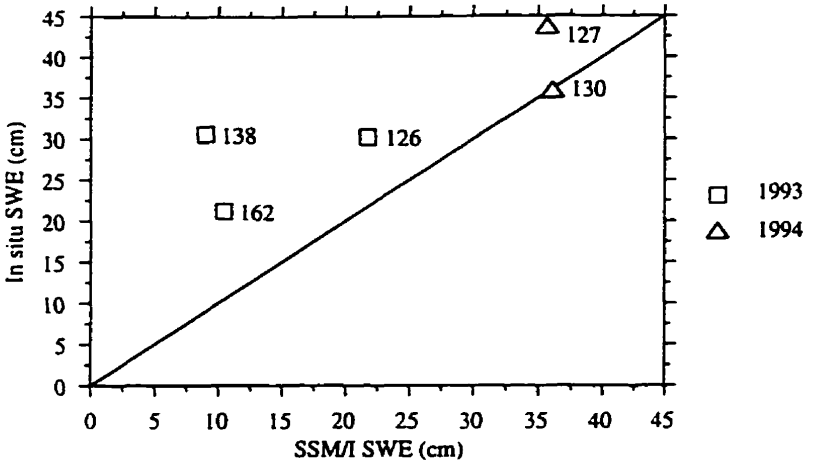

Figure 5.4 Bivariate plot of in situ versus SSM/I SWE. Julian days included in the graph.

5.3.2 Ice Heterogeneity as a Source of Variation

With the lack of empirical measurements, theoretical sensitivity trials are employed here to assess the effect of heterogeneity in the underlying ice. The spatial pattern of FYI and MYI from Figure 5.2 is still apparent after applying the randomly generated emissivities for FYI and MYI (Figure 5.5). All 6 frequency/polarization are similar in nature, with only 19GHz H pol being shown. The smaller standard deviation of FYI leads to a more uniform emissivity, as opposed to the highly speckled MYI areas.

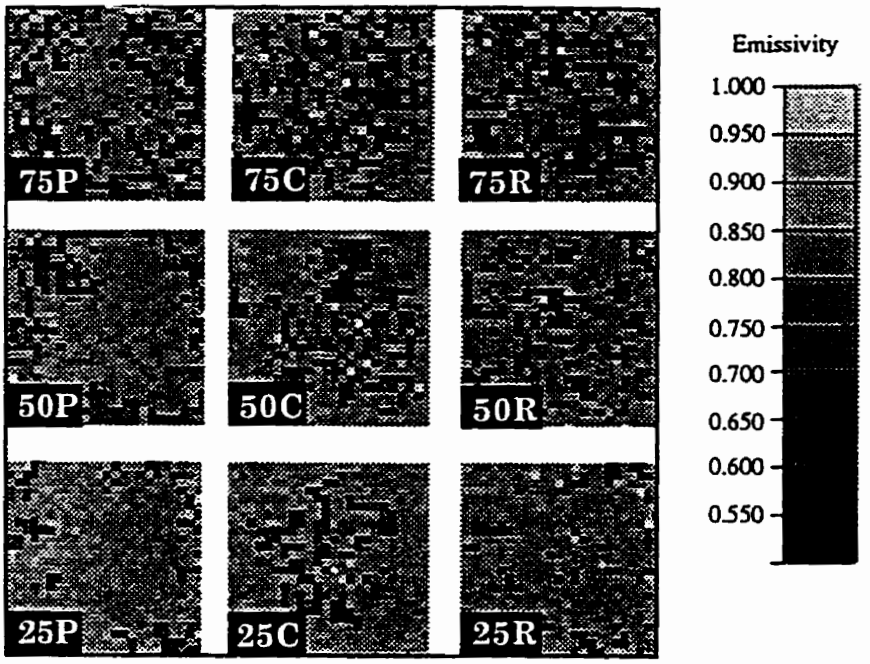

Figure 5.5 Emissivity variations of MYI overlaid on original ice concentration patterns.

Segmenting into the nine case situations, emissivity is shown to vary with frequency, polarization and percent composition of FYI (Figure 5.6). Emissivity decreases with increasing frequency and is larger for V polarization. As expected, emissivity is highest for 25% FYI and lowest for 75% FYI. With the addition of SSM/I antenna patterns, the spatial location of the ice becomes important. Relative to the initial run, cases with FYI in the centre of the field of view display increases in emissivity, while cases with FYI on the periphery display decreases. When the ice is randomly distributed emissivity does not change substantially.

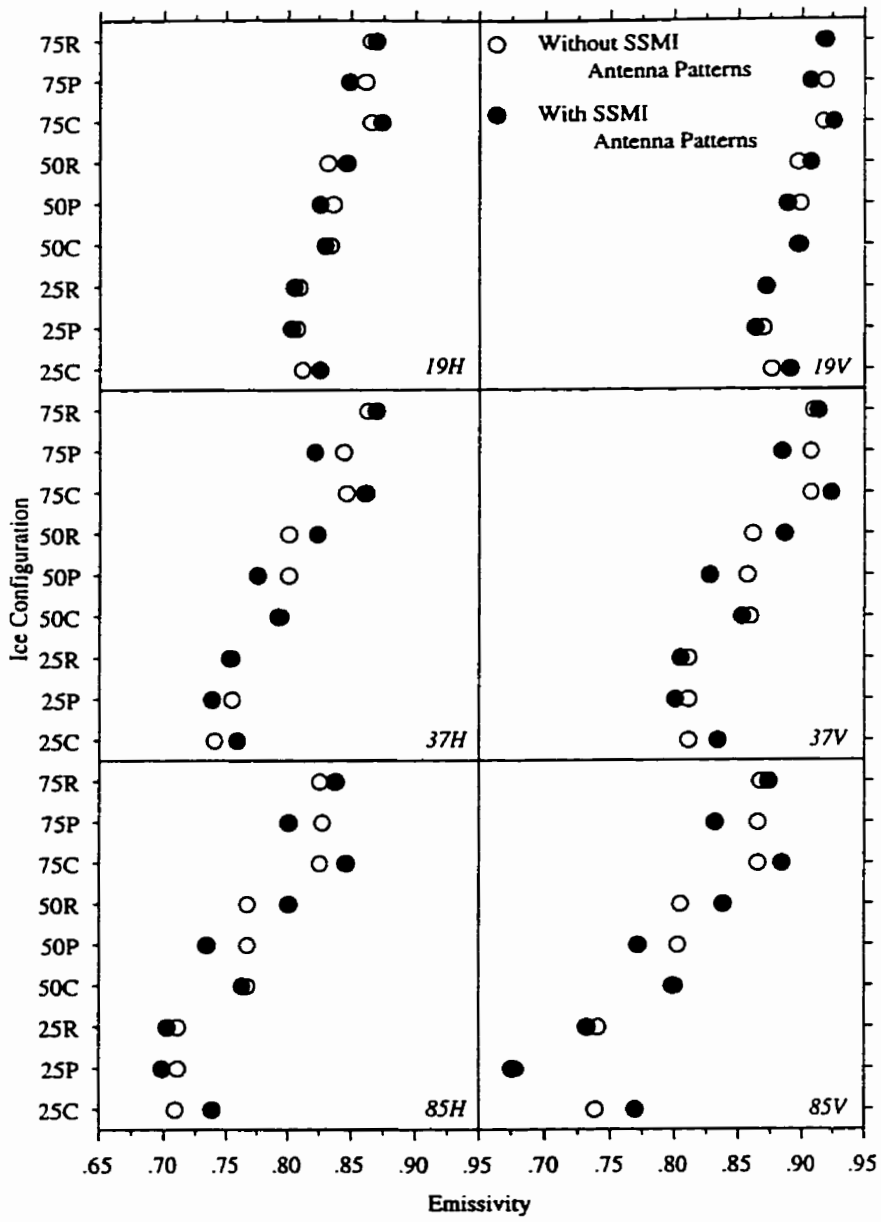

Figure 5.6 Emmisivity variation as a function of frequency, ice configuration and SSM/I antenna patterns.

Since the algorithm used for SWE estimation in this study [5.1] uses 19 and 37GHz V brightness temperatures, emissivity values were converted to brightness temperatures with prescribed ice temperatures (Figure 5.7). For an ice temperature of 270K, T_Bs range from less than 220K to more than

250K. Other ice temperatures yield similar ranges in the acquired brightness temperature.

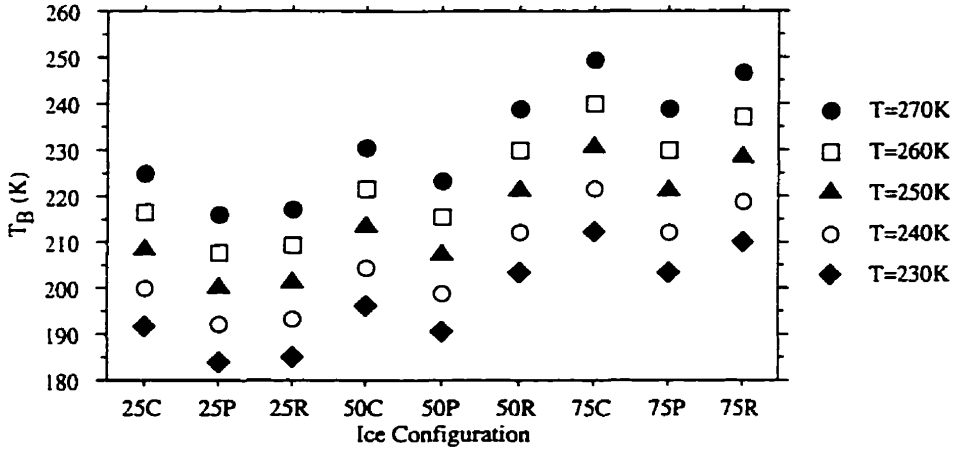

Figure 5.7 37V T_B based on ice type and temperature. 19V is similar.

Computation of SWE with [5.1] was used to examine effects of the range in brightness temperatures. Since the sensitivity trials do not place any snow on the ice, a value near zero would be considered accurate. Even though [5.1] has not been developed specifically for the Arctic, it appears it may be useful in deriving SWE over predominately FYI surfaces (Table 5.5), as SWE values are low, especially with colder ice. This table also shows the importance of ice location within a pixel. With FYI on the periphery, such as case 75P, results degrade substantially. In fact, a scene with 50% FYI located in the centre includes less error than one with 75% located on the periphery. When MYI begins to dominate the scene, SWE estimates with the current parameters of [5.1] could overestimate snow water equivalence by over 45cm. This is a result of the difference in emissivity between MYI and FYI. Whereas average emissivity for FYI is 0.941 at 19GHz and 0.955 at 37GHz, it is 0.850 at 19GHz and 0.764 at 37GHz (Table 5.3). The increased difference in MYI will equate to a larger difference in T_Bs. This translates

to an increased gap in 37v-19v in [5.1], which leads to the overestimation. In these cases, the spatial location of FYI is not important, as substantial error is noticeable even when FYI is centered within the FOV (e.g. 25C). Since the variance in MYI emissivities is high, it would not be possible to simply apply an offset to the SWE algorithm based on MYI percentage. For the precise use of SWE estimates, these results show it is important to monitor scenes that are principally FYI.

Table 5.5 SWE derived with [5.1] and prescribed ice temperatures.

Ice Config.	T=270K	T=260K	T=250K	T=240K	T=230K
25P	45.41	43.69	41.96	40.24	38.51
25C	39.50	37.99	36.49	34.98	33.48
25R	47.63	45.82	44.01	42.21	40.40
50P	42.45	40.84	39.22	37.61	35.99
50C	15.11	14.51	13.90	13.30	12.70
50R	29.89	28.74	27.59	26.44	25.29
75P	15.85	15.22	14.59	13.96	13.33
75C	0.33	0.27	0.22	0.16	0.11
75R	2.55	2.41	2.27	2.13	2.00

5.3.3 SAR Characterization of Spatial Heterogeneity

Based on the above results, it becomes clear successful SWE derivation must take into account the underlying ice type (as well as spatial pattern). Using the NASA Team Algorithm [5.2, 5.3], both 1993 and 1994 appear to

have substantial amounts of MYI within each pixel (Figure 5.8). When the region of interest is expanded it is apparent 1994 contains more MYI (Figure 5.9).

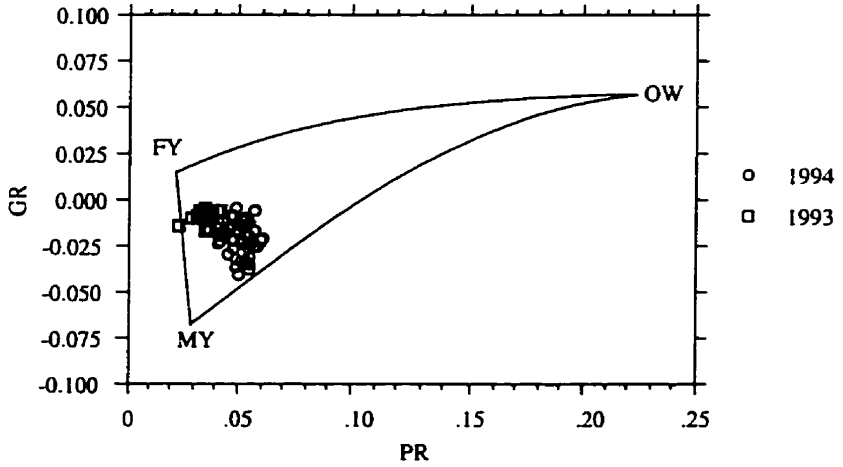

Figure 5.8 Ice type during 1993 and 1994 as determined by the NASA Team Algorithm.

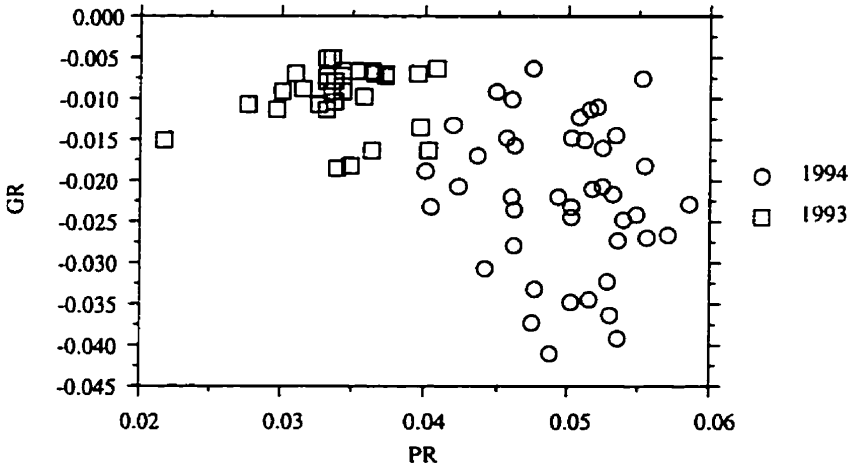

Figure 5.9 Enlarged portion of Figure 5.8 outlining ice type during 1993 and 1994 as determined by the NASA Team Algorithm.

With the NASA Team Algorithm, only the general character of an SSM/I pixel can be determined. However, the use of SAR can classify the pixel with greater resolution. In 1993 (Figure 5.10), the image appears to have a

mixture of MYI and FYI. Significant amounts of MYI are noticeable southeast of Lowther Island and east of Young Island. As a result, sectors 6, 8 and 9 would not yield accurate SWE estimates. Sectors 2-5 and 7 appear to be predominately FYI (Table 5.6), so variations in emissivity would more likely be a result of snowpack properties. Sector 1 contains a large land mass from Bathurst Island. Gan (1996) has pointed out the difficulty in obtaining SWE over this type of surface.

1994 (Figure 5.11) is noticeably MYI deficient in comparison with 1993. This is not in accordance with the SSM/I results, but may be due to the size of the ERS-1 scene - the SAR image does not cover the entire region of the SSM/I image. From a SWE derivation perspective, sectors 4,5,7 and 9 are composed mainly of FYI (Table 5.7). The ice types in sectors 6 and 8 are mostly FYI, but Lowther and Griffith Islands could obscure the ability of SWE estimation. Bathurst and Cornwallis Islands dominate sectors 1-3.

1995 (Figure 5.12) demonstrates MYI dominates this region in some years. This would overestimate SWE in sectors 1-4 and 6-7. Sector 5 could yield acceptable results since FYI dominates the centre of the pixel. Sectors 8 and 9 do contain more FYI (Table 5.8), with Lowther Island posing a possible problem in sector 8.

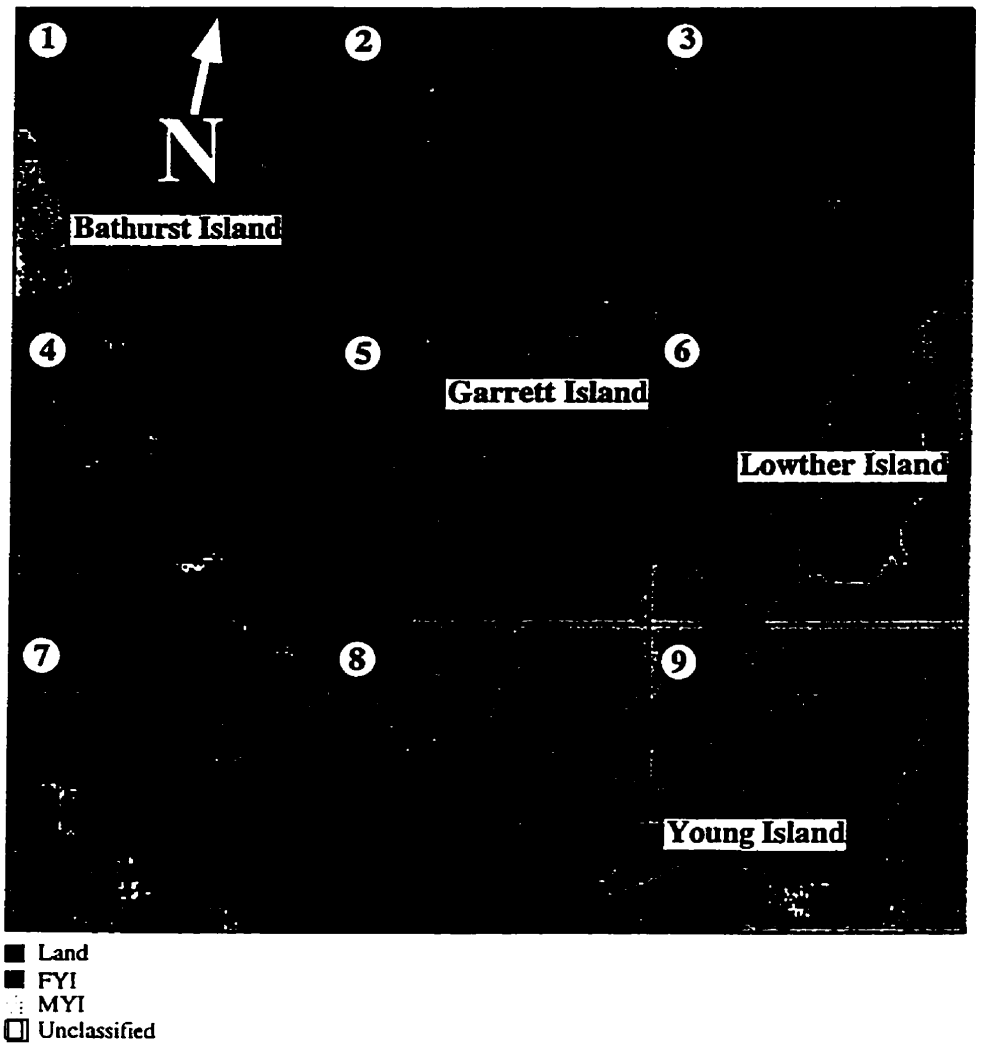

Figure 5.10 ERS-1 classified image from May 13, 1993. Boxed areas indicate one SSM/I pixel (25km^2). Numbers are used to distinguish the boxed areas in the text.

Table 5.6 Ice type composition of ERS-1 classified image from May 13, 1993.

Sector	%FYI	%MYI	%Land	%Unclassified
1	32.1	3.2	63.6	0.1
2	85.9	0.1	14.0	0.0
3	98.7	2.3	0.0	0.0
4	97.2	2.6	0.0	0.2
5	89.4	8.2	2.4	0.0
6	55.5	23.6	20.0	0.9
7	94.1	4.7	0.0	1.2
8	67.1	27.4	2.9	2.5
9	25.8	70.0	1.5	2.7

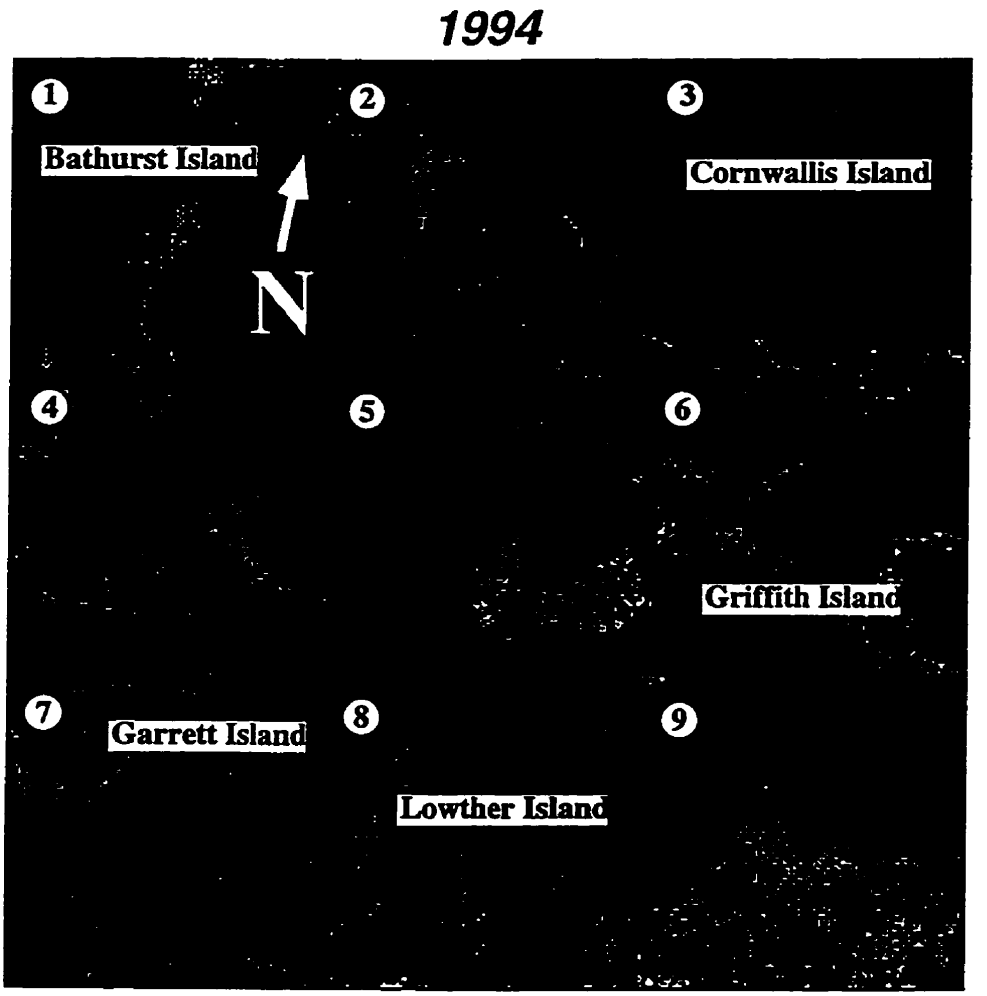

Figure 5.11 ERS-1 classified image from May 7, 1994. Boxed areas indicate one SSM/I pixel (25km^2). Numbers are used to distinguish the boxed areas in the text.

Table 5.7 Ice type composition of ERS-1 classified image from May 7, 1994.

Sector	%FYI	%MYI	%Land	%Unclassified
1	57.7	0.5	41.2	0.6
2	37.7	0.5	60.9	0.9
3	2.1	0.0	97.8	0.1
4	94.8	1.3	3.8	0.1
5	96.2	2.0	1.0	0.8
6	82.1	2.0	16.7	0.2
7	97.3	0.6	2.1	0.0
8	81.4	1.0	17.3	1.2
9	96.6	3.4	0.0	0.0

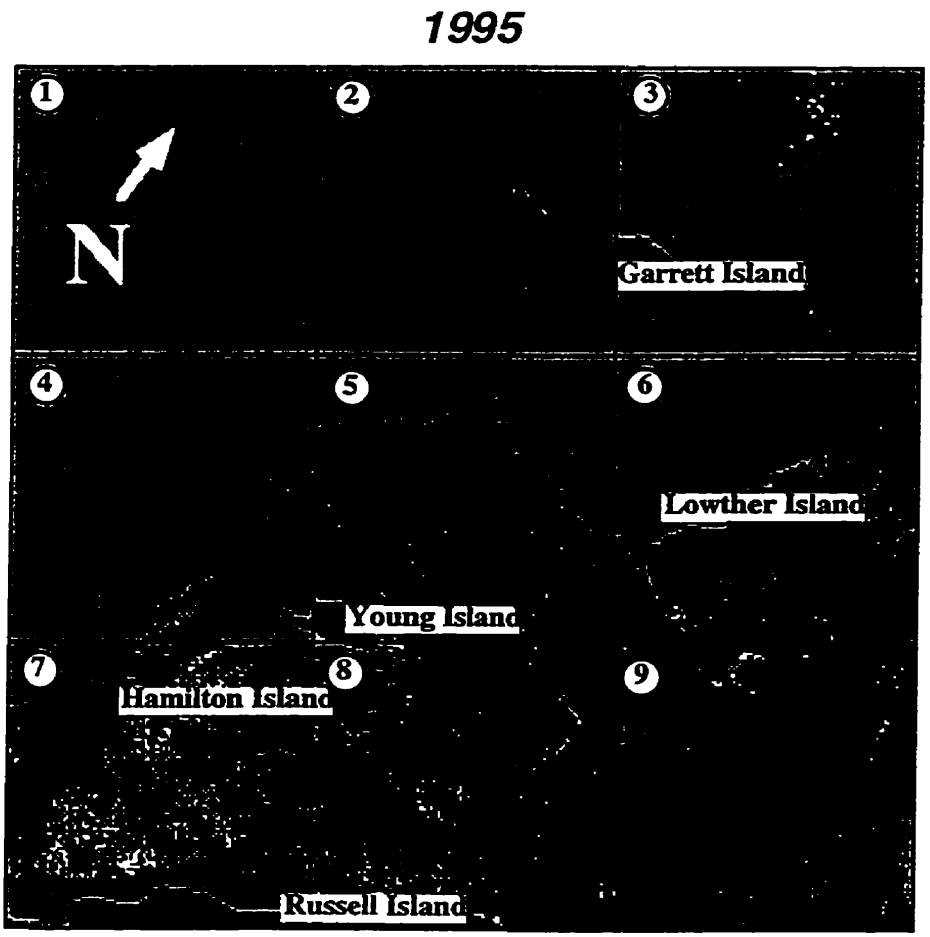

Figure 5.12 ERS-1 classified image from April 19, 1995. Boxed areas indicate one SSM/I pixel (25km^2). Numbers are used to distinguish the boxed areas in the text.

Table 5.8 Ice type composition of ERS-1 classified image from April 19, 1995.

Sector	%FYI	%MYI	%Land	%Unclassified
1	0.0	100.0	0.0	0.0
2	0.5	98.9	0.2	0.4
3	1.2	97.4	1.4	0.0
4	9.7	88.3	1.1	0.9
5	56.4	39.3	2.3	2.0
6	21.7	61.2	16.1	1.0
7	41.6	45.1	7.5	5.8
8	69.7	27.6	0.8	1.9
9	88.2	9.5	0.0	2.3

5.4 Conclusions

Several objectives were presented in the beginning of this chapter:

2 - *How does variation in the underlying ice type effect SSM/I derivation of SWE?*

2A - Are the SWE derivations from an in situ microwave radiometer and a satellite based microwave radiometer associated?

2B - To what extent does variation in the underlying ice type (FYI vs. MYI) affect emissivity on the F-13 SSM/I sensor?

2C - What does real world underlying ice type variability look like?

Although the 5 points listed here are positively related, it is not appropriate to do a statistical test to determine whether this relationship has statistical significance. However, it appears the presence of water in liquid phase forces an underestimation of SWE with a current terrestrial based SWE algorithm.

The sensitivity trials employed here showed emissivity decreased significantly with (a) decreasing FYI ice type and (b) with an increase in MYI in the centre of the pixel. The increase in derived SWE was a result of an increase in the emissivity difference for MYI. As a result, derived SWE could be in error by over 45cm.

In all years a mixture of FYI and MYI was noted. The ERS-1 classification stated 1994 contained the most FYI and would be the best candidate to explore SSM/I derived SWE. Conversely, 1995 was dominated by MYI, with 1993 being mainly FYI, but also containing some MYI in certain regions. The SSM/I classification noted larger MYI contents in 1994, with less in 1993. However, since the ERS-1 image has greater spatial resolution, it should be more precise in ice classification.

These results show MYI significantly overestimates SWE with the algorithm used on the Canadian prairies. Some method of analyzing the ice concentration within an SSM/I pixel is needed to adequately monitor SWE. Although the NASA Team Algorithm can describe the general make-up of a pixel, this work has also shown the spatial pattern of ice is important. To assess that, SAR imagery should be used.

CHAPTER 6 - Summary and Conclusions

6.1 Summary

The introductory chapter signaled the marine cryosphere as a region playing a principal role in global change and in our understanding of such change. It suggested a variation in the spatial and temporal extent of snow may be one repercussion of warming in the cryosphere. Furthermore, the initial chapter stated measuring SWE is an effective way to monitor any variations in this snow cover.

Chapter two delineated the physical aspects of the marine cryosphere. It described the formation and evolution of a seasonally dynamic snow covered sea ice volume. This chapter also portrayed the snow cover as an

integral component of mass and energy fluxes, as well as a controlling force in sea ice growth and decay. It was also shown how changes in the snow cover could affect local and global climate, as well as ecology in the marine cryosphere.

Chapter three illustrated how the physical properties of snow and ice interact with microwave energy. It suggested SWE is an effective way to monitor any changes in the snowpack and portrayed sea ice as the main source of microwave emission, with snow cover being the major source of microwave attenuation. This chapter also described theoretical models to predict the dielectric properties of the snow and ice and provided experimental findings from the recent past.

Chapter four incorporated theory from chapters two and three to assess the ability of an in-situ microwave radiometer in SWE estimation. The primary steps included monitoring the vertical profiles, seasonal evolutions and diurnal ranges in the physical and electrical properties of the snow and ice. Statistical links between T_B and SWE were not apparent when the full suite of observations were used. However, investigation of the *am, noon and pm* sets noted a significant difference in liquid water content and dielectric loss - the morning set was significantly drier than either the noon or pm. Upon segmenting the data into the three time periods, re-analysis showed a statistical link between the am T_B and SWE. Noon and pm sets showed no correlation. The fourth chapter concluded by stating SWE can be derived when liquid water contents are accounted for.

Chapter five scaled the results from chapter four up to satellite based microwave radiometry, since the marine cryosphere is characterized by a large geographic area. The sensitivity trials noted varying either the ice type or the spatial pattern of ice resulted in emissivity differences. These differences were shown to cause potential error in SWE derivation. In particular, the addition of MYI forced an underestimation of SWE with the current SWE algorithm used in the Canadian prairies. Segmentation of SSM/I imagery with the NASA Team Algorithm noted 1993 and 1994 contained mixtures of FYI and MYI, while Bayesian classification of ERS-1 imagery also noted the spatial arrangement of the ice in these years. Chapter five ended by noting variation in the underlying ice is a significant source of variation that SWE algorithms must account for.

6.2 Conclusions

In the initial chapter, the following scientific objective was proposed:

> *Science Objective: "To provide insight on the development of SWE algorithms for snow covered sea ice using microwave radiometry."*

Based on the results presented in this thesis, the following conclusions can be drawn:

1) The diurnal separation of water in liquid phase can be exploited in SWE derivation over first-year sea ice. In particular, it was shown that the

scattering properties of a dry snowpack can be related to the snow water equivalence. However, the presence of liquid water forces an underestimation of SWE with current algorithms using the ratio of 19 and 37GHz. It was shown that multiple regression techniques may be a better avenue to pursue.

2) The presence of multiyear ice confuses SWE estimation due to the large emissivity variations in MYI. Even with a dry snowpack, the presence of MYI causes an overestimation of SWE due to its lower emissivity. The spatial location of MYI within a pixel was also noted to be important. If MYI is located towards the periphery of the sensor's field of view, the overestimation is reduced.

3) Although this work has pointed out that SWE derivation is possible over first-year ice surfaces, a fully operational SWE algorithm remains to be developed. Such an algorithm will have to first identify the percentage of water in liquid phase within the snowpack. If it is found to be negligible, then the algorithm must examine the spatial heterogeneity of the underlying ice type. Based on the results of this thesis, only in the situation where FYI dominates the scene could a SWE retrieval then be made.

Several factors limit the results presented in this work. For chapter three, the major provisions regard the small sample sizes present in both the in situ and SSM/I analyses. Despite the seemingly good relationship present, C-ICE 96 was the premiere of the SBR system in Arctic SWE analyses. It covers only a two month window in the spring of 1996 and all samples were

collected at a fixed site. It is therefore not possible to comment on the applicability of these results over different ice types. It cannot be guaranteed these results would be manifest in other areas of FYI, or even in other years. For example, Hallikainen (1989) noted significant differences in microwave emission over Finland from 1979 to 1982 even though the SWE was the same. Hall *et al.* (1991) observed a similar effect over Alaska. These discrepancies have not been reported by other authors, nor is it clear why the variations exist. Further research is necessary to understand this potential problem.

In chapter 4, the major limitations are the lack of real data to support the findings. Early SIMMS years monitored snow only in 3 day intervals and at few sites. In the latter years (after 1994), where snow information was collected for many months on daily scales, SSM/I data is sparse, or not available. Further, even though SIMMS/C-ICE snow researchers sample from many sites, all are within a short distance of one another when the scale of SSM/I is considered. Truly adequate in situ sampling would require collection over the entire Arctic archipelago, something which is not feasible.

6.3 Future Directions

It can be appreciated that the process of deriving SWE over the cryosphere is an inherently difficult task. However, several advances in the next few years should alleviate some of these problems. For instance, the Advanced Microwave Scanning Radiometer (AMSR), to be launched in 2000, has twice the spatial resolution of SSM/I at 19 and 37GHz (12.5km), while 85GHz is

even finer, with a resolution of 5km. The smaller field of view should result in more homogenous pixels, enhancing the possibility of SWE retrievals. The AMSR is a twelve channel, six frequency passive microwave radiometer system. It measures vertically and horizontally polarized brightness temperatures at 6.925, 10.65, 18.7, 23.8, 36.5 and 89.0GHz. The AMSR is a part of NASA's PM-1 series of Earth Observing Science (EOS) satellites, developed in conjunction with the Mission to Planet Earth (MTPE).

Future research should focus more on the effects of water in liquid phase. For instance, if we can systematically characterize the exact contribution of wet snow to emission, then it stands to reason we could account for wet snow in the SWE algorithm. The use of lower frequencies may be useful in such an endeavour.

Questions remain surrounding the problem of MYI. The theoretical basis for SWE is that changes in SWE cause the majority of attenuation in the T_B. FYI over 10mm has a fairly consistent emissivity value, but MYI is highly variable. This variability currently precludes the accurate retrieval of SWE over MYI surfaces. As well, the distribution of snow over MYI is much more variable than snow over FYI. In rough topography, snow depths can range from zero to well over a metre within a few metres. Combined, these two points emphasize the extreme difficulty involved in trying to derive SWE over MYI surfaces.

Continued avenues of research should also attempt to draw samples from a large spatial region of in situ SWE. This should be linked to a detailed study

of the underlying ice. Combining these two with satellite based microwave radiometry could yield a successful SWE algorithm for the marine cryosphere.

Cited References

Aagaard, K., and E.C. Carmack. 1994. The Arctic Ocean and climate: A perspective. In The Polar Oceans and Their Role in Shaping the Global Environment AGU Geophysical Monograph 85. *eds.* O. M. Johannessen, R. D. Muench, and J. E. Overland. American Geophysical Union, Washington, D.C. pp. 5-20.

Aagaard, K. and E.C. Carmack. 1989. The role of sea ice and other fresh water in the Arctic circulation. *Journal of Geophysical Research.* 94:14485-14498.

Akitaya, E. (1975) IAHS-ASIH Publication. 114:42-48.

Arcone, S.A., A.G. Gow, and S. McGrew. 1986. Structure and dielectric properties at 4.8 and 9.5GHz of saline ice. *Journal of Geophysical Research (C12).* 91:14 281-14 303.

Barber, D.G. 1993. Assessment of the Interaction of Solar Radiation (0.3 to 3.0 μm) with a Seasonally Dynamic Snow Covered Sea Ice Volume, from Microwave (2.0 to 5.0 cm) Scattering. EOL Technical Report Series ISTS-EOL-TR93-002. University of Waterloo. Waterloo, Ont.

Barber, D.G., T.N. Papakyriakou, E.F. LeDrew, and M.E. Shokr. 1995. An examination of the relation between the spring period evolution of the scattering coefficent (σ°) and radiative fluxes over landfast sea ice. *International Journal of Remote Sensing.* 16:3343-3363.

Barber, D.G., T.N. Papakyriakou, and E.F. LeDrew. 1994. On the relationship between energy fluxes, dielectric properties, and microwave scattering on snow covered first-year sea ice during the spring transitional period. *Journal of Geophysical Research.* 99(C11):22 401-22 411.

Barry, R.G., J.M. Fallot, and R.L. Armstrong. 1995. Twentieth-century variability in snow-cover and approaches to detecting and monitoring changes: status and prospects. *Progress in Physical Geography.* 19:520-532.

Basharinov, A.E., A.S. Gurvich, S.T. Egorov, V.I. Zhukov, A.A. Kurskaya, L.I. Malafeev, D.T. Mateev, A.S. Mikhailov, and A.M. Shutko. 1971. Results of observations of the thermal radio emission of earth's surface in an experiment on the Cosmos-243 satellite. *Kosmonaut Issled.* 9:268-273.

Broecker, W., and T. H-Peng. 1989. The cause of the glacial to interglacial atmospheric CO_2 change: A polar alkalinity hypothesis. *Global Biogeochemistry Cycles.* 3:15-239.

Brown, R.D. and P. Cote. 1992. Interannual Variability of Landfast Ice Thickness in the Canadian High Arctic, 1950-89. *Arctic*. 45:273-284.

Bryan, F. 1986. High-latitude salinity effects and interhemispheric thermohaline circulations. *Nature*. 323:301-304.

Burton, W.K., N. Cabrera, and F.C. Frank. 1951. The growth of crystals and the equilibrium structure of their surfaces. *Philosophical Transactions of the Royal Society of London*. 243:299-358.

Campbell, W.J., P. Gloersen, W.J. Webster, T.T. Wilheit, and R.O. Ramseier. 1976. Beaufort sea ice zones as delineated by microwave imagery. *Journal of Geophysical Research*. 81:1103-1110.

Carmack, E.C., R.W. Macdonald, R.G. Perkin, F.A. McLaughlin, and R.J. Pearson. 1995. Evidence for warming of Atlantic water in the southern Canadian Basin of the Arctic Ocean: Results from the Larsen-93 expedition. *Geophysical Research Letters*. 22:1061-1064.

Carsey, F.D. 1992. Microwave Remote Sensing of Sea Ice. AGU Geophysical Monograph 68. Washington, DC. 462 pp.

Carsey, F.D. 1982. Review and status of remote sensing of sea ice. *IEEE Journal of Oceanic Engineering*. 14:127-138.

Carsey, F.D., R.G. Barry, D.A. Rothrock, and W.F. Weeks. 1992. Status and future directions for sea ice remote sensing. In Microwave Remote Sensing of Sea Ice. AGU Geophysical Monograph 68. *ed.* F. Carsey. pp. 443-446.

Cavalieri, D.J., P. Gloersen, and W.J. Campbell. 1984. Determination of sea ice parameters with the Nimbus 7 SMMR. *Journal of Geophysical Research*. 89(D4):5355-5369.

Cavalieri, D., J. Crawford, M.R. Drinkwater, D.T. Eppler, L.D. Farmer, R.R. Jentz, and C.C. Wackerman. 1991. Aircraft active and passive microwave validation of sea ice concentration from the Defense Meteorological Satellite Program special sensor microwave Imager. *Journal of Geophysical Research*. 96(C12):21,989-22,008.

Cess *et al.*, 1991. Interpretation of snow-climate feedback as produced by 17 general circulation models. *Science*. 888-891.

Chang, A.T.C., J.L. Foster, and A. Rango. 1991. utilization of surface cover composition to improve the microwave determination of snow water equivalent in a mountain basin. *International Journal of Remote Sensing*. 12:2311-2319.

Chang, A.T.C., J.L Foster, and D.K. Hall. 1987. Nimbus-7 derived global snow cover parameters. *Annals of Glaciology*. 9:39-44.

Chang, A.T.C., P. Gloersen, P. Schmugge, T.T. Wilheit, and H.J. Zwally. 1976. Microwave emission from snow and glacier ice. *Journal of Glaciology*. 16:23-29.

Chapman, W.L., and J.E. Walsh. 1993. Recent variations of sea ice and air temperature in high latitudes. *Bulletin of the American Meteorological Society*. 74:33-47.

Colbeck, S.C. 1987. Snow Metamorphism and Classification. In Seasonal Snow covers: Physics, Chemistry, Hydrology. *eds*. H.G. Jones and W.J. Orville-Thomas.

Colbeck, S.C. 1986. Classification of seasonal snow cover crystals. *Water Resources Research*. 22:59S-70S.

Colbeck, S.C. 1983. Theory of metamorphism of dry snow. *Journal of Geophysical Research*.. 88:5475-5482.

Comiso, J.C. 1990. Arctic multiyear ice classification and summer ice cover using passive microwave satellite data. *Journal of Geophysical Research*. 95(C8):13 411-13 422.

Comiso, J.C. 1986. Characteristics of Arctic winter sea ice from satellite multispectral microwave observations. *Journal of Geophysical Research*. 91(C1):975-991.

Comiso, J.C., Grenfell, T.C., Bell, D.L., Lange, M.A., and S.F. Ackley. 1989. Passive microwave in-situ observations of winter Weddell sea ice. *Journal of Geophysical Research*. 95(C8):10891-10905.

Cox, G.F.N., and W.F. Weeks. 1988. Numerical simulations of the profile properties of undeformed first-year sea ice during the growth season. *Journal of Geophysical Research*. 93:12,449-12,460.

Cox, G.F.N., and W.F. Weeks. 1975. Brine drainage and initial salt entrapment in sodium chloride ice. CRREL Research report 345. Hanover, NH, USA. 85 pp.

Cumming, W. 1952. The dielectric properties of ice and snow at 3.2cm. *Journal of Applied Physics*. 23:768-792.

de Quervain, M.R. 1963. On the metamorphism of snow. In Ice and Snow: properties, processes, and applications - proceedings of a conference held at MIT, Feb 12-16,1962. The MIT Press, Cambridge, MA, pp. 377-390.

Dickson, R.R., J. Meincke, S.A. Malmberg, and A.J. Lee. 1988. The "Great Salinity Anomaly" in the northern North Atlantic 1968-1982. *Progress in Oceanography*. 20:103-151.

Doronin, Y.P., and D.E. Kheisin. 1975. Sea Ice. Girdrometeoizdat Publishers, St. Petersburg. 323pp.

Drinkwater, M.R. and G.B. Crocker. 1988. Modelling Changes in the Dielectric and Scattering Properties of Young Snow-Covered Sea Ice at GHz Frequencies. *Journal of Glaciology*. 34:274-282.

Eicken, H., M.A. Lange, and G.S. Dieckmann. 1991. Spatial variability of sea-ice properties in the Northwestern Weddell Sea. *Journal of Geophysical Research*. 96:10 603-10 615.

Eide, L.I., and S. Martin. 1975. The formation of brine drainage features in young sea ice. *Journal of Glaciology*. 14:137-154.

Eppler, D.T., L.D. Farmer, A. L. Lohanick, M.R. Anderson, D.J. Cavalieri, J. Comiso, P. Gloersen, C. Garrity, T.C. Grenfell, M. Hallikainen, J.A. Maslanik, C. Mätzler, R.A. Melloh, I. Rubinstein, and C.T. Swift. 1992. Passive microwave signatures of sea ice. In Microwave Remote Sensing of Sea Ice. AGU Geophysical Monograph 68. *ed*. F. Carsey. pp. 41-71.

Eppler, D.T., L.D. Farmer, A.W. Lohanick, and M. Hoover. 1986. Classification of sea ice types with single-band (33.6GHz) airborne passive microwave imagery. *Journal of Geophysical Research*. 91(C9):10 661-10 695.

Fukusako, S. 1990. Thermophysical properties of ice, snow, and sea ice. *International Journal of Thermophysics*. 11:353-372.

Garrity, C. 1993. Passive microwave remote sensing of snow covered floating ice during spring conditions in the Arctic and Antarctic. AES MWG-OR 93-1. 348pp.

Garrity, C. 1991. Passive microwave remote sensing of snow covered floating ice during spring conditions in the Arctic and Antarctic. Ph.D. dissertation, York University, CRESS department, North York, Ontario.

Garrity, C. and B. Burns. 1988. Electrical and Physical Properties of Snow in Support of BEPERS-88, Technical Report MWG 88-11. York University, North York, Ontario. 65 pp.

Gloersen, P., and W.J. Campbell. 1991. Recent variations in Arctic and Antarctic sea-ice covers. *Nature*. 352:33-36.

Gloerson, P., and D.J. Cavalieri. 1986. Reduction of weather effects in the calculation of sea ice concentration from microwave radiances. *Journal of Geophysical Research*. 91(C3):3913-3919.

Gloersen, P., W. Nordberg, T.J. Schmugge, and T.T. Wilheit. 1973. Microwave signatures of first-year and multiyear ice. *Journal of Geophysical Research*. 78:3564-3572.

Goodison, B.E. 1997. The cryosphere: An indicator of climate change? Geomatics in the Era of Radarsat Conference. Ottawa, ON. May 26-30, 1997. 13 pp.

Goodison, B.E. 1990. Remote Sensing of Snowcover. In The Canadian Remote Sensing Contribution to Understanding Global Change. *eds*. E.F. LeDrew, M. Stone, and F. Hegyi. pp. 93-110.

Goodison, B.E., A.E. Walker, and F.W. Thirkettle. 1990. Determination of snow water equivalent on the Canadian prairies using near real-time passive microwave data. Proceedings of the Workshop on Applications of Remote Sensing in Hydrology, Saskatoon, Canada. *eds*. G.W. Kite and A. Wankiewicz. pp. 297-309.

Grenfell, T.G. 1992. Surface-based passive microwave studies of multiyear sea ice. *Journal of Geophysical Research*. 97(C3):5063-5074.

Grenfell, T.C. 1986. Surface-based passive microwave observations of sea ice in the Bering and Greenland seas. *IEEE Transactions on Geoscience and Remote Sensing*. GE-24:378-382.

Grenfell, T.G. 1979. The effects of ice thickness on the exchange of solar radiation over the Polar Oceans. *Journal of Glaciology*. 22:305-320.

Grenfell, T.G., D. Bell, A. Lohanick, C. Swift, and K. St. Germain. 1988. Multifrequency passive microwave observations of saline ice grown in a tank. Proceedings of the IGARSS'88 Symposium. pp. 1687-1690.

Grenfell, T.C and J.C. Comiso. 1986. Multifrequency passive microwave observations of first-year sea ice grown in a tank. *IEEE Transactions on Geoscience and Remote Sensing*. GE-24:826-831.

Grenfell, T.G., and A.W. Lohanick. 1985. Variations of the microwave signatures of sea ice during the late spring and early summer near Mould Bay, NWT. *Journal of Geophysical Research*. 90(C3):5063-5073.

Grenfell, T.G, and D.K. Perovich. 1984. Spectral albedo of sea ice and incident solar irradiance in the Southern Beaufort Sea. *Journal of Geophysical Research*. 89(C3):3573-3580.

Hall, D.K., M. Sturm, C.S. Benson, A.T.C. Chang, J.L. Foster, H. Garbeil, and E. Chacho. 1991. Passive microwave remote and in situ measurements of Arctic and subarctic snow covers in Alaska. *Remote Sensing of Environment*. 38:161-172.

Hall, D.K., J.L. Foster, and A.T.C. Chang. 1982. Measurement and modelling of microwave emission from forested snowfields in Michigan. *Nordic Hydrology*. 13:129-138.

Hallikainen, M.T. 1989. Microwave radiometry of snow. *Advanced Space Research*. 9:267-275.

Hallikainen, M.T. 1983. A new low-salinity sea ice model for UHF radiometry. *International Journal of Remote Sensing*. 4:655-661.

Hallikainen, M.T. 1977. Dielectric properties of NaCl at 16GHz. Report S-107, Helsinki University of Technology, Radio Laboratory. 37 pp., Espoo, Finland.

Hallikainen, M., and D.P. Winebrenner. 1992. The physical basis for sea ice remote sensing. In Microwave Remote Sensing of Sea Ice. AGU Geophysical Monograph 68. *ed.* F. Carsey. pp. 29-44.

Hallikainen, M.T. and P.A. Jolma. 1986. Retrieval of the Water Equivalent of Snow Cover in Finland by Satellite Microwave Radiometry. *IEEE Transactions on Geoscience and Remote Sensing*. 24:855-862.

Haykin, S., E. Lewis, K. Raney and J.R. Rossiter. 1994. *Remote Sensing of Sea Ice and Icebergs*. John Wiley & Sons, Toronto.

Henderson-Sellers, A., and P.J. Robinson. 1987. Contemporary Climatology. Longman Scientific & Technical. New York. 439 pp.

Hoekstra, P. and P. Cappillino 1971. Dielectric properties of sea and sodium chloride ice at UHF and microwave frequencies. *Journal of Geophysical Research*. 76:4922-4931.

Hollinger, J.P., B.E. troy, Jr., R.O. Ramseier, K.W. Asmus, M.F. Hartman, and C.A. Luther. 1984. Microwave emission from high Arctic sea ice during freeze-up. *Journal of Geophysical Research*. 89(C5):8104-8122.

IPCC. 1995. Climate change 1995. Impacts, adaptations and mitigation of climate change. Contribution of Working Group II to the Second Assessment Report of the Intergovernmental Panel on Climate Change. Cambridge University Press. 877 pp.

IPCC. 1990. Climate change: The IPCC scientific assessment. *eds*. J.T. Houghton, G.J. Jenkins, and J.J. Ephraums. Cambridge University Press. 365 pp.

Jewett, S.C., and H.M. Feder. 1980. Autumn food of adult starry flounder Platichthys stellatus from the NE Bering Sea and the SE Chukchi Sea. *Journal of International Exploration*. 39:7-14.

Johannessen, O.M., M. Miles, and E. Bjorgo. 1995. The Arctic's shrinking sea ice. *Nature*. 376:126-127.

Kong, J.A., R. Shin, J.C. Shiue, and L. Tsang. 1979. Theory and experiment for passive microwave remote sensing of snowpacks. *Journal of Geophysical Research*. 84(B10):5669-5673.

Kotlyakov, V.M., and M.G. Grosswald. 1990. Interaction of Sea Ice, Snow and Glaciers with the Atmosphere and Ocean (Part III). *Polar Geography and Geology*. 14: 155-163

LaChapelle, E.R., and R.L. Armstrong. 1977. Temperature patterns in an alpine snow cover and their influence on snow metamorphism.

Technical report, Institute for Arctic and Alpine Research. University of Colorado. Boulder, CO.

Langham, E.J. 1981. Physics and properties of snow cover. In Handbook of snow. *eds*. D.M.Gray, and D.H. Male. Pergamon Press Canada Ltd, Willowdale, Ont. pp.275-337.

Langleben, M.P. (1969) Albedo and degree of puddling of a melting cover of sea ice. *Journal of Glaciology*. 8:407-413.

Ledley, T.S. 1991. Snow on sea ice: Competing effects in shaping climate. *Journal of Geophysical Research (D9)*. 96:17 195-17 208.

LeDrew, E.F. 1990. Influence of Polar regions on Climate Variability and Change., In: Encyclopedia of Earth System Science. *ed*. by W.A. Nierenberg. Academic Press.

Lohanick, A.W. 1993. Microwave brightness temperatures of laboratory-grown undeformed first-year ice with an evolving snow cover. *Journal of Geophysical Research*. 98(C3):4667-4674.

Lohanick, A.W. 1990. Some observations of established snow cover on saline ice and their relevance to microwave remote sensing. In Sea Ice Properties and Processes, Proceedings of the W.W. Weeks Sea Ice Symposium, *eds*. S.A. Ackley and W.W. Weeks, CRREL Monograph 90-1:61-67, US Army Cold Regions Research and Engineering Laboratory, NH, USA.

Lohanick, A.W. and T.C. Grenfell. 1986. Variations in brightness temperature over cold first-year sea ice near Tuktoyaktuk, NT. *Journal of Geophysical Research*. 91(C4):5133-5144.

Male, D.H. 1980. The seasonal snowcover. In Dynamics of snow and ice masses. *ed*. Colbeck, S.C. Academic Press, New York, NY. pp.305-396.

Manabe, S., and R.J. Stouffer. 1988. Two stable equilibria of a coupled ocean-atmosphere model to gradual changes of atmospheric CO_2. Part II: Seasonal response. *Journal of Climate*. 5:105-126.

Marshall, J.S. and K.L.S. Gunn. 1952. Measurement of snow parameters by radar. *Journal of Meteorology*. 9:322-938.

Martin, S. 1979. A field study of brine drainage and oil entrainment in first-year sea ice. *Journal of Glaciology*. 22:473-502.

Mason, B.J. 1992. Snow crystals, natural and man-made. *Contemporary physics*. 33:227-243.

Massom, R. (1991) Satellite Remote Sensing of Polar Regions. Lewis Publishers. Boca Raton, FL.

Mätzler, C., and U. Wegmüller. 1987. Dielectric properties of freshwater ice at microwave frequencies. *Journal of Physics D: Applied Physics*. 10:1623-1630.

Mätzler, C., E. Schanda, and W. Good. 1982. Towards definition of optimum sensor specifications for microwave remote sensing of snow. *IEEE Transactions on Geoscience and Remote Sensing*. GE20:57-66.

Maykut, G.A. 1986. Chapter 5: The surface heat and mass balance. In: Geophysics of Sea Ice. *ed*. N. Untersteiner. Dordrecht: Martinus Nijhoff Pub., pp. 395-463.

Maykut, G.A. and N. Untersteiner. 1971. Some results from a time-dependent thermodynamic model of sea ice. *Journal of Geophysical Research,*. 76:550-1575.

Meeks, D.C., G.A. Poe, and R.O. Ramseier. 1974. A study of microwave emission properties of sea ice - AIDJEX 1972, Aerojet Electrosystems Co., University of Washington. Final report, 1786FR-1.

Mellor, M. 1977. Engineering properties of snow. *Journal of Glaciology*. 19:15-66.

Mellor, M. 1965. Optical properties of snow. CRREL Research Report 169. 20 pp.

Mikhalevsky, P.N., A.B. Baggeroer, A. Gavrilov, and M. Slavinsky. 1995. Experiment tests use of acoustics to monitor temperature and ice in the Arctic Ocean. EOS Transactions, American Geophysical Union, 76:265.

Misurak, K.M. 1994. Section 5.2 Snow geophysical properties. In Misurak, K.M., D.G. Barber, and E.F. LeDrew. SIMMS'94 Data Report. Earth Observation Laboratory Technical Report, ISTS-EOL-SIMS-TR-94-001.

Misurak, K.M. 1993. Section 6.1 Snow geophysical properties. In Misurak, K.M., D..G. Barber, and E.F. LeDrew. SIMMS'93 Data Report. Earth Observation Laboratory Technical Report, ISTS-EOL-SIMS-TR-93-007.

Mote, T.L., and M.R. Anderson. 1995. Variations in snowpack melt on the Greenland ice sheet based on passive-microwave measurements. *Journal of Glaciology*. 41:51-60.

Nakawo, M. and N.K. Sinha. 1981. Growth Rate and Salinity Profile of First-Year Sea Ice in the High Arctic. *Journal of Glaciology*. 27:315-330.

Nansen, F. 1902. The oceanography of the North Polar Basin, Norwegian North Polar Expedition. 1893-1896, Scientific Research. V(IX), 427 p.

Neumann, G. and W.J. Pierson, Jr. 1966. *Principles of Physical Oceanography*. Prentice-Hall. New Jersey, USA. 545pp.

NSIDC. 1996. Snow and Ice. 1996. Boulder, CO. 32pp.

Nyfors, E. 1983. On the dielectric properties of dry snow in the 800MHz to 13GHz region. Helsinki University Technological Radio Lab. Report S135.

Oke, T.R. 1987. Boundary Layer Climates. Methuen & Co., Ltd. 372 pp.

Onstott, R.G., Grenfell, T.C., Mätzler, C., Luther, C.A., and E.A. Svendsen. 1987. Evolution of microwave sea ice signatures during early summer and midsummer in the marginal ice zone. *Journal of Geophysical Research.* 92:6825-6835.

Perla, R. 1991. Real permittivity of snow at 1MHz and 0°C. *Cold Regions Science and Technology.* 19:215-219.

Perovich, D.K. and A.J. Gow 1991. A statistical description of the microstructure of young sea ice. *Journal of Geophysical Research.* 96:16 943-16 953.

Rind, D., R. Healy, C. Parkinson, and D. Martinson. 1995. The role of sea ice in 2X CO2 climate sensitivity. Part I: The total influence of sea ice thickness and extent. *Journal of Climate* 8:449-463.

Sakazume, S. and N. Seki. 1978. On the thermal properties of ice and snow in a low temperature region. *Japanese Society of Mechanical Engineers.* 46:1119.

Schemenauer, R.S., Berry, M.O., and J.B. Maxwell. 1981. Snowfall formation. In Handbook of snow. *eds.* D.M.Gray and D.H. Male. Pergamon Press Canada Ltd, Willowdale, Ont. pp. 127-152.

Smith, T.G., and I. Stirling. 1977. Variation in the density of ringed seal (Phoca Hispida) birth layers in the Amundsen Gulf, NWT. *Canadian Journal of Zoology.* 56:1066-1070.

Steffen *et al.* 1992. The estimation of geophysical parameters using passive microwave algorithms. In Microwave Remote Sensing of Sea Ice. AGU Geophysical Monograph 68. *ed.* F. Carsey. pp. 201-231.

Steffen, K., and J.A. Maslanik. 1988. Comparison of Nimbus 7 Scanning Multichannel Microwave Radiometer radiance and derived sea ice concentrations with Landsat imagery for the North Water area of Baffin Bay. *Journal of Geophysical Research.* 93(C9):10,769-10,781.

Tinga, W.R., W.A.G. Voss, and D.F. Blossey. Generalized approach to multiple dielectric mixture theory. *IEEE Transactions on Antennas and Propagation.* 44:3897-3902.

Tiuri, M.E., A.H. Sihvola, E.G. Nyfors and M.T. Hallikainen. (1984) The Complex Dielectric Constant of Snow at Microwave Frequencies. *IEEE Journal of Oceanic Engineering.* OE-9:377-382.

Tucker, W.B., III, D.K. Perovich, A.J. Gow, W.F. Weeks, and M.R. Drinkwater. 1992. Physical properties of sea ice relevant to remote sensing. In Microwave Remote Sensing of Sea Ice. AGU Geophysical Monograph 68. *ed.* F. Carsey. pp. 10-28.

Tucker, W.B., A.J., and J.A. Richter. 1984. On small-scale variations in first-year sea ice. *Journal of Geophysical Research*. 89:6505-6514.

Ulaby, F.T., R.K. Moore, and A.K. Fung. 1986. Microwave Remote Sensing: Active and Passive: Volume III: From Theory to Application. Addison-Wesley Publishing Company, Massachusetts.

Vant M.R. 1976. A combined empirical and theoretical study of the dielectric properties of sea ice over the frequency range 100MHz to 40GHz. Technical report, Carleton University, Ottawa, Canada.

Walker, A.E., and B.E. Goodison. 1993. Discrimination of a wet snow cover using passive microwave satellite data. *Annals of Glaciology*. 17:307-311.

Weeks, W.F. and S.F. Ackley, 1986. The growth, structure, and properties of sea ice. in The Geophysics of Sea Ice. *ed*. N. Understeiner. NATO Series B: Physics vol. 146. Plenum press, New York, USA. Pp 9-164.

Weeks,W.F. and G. Lofgren 1967. The effective solute distribution during the freezing of NaCl solutions. Proceedings of the International Conference on Low Temperature Science, Physics of Snow and Ice. *ed*. H. Oura, Institute of Low Temperature Science, Hokkaido University, Sapporo, japan. Pp. 579-597.

Welch, H.E., M.A. Bergmann, T.D. Siferd and P.S. Amarualik. 1991. Seasonal development of ice algae near Chesterfield Inlet, N.W.T., Canada. *Canadian Journal of Fisheries and Aquatic Sciences*.48:2395-2402.

Welch, H.E. and M.A. Bergmann. 1989. Seasonal development of ice algae and its prediction from environmental factors near Resolute, NT, Canada. *Canadian Journal of Fisheries and Aquatic Sciences*. 46:1793-1804.

Wilheit, T., J. Blin, W. Campbell, A. Edgerton, and W. Nordberg. 1972. Aircraft measurements of microwave emission from Arctic sea ice. *Remote Sensing of the Environment*. 2:129-139.

Yoshida, Z. (1955) Physical studies on deposited snow: Thermal properties. Institute of Low Temperature Science. Hokkaido Univ., Sapporo, Ser.A.No.27, pp. 19-74.

World Meteorological Organization. 1970. Snow and Ice.

Appendices

Appendix A: Acronyms & Abreviations

AIDJEX	Arctic Ice Dynamic Joint Experiment
AMSR	Advanced Microwave Scanning Radiometer
C-ICE	Collaborative-Interdisciplinary Cryospheric Experiment
DMSP	United States Defense Meteorological Satellite Program
ERS-1	Earth Resources Satellite
ESMR	Electronically Scanning Microwave Radiometer
FYI	First-year ice
GCM	General circulation models
IPCC	Intergovernmental Panel on Climate Change
MYI	Multiyear ice
NASA	National Aeronautics Space Agency
OW	Open Water
SBR	Surface Based Radiometer
SIMMS	Seasonal Sea Ice Monitoring and Modelling
SMMR	Scanning Multichannel Microwave Radiometer
SSM/I	Special Sensor Microwave/Imager
SWE	Snow water equivalence

Appendix B: List of Symbols

$K\downarrow$	Downwelling shortwave radiation
$K\uparrow$	Upwelling shortwave radiation
λ_o	Wavelength of free space
α	Albedo
ε	Complex dielectric constant
ε''	Dielectric loss
e	Emissivity
ε'	Permittivity
GHz	Gigahertz
H	Horizontal polarization
K	Kelvin
λ_{se}	Thermal conductivity of snow
ρ	Density
S_i	Ice salinity
S_w	Water salinity of in parts per thousand (‰)
T_f	Freezing temperature of water
V	Vertical polarization
V_i	Volume of ice
°C	Degrees Celcius
T_B	Brightness Temperature
kg	Kilogram
EM	Electromagnetic spectrum
V_b	Volume of brine
‰	parts per thousand (ppt)
FOV	Field of view

Appendix C: List of Terms

Pendular Regime: Liquid water content within a snowpack is general less than 7% by volume.

Funicular Regime: Liquid water content within a snowpack is general greater than 7% by volume.

Emissivity: a ratio of the emission an object radiates compared to what a blackbody at the same temperature would radiate.

Permittivity: A dielectric measure of the amount of energy which penetrates into a medium.

Loss: A dielectric measure that describes what happens to energy once it has penetrated a medium.

GR: The gradient ratio. A comparison of 19GHz and 37GHz at V polarization.

PR: The polarization ratio. A comparison of 19GHz at V and H polarizations.

Appendix D: Normality Plots from Chapter 3

A•All Samples Combined

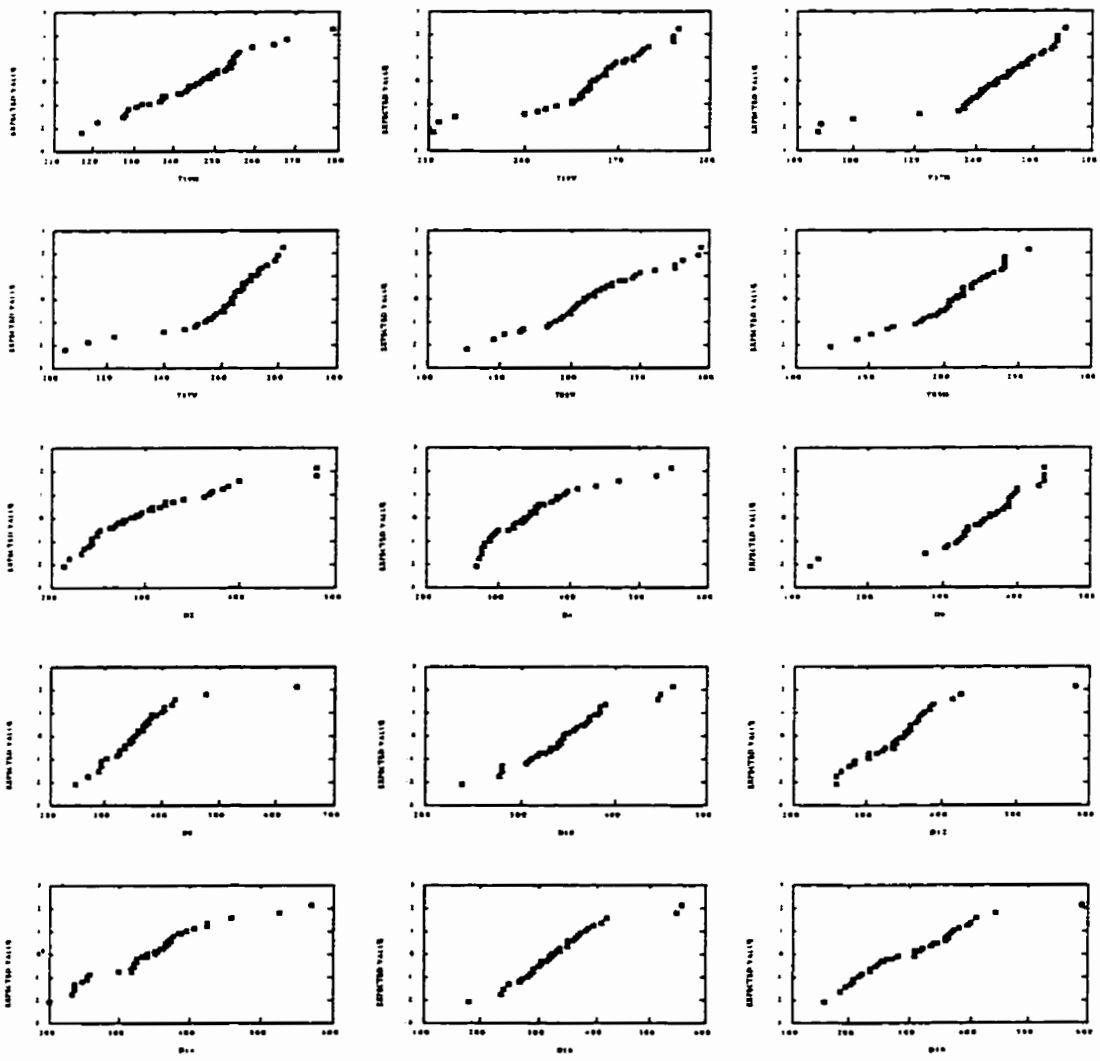

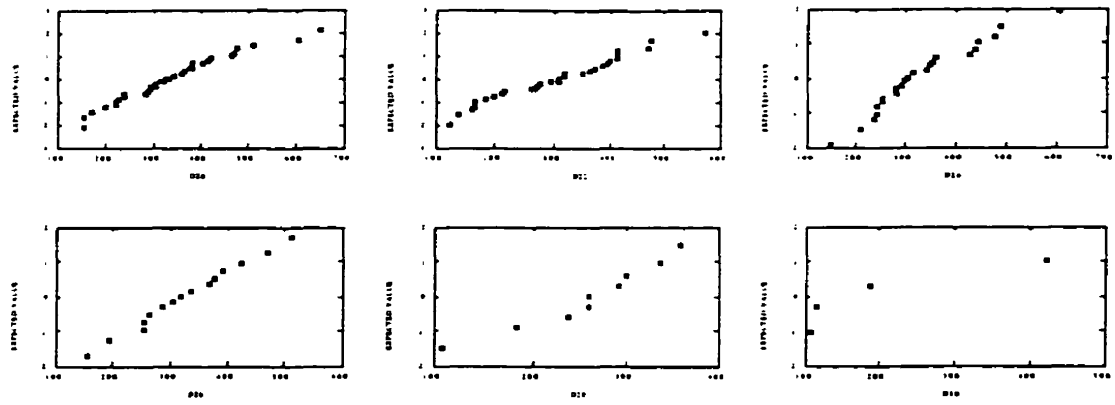

B• AM Subset

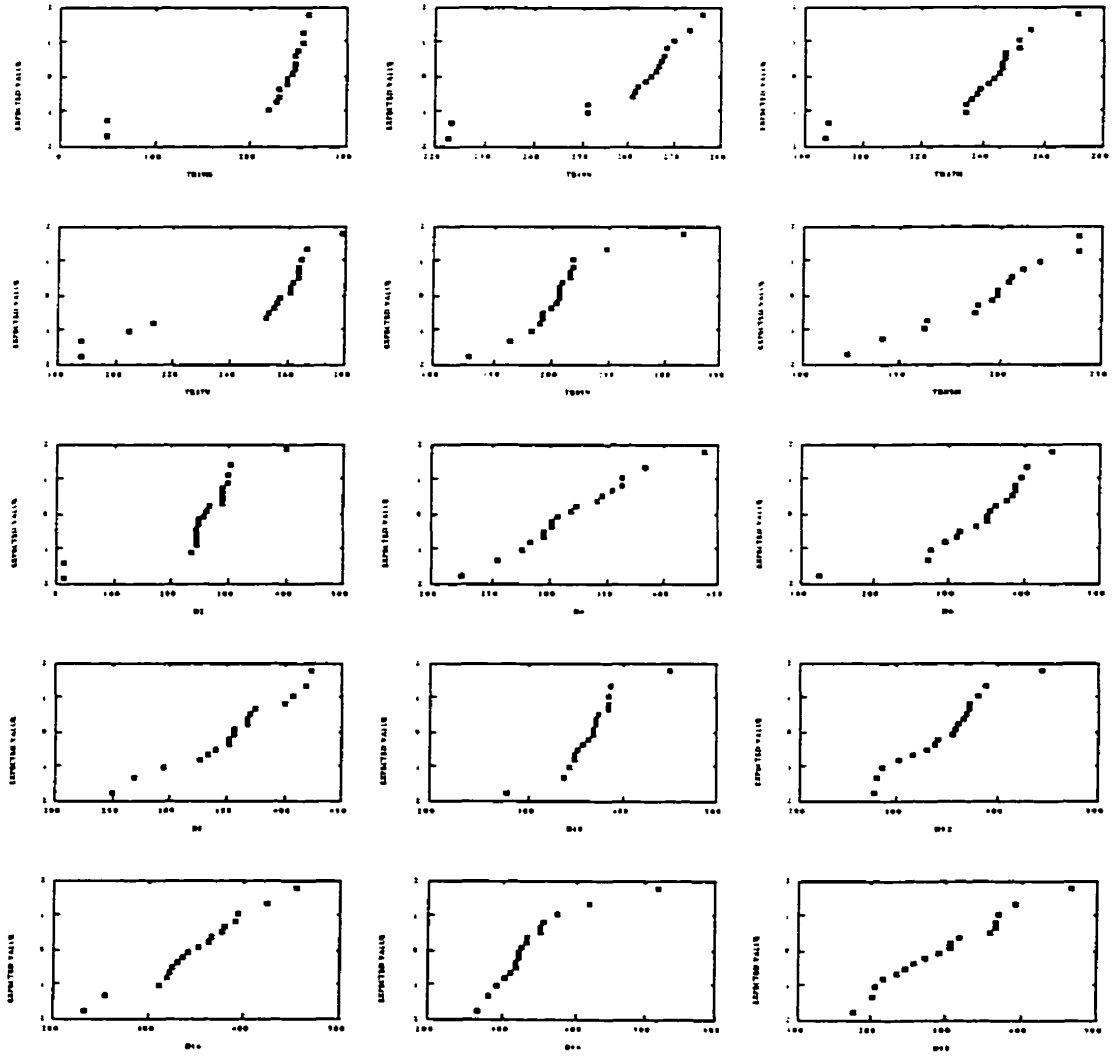

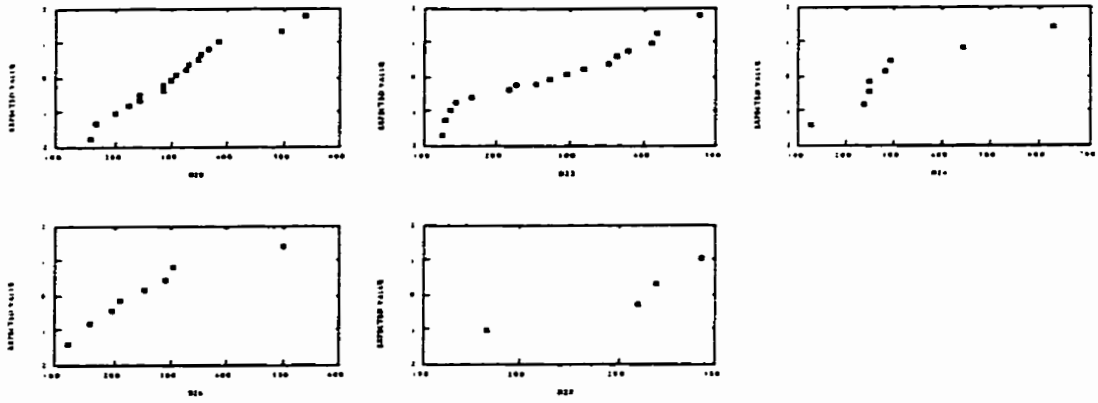

Appednix E: ANOVA Results from Chapter 3

A• All Samples Combined

ANOVA Table
SWE vs. TB 19H

	DF	Sum of Squares	Mean Square	F-Value	P-Value
Regression	1	31.431	31.431	8.133	.0064
Residual	48	185.506	3.865		
Total	49	216.937			

ANOVA Table
SWE vs. TB 19V

	DF	Sum of Squares	Mean Square	F-Value	P-Value
Regression	1	12.662	12.662	3.098	.0841
Residual	53	216.592	4.087		
Total	54	229.254			

ANOVA Table
SWE vs. TB 37H

	DF	Sum of Squares	Mean Square	F-Value	P-Value
Regression	1	42.532	42.532	12.201	.0010
Residual	54	188.240	3.486		
Total	55	230.772			

ANOVA Table
SWE vs. TB 37V

	DF	Sum of Squares	Mean Square	F-Value	P-Value
Regression	1	35.277	35.277	9.744	.0029
Residual	54	195.495	3.620		
Total	55	230.772			

ANOVA Table
SWE vs. TB 85H

	DF	Sum of Squares	Mean Square	F-Value	P-Value
Regression	1	20.147	20.147	5.069	.0293
Residual	45	178.841	3.974		
Total	46	198.988			

ANOVA Table
SWE vs. TB 85V

	DF	Sum of Squares	Mean Square	F-Value	P-Value
Regression	1	41.850	41.850	11.962	.0011
Residual	54	188.922	3.499		
Total	55	230.772			

B• AM Subset

ANOVA Table
SWE vs. T19H

	DF	Sum of Squares	Mean Square	F-Value	P-Value
Regression	1	66.737	66.737	30.401	<.0001
Residual	13	28.538	2.195		
Total	14	95.275			

ANOVA Table
SWE vs. T19V

	DF	Sum of Squares	Mean Square	F-Value	P-Value
Regression	1	71.684	71.684	37.940	<.0001
Residual	14	26.452	1.889		
Total	15	98.137			

ANOVA Table
SWE vs. T37H

	DF	Sum of Squares	Mean Square	F-Value	P-Value
Regression	1	91.223	91.223	140.551	<.0001
Residual	15	9.736	.649		
Total	16	100.959			

ANOVA Table
SWE vs. T37V

	DF	Sum of Squares	Mean Square	F-Value	P-Value
Regression	1	90.301	90.301	127.090	<.0001
Residual	15	10.658	.711		
Total	16	100.959			

IMAGE EVALUATION TEST TARGET (QA-3)

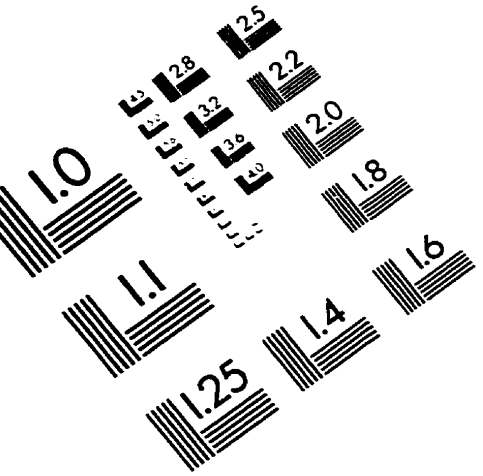

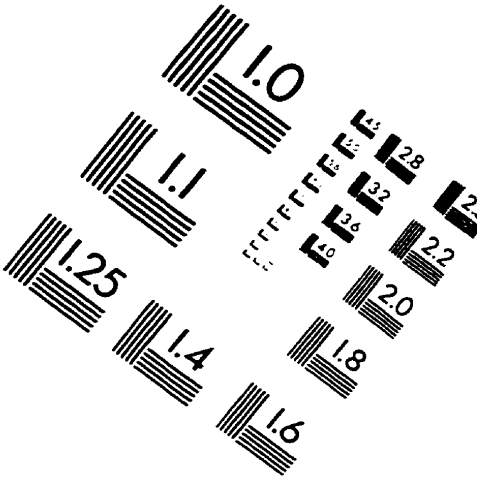

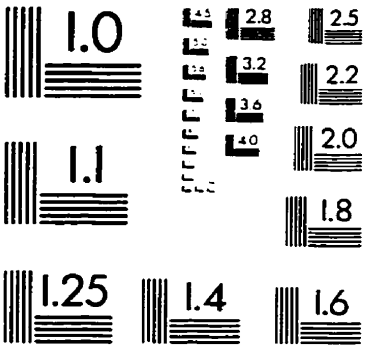

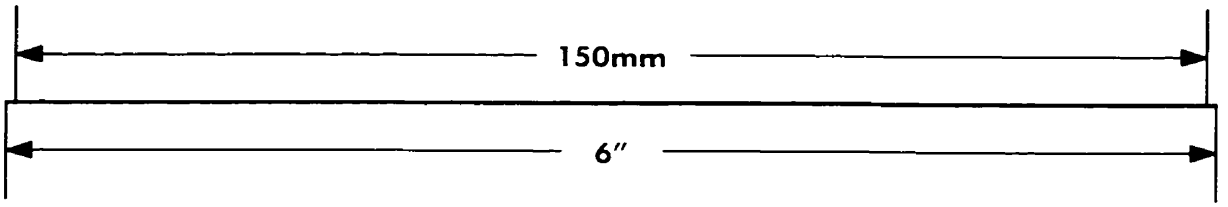

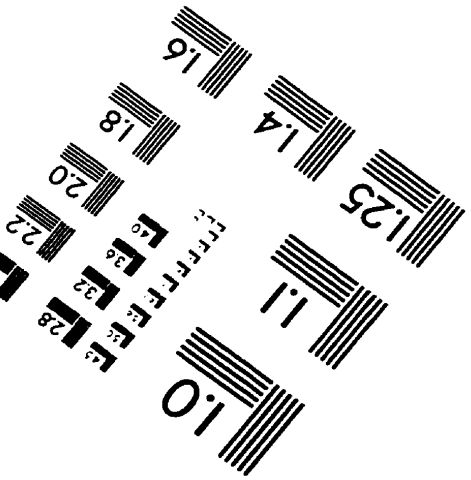

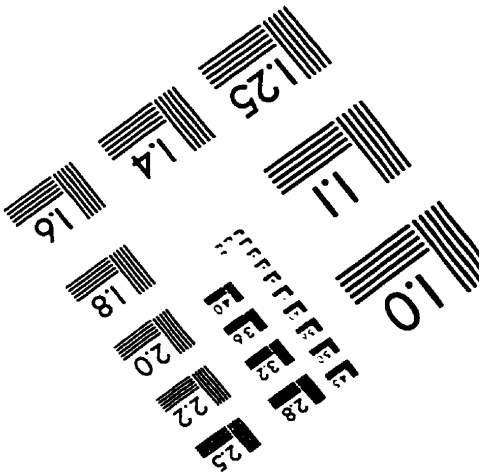

APPLIED IMAGE, Inc
1653 East Main Street
Rochester, NY 14609 USA
Phone: 716/482-0300
Fax: 716/288-5989